Project No. 609687

FP7-ENERGY-2013-IRP

ELECTRA

European Liaison on Electricity Committed Towards long-term Research Activities for Smart Grids

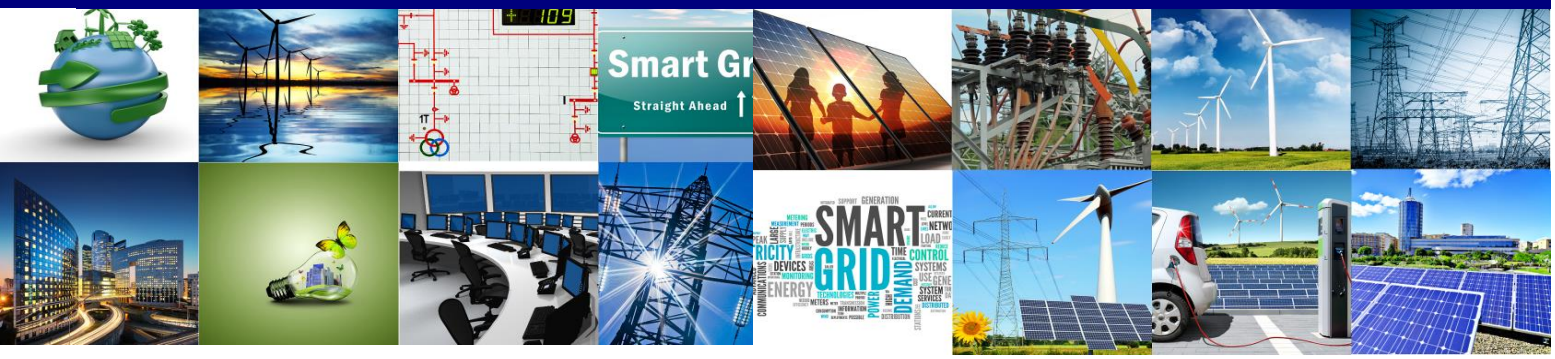

WP 6

Control schemes for the use of flexibility

Deliverable 6.4

Simulations based evaluation of the ELECTRA WoC solutions for voltage and balance control - Stand-alone Use Case simulation results

01/03/2018

ID&Title	**D6.4** Simulations based evaluation of the ELECTRA WoC solutions for voltage and balance control - Stand-alone Use Case simulation results	Number of pages:	108

Short description (Max. 50 words):

Within IRP ELECTRA six control schemes were developed to control power system voltage and balancing (frequency) in the Web-of-Cells architecture. This document summarizes and presents simulations proving that the Web-of-Cells can be controlled in a stable way by each of these six control schemes in stand-alone mode.

Version	Date	Modification's nature
V0.1	30/06/2017	First Draft
V0.02	24/10/2017	Revised Draft
V0.03	31/10/2017	2nd Revised Draft
V1.00	31/10/2017	Under 1st Review
V1.01	01/02/2018	Under 2nd Review
V2.00	01/03/2018	Released

Accessibility

☒ PU, Public

☐ PP, Restricted to other program participants (including the Commission Services)

☐ RE, Restricted to other a group specified by the consortium (including the Commission Services)

☐ CO, Confidential, only for members of the consortium (including the Commission Services)

If restricted, please specify here the group:	

Owner / Main responsible:		
WP 6.2 Task Leader:	Berend Evenblij (TNO)	
Reviewed by:		
WP 6 Leader: Technical Project Coordinator:	Seppo Hänninen (VTT Ltd) Helfried Brunner (AIT)	01/02/2018
Final Approval by:		
ELECTRA Technical Committee TOQA appointed Reviewer:	Helfried Brunner (AIT) Thomas Strasser (AIT)	15/02/2018

Authors

Name	Last Name	Organization	Country
Berend	Evenblij	TNO	The Netherlands
Kai	Heussen	DTU	Denmark
Junjie	Hu	DTU	Denmark
Michel	Rezkalla	DTU	Denmark
Mattia	Marinelli	DTU	Denmark
Seppo	Hänninen	VTT	Finland
Riku	Pasonen	VTT	Finland
Julia	Merino	TECNALIA	Spain
Emilio	Rodríguez	TECNALIA	Spain
Evangelos	Rikos	CRES	Greece
Michal	Kosmecki	IEN	Poland
Efren	Guillo-Sansano	USTRATH	United Kingdom
Mazher	Syed	USTRATH	United Kingdom
Kevin	Johnstone	USTRATH	United Kingdom

Copyright

Consisting of:

Coordinator	
Ricerca Sul Sistema Energetico – (RSE)	Italy
Participants	
Austrian Institute of Technology GmbH - (AIT)	Austria
Vlaamse Instelling Voor Technologisch Onderzoek N.V. - (VITO)	Belgium
Belgisch Laboratorium Van De Elektriciteitsindustrie - (LABORELEC)	Belgium
Danmarks Tekniske Universitet - (DTU)	Denmark
Teknologian Tutkimuskeskus - (VTT)	Finland
Commissariat A L'Energie Atomique Et Aux Energies Alternatives - (CEA)	France
Fraunhofer-Gesellschaft Zur Förderung Der Angewandten Forschung E.V – (IWES)	Germany
Centre For Renewable Energy Sources And Saving - (CRES)	Greece
Agenzia Nazionale per Le Nuove Tecnologie, L´Energia E Lo Sviluppo Economico Sostenibile - (ENEA)	Italy
Fizikalas Energetikas Instituts - (IPE)	Latvia
SINTEF Energi AS - (SINTEF)	Norway
Instytut Energetyki - (IEN)	Poland
Instituto De Engenharia De Sistemas E Computadores Do Porto - (INESC_P)	Portugal
Fundacion Tecnalia Research & Innovation - (TECNALIA)	Spain
Joint Research Centre European Commission - (JRC)	Belgium
Nederlandse Organisatie Voor Toegepast Natuurwetenschappelijk Onderzoek – (TNO)	Netherlands
Turkiiye Bilimsel Ve Teknolojik Arastirma Kurumu - (TUBITAK)	Turkey
University Of Strathclyde - (USTRATH)	UK
European Distributed Energy Resources Laboratories (DERlab)	Germany
Institute for Information Technology at University of Oldenburg (OFFIS)	Germany

Executive summary

This report describes the simulation-based validation of the six selected ELECTRA Web-of-Cells control schemes represented individual use cases. The six control schemes and related use cases are the following:

- Inertia control: Inertia Response Power Control (IRPC)
- Frequency control: Adaptive Frequency Containment Control (FCC)
- Balance control:
    - Balance Restoration Control (BRC)
    - Balance Steering Control (BSC)
- Voltage control:
    - Primary Voltage Control (PVC)
    - Post-Primary Voltage Control (PPVC)

The controllers are simulated in a grid divided in a number of cells according to the ELECTRA Web-of-Cells concept. This concept is a proposed control scheme for the real-time frequency/balance and voltage control of the future power grid. It is designed for a future where large parts of traditional synchronous generators – connected to the high voltage grid – are replaced by large amounts of smaller – intermittent – renewables at all voltage levels, and where flexible loads and affordable storage is omnipresent. It applies a 'solve local problems locally' paradigm, where the responsibility for detecting the need for activating reserves, as well as the responsibility to do activations in a grid secure manner, is delegated to smaller grid areas – called cells. This results in a distributed control strategy, where system balance is restored in a bottom-up, grid-secure manner, through the combined functionality of Inertia Response Power Control, Adaptive Frequency Containment Control, Balance Restoration Control and Balance Steering Control. The control actions are based on local observables where a continuous voltage control (through the combined functionality of Post-Primary Voltage Control and Primary Voltage Control) minimizes losses and avoids local voltage problems at all voltage levels.

For each of the six control schemes simulations have been performed, that make clear whether and how far the control schemes are able to keep the Web-of-Cells power system stable. The reports of the individual simulations are include in six annexes to this deliverable. In each of these annexes the focus is on the control scheme in stand-alone mode, i.e. it is primarily not a combined simulation of two or more control schemes. In the case a control scheme needs for its performance the activity of other one(s), these are implemented as well in the simulation.

Another aspect is the number of cells involved. The focus of the presented evaluation is on the functionality of the Web-of-Cells concept and not on its scalability. That is the reason why the number of cells in the test grids is limited to a maximum of four.

The specific tasks of the control schemes can be summarized as follows:

- IRPC: limit the rate of change of frequency
- FCC: limit the deviation of the frequency
- BRC: bring back the frequency to rated value
- BSC: rearrange the power flows, so that reserves in use are made available
- PVC: keep the voltages within limits
- PPVC: rearrange use of resources that keep the voltage, so that resources are optimally used.

Almost all the control schemes performed according to expectation, i.e., each of them is doing what it was designed for. The only exception is IRPC. IRPC, however, in combination with FCC still gives good results. The IRPC seems to do only partly what is was intended for, whereas FCC apparently is still able to keep the frequency within boundaries. A stable grid might be the consequence, with a much faster changing frequency than was the case in the past.

The ultimate conclusion is that the collection of IRPC, FCC, BRC, BSC, PVC and PPVC within the WoC concept apparently strikes the balance of doing locally what can be done locally and do more globally which needs a more global approach. The practical consequence is that the WoC concept supports the future scenario of renewable local supply for local demand.

Terminologies

Table 1: Key definitions in the ELECTRA IRP

Term	Definition
Control Triple	A set consisting of {Control Aim, Observable, System Input Signal}, which is the basis of a control loop.
Control Aim	A concise statement describing the control purpose of a control loop.
Observable	A uniquely valued function of a number of measurable quantities in a physical system. An observable can either be a scalar or vector (“State Vector”) that is calculated from measured (observed) values in the present or past.
Transition Time	Time for system response or system control loops to complete the transition from a stationary system state to the next stationary state, after a switching event occurs within a power system.
Control Time Scale	A characteristic Transition Time at which a control loop operates. In this document the following Control Time Scales (CTS) are used: • CTS_0: System response • CTS_1: Primary Level • CTS_2: Secondary Level • CTS_3: Tertiary Level
System Input Signal	A (scalar or vector) signal that is input to the power system, in order to change the value of an observable.
Observable algorithm	A detailed description of (or reference to) a specific set of operations that convert measurable values into an observable.
Control Topology Level	A characteristic Topology Level at which a control loop operates. Here the following Control Topology Levels (CTLs) are used: • CTL_0: Physical (single) Device Level • CTL_1: Flexible (aggregate) Resource Level • CTL_2: Cell level • CTL_3: Inter-cell level (For more detailed definition of the Control Topology Levels see the chapter 21.5. "Working procedure for selecting control functions for Use Cases")
Balance Control	Control loops that control the cell balance which is defined as the aggregated power flow profiles over the tie-lines (i.e> import/export profiles).

Term	Definition
Voltage Control	Voltage control: control loops that ensure that voltage at each node keeps within operational limits, in a stable, secure and reliable way. Voltage control includes the needed control of power flow in all cables and lines in the network, with methods depending on the used power system technologies (AC, DC).
N.B: The definitions of "Balance Control" & "Voltage Control" comprise a generic physical description of the control challenge, which is both technology independent and voltage level independent. So these generic definitions can be applied to all power system technologies. such as AC, DC, and to all voltage levels HV, MV, LV, et cetera.	
Cell	An ELECTRA Cell is a portion of the power grid able to maintain an agreed power exchange at its boundaries by using the internal flexibility of any type available from flexible generators/loads and/or storage systems. The total amount of internal flexibility in each cell shall be at least enough to compensate the cell generation and load uncertainties in normal operation.

Abbreviations

Abbreviation	Meaning
AC	Alternating Current
AD	Analogue to Digital
ALF	Accuracy Limit Factor
BRC	Balance Restoration Control
BRP	Balance Responsible Party
BSC	Balance Steering Control
CPFC	Cell Power Frequency Characteristic
CT	Current Transformers
CTL	Control Topology Level
CTS	Control Time Scale
CVD	Capacitive Voltage Divider
CVT	Capacitor Voltage Transformers
DAE	Differential Algebraic Equations
DAQ	Data Acquisition
DC	Direct Current
DER	Distributed Energy Resources
DFT	Discrete Fourier Transform
DOW	Description Of Work
DSO	Distribution System Operator
DSOGI	Dual Second-Order Generalised Integrator
EMU	Electromagnetic Unit
ENOB	Effective Number Of Bits
ESS	Energy Storage System
EU	European Union
EV	Electric Vehicle
FCC	Frequency Containment Control
FIR	Finite Impulse Response
FLL	Frequency Locked Loop
FS	Security Factor
GOOSE	Generic Object Oriented Substation
GPS	Global Positioning System
H	Inertia Constant

HV	High Voltage
HVDC	High Voltage Direct Current
ICT	Information and Communication Technology
IEC	International Electrotechnical Committee
IED	Intelligent Electronic Device
IFSC	Institute Of Santa Catarina
IRP	Integrated Research Program
IRPC	Inertia Response Power Control
J	Moment of inertia
LED	Light-emitting diode
LSB	Least Significant Bit
LV	Low Voltage
MV	Medium Voltage
NH	Noord Holland
NPFC	Network Power Frequency Characteristic
ODE	Ordinary Differential Equations
OLTC	On-Load Tap Changer
PCC	Point of Common Coupling
PI	Proportional-Integral
PLC	Power Line Carrier
PLL	Phase Locked Loop
PMU	Phasor Measurement Unit
PPVC	Post-Primary Voltage Control
PV	Photo Voltaic
PVC	Primary Voltage Control
PWM	Pulse-width modulation
RES	Renewable Energy Sources
RMS	Root-Mean-Square
ROCOF	Rate-Of-Change-Of-Frequency
SCADA	Supervisory Control And Data Acquisition
SE	State Estimator
SF	Safety Factor
SG	Synchronous Generator
SNR	Signal-to-Noise Ratio
SOC	State Of Charge (Of Energy Storage System)

SRPS	Single Reference Power System
SVC	Static Var Compensator
TSO	Transmission System Operator
UC	Use Case
VCD	Voltage Capacitive Dividers
VSC	Voltage Source Converter
VT	Voltage Transformer
WG	Wind Generation
WoC	Web-of-Cells
WP	Workpackage
WT	Wind Turbine

Table of contents

List of figures and tables

1 Introduction

1.1 Project context

The present document includes the simulation-based validation of the six selected ELECTRA Web-of-Cells power system control schemes represented individual use cases.

The ELECTRA Web-of-Cells concept is a proposed control scheme for the real-time frequency/balance and voltage control of the future grid. The six use cases were derived in a structured top-down manner in from the six high-level functionalities [1, 2], which are namely:

- Inertia control: Inertia Response Power Control (IRPC)
- Frequency control: Adaptive Frequency Containment Control (FCC)
- Balance control:
  - Balance Restoration Control (BRC)
  - Balance Steering Control (BSC)
- Voltage control:
  - Primary Voltage Control (PVC)
  - Post-Primary Voltage Control (PPVC)

The detailed functional architecture of these 6 ELECTRA Web-of-Cells control scheme Use Cases with “Black-Box” and “Grey-box” descriptions of the functions involved is covered by [2]. The “White-box-descriptions” of these functions are presented in [3]. In present document these functions are validated by simulations.

1.2 General description of the simulated control schemes

The tests are done by simulations in the context of each of the six Use Cases. The basic structure of the control scheme for each Use Case is presented in Figure 1.

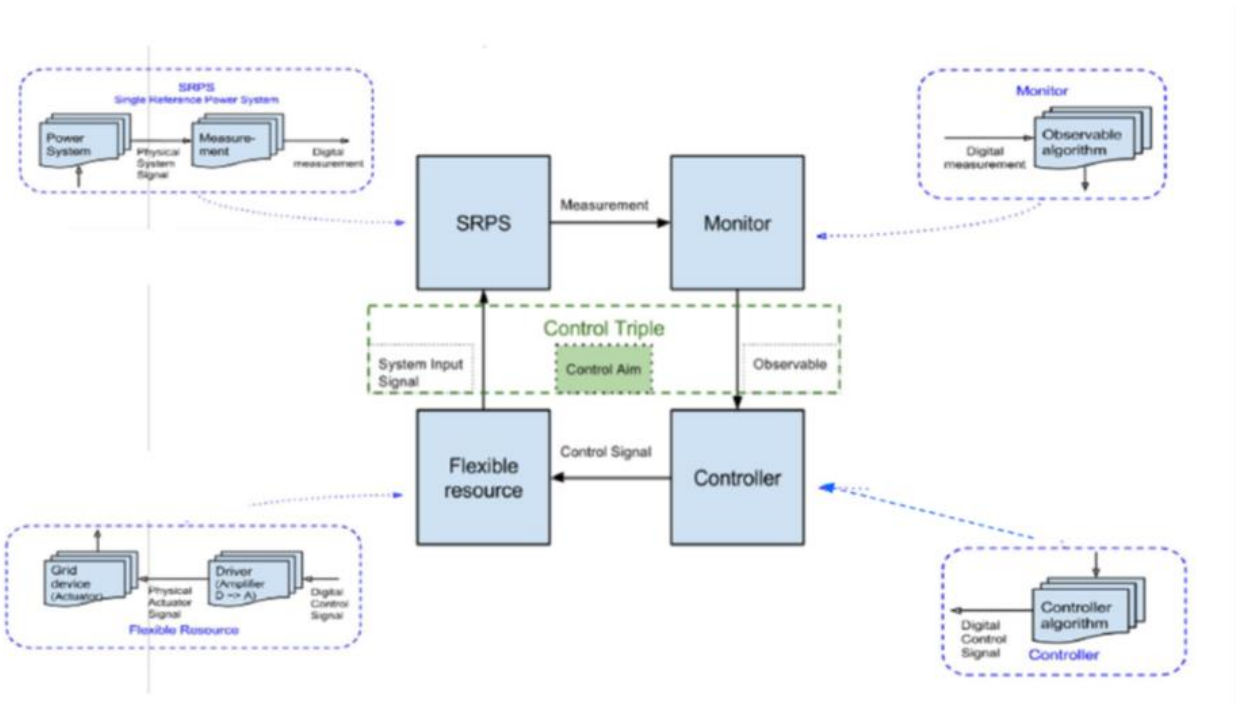

Figure 1: The control triple structure [4]

Each control scheme has the same structure as depicted in Figure 1. It consists of the blocks “Monitor” and “Controller”. The device that converts the control signal (for instance a setpoint for real power) into physical quantities (in this case physical currents or physical real power) also belongs to the control scheme. These devices are indicated by the block “Flexible resource”. The blocks SRPS (i.e. Single Reference Power System) represents the grid where the control scheme is active.

Behind the blocks “Monitor” and “Controller” are the algorithms of the specific control scheme representing the six use cases. Behind the block “Flexible resource” is the model of a physical device (as for instance a PV installation) or a cluster of such devices. In the latter case the resource correspond to an aggregation of a number of physical devices. Behind the block “SRPS” is the selected grid model.

The Observable Algorithm is the detailed description of (or reference to) a specific set of operations that convert measurable values into an observable. In Figure 1 it corresponds to the upper right blue square “Monitor” that contains the Observable Algorithms.

The Controller Algorithm transforms the Observable into a control signal. See the lower right blue square “Controller” in Figure 1.

For each control scheme the observable algorithms and controller algorithms are the starting point (they come from previous work in the project). For the purpose of the present document a test-grid is chosen (Single Reference Power System - SRPS) and a scenario (a certain sequence of events in that grid) as well as a device or devices (flexible resource) that can perform the task of converting the control signal into a physical quantity the affects the operation of the grid.

1.3 Outline of the report

This deliverable contains simulation results for each of the Use Cases or cell-control schemes on the stage of the Web-of-Cells. The deliverable consist of the main document and six annexes. The detailed simulation reports are included in the annexes after present main document.

- Annex 1: Inertia Response Power Control (IRPC)
- Annex 2: Adaptive Frequency Containment Control (FCC)
- Annex 3: Balance Restoration Control (BRC)
- Annex 4: Balance Steering Control (BSC)
- Annex 5: Primary Voltage Control (PVC)
- Annex 6: Post-Primary Voltage Control (PPVC)

Each annex has its own topology and scenario. These are chosen on basis of the character of each Use Case. Topology and scenario vary widely from Use Case to Use Case, in particular due to the different time scales of the Use Cases. Each report contains the conclusions specific to its Use Case.

This document gives in chapter 1 the general description of the simulated control schemes and an outline of this deliverable. The chapter 2 gives the concise introduction into the main characteristics and findings of each of the simulation reports. This is for the purpose of making the reading of the report more easy and facilitating the reader in the process of making his or her own overall picture. This summarizing and condensed text however does not replace the detailed reports on the individual Use Cases.

The nature of the conclusions differs widely from Use Case to Use Case. Moreover, the stand-alone character of the simulations hardly allows for a general conclusion that is more than a compilation of the individual ones. Nevertheless, a short discussion presents an overall conclusion in the last chapter 3.

2. Synopsis of control scheme simulations

The following chapter summarizes the evaluation of the six control schemes. The structure for the text for each control scheme is the same and os organized as follows

First a brief characterization of the setup of the simulation is given (under the heading “Setup”): the simulated grid, the monitored quantity or observable, and the resources that are used to control the observable. In order to disturb the steady state value of the observable a certain event or series of events have to take place. These events that trigger the dynamic response are given next, under the heading “Characterization of scenario”. The main findings of the simulations are presented, illustrated by some illustrative results in the sections “Main findings” and “Illustrative results” respectively. The section closes with general conclusions and conclusion specific for the Web-of-Cells concept respectively in “Conclusions in general” and “Conclusions for WoC concept”.

2.1 Inertia Response Power Control - IRPC

2.1.1 Setup

SRPS	Pan European network
Monitor	Frequency and Rate of Change of Frequency (RoCoF)
Flexible resource	Aggregated unidirectional charging of electric vehicles

2.1.2. Characterization of scenario

In this study, two different techniques have been implemented and investigated to enhance the frequency dynamics after a power imbalance. Both IRPC and FCC have been implemented and analyzed using the power system simulation software PowerFactory. The controllers employ the EVs as flexibility resources. The EVs are not equipped with vehicle to grid (V2G) capability. In fact, the controllers can only modulate the charging current between 6 and 16 A as imposed by the standards. The pan-European power system has been used for this study.

The total number of unidirectional charge EVs is equal to 50000 (126 MW at 11A per phase). It allows a total EVs flexibility of ±57.5 MW. In the three scenarios the system response is triggered by the loss of one of the slack machines (P_{loss}=136MW versus P_{load}=2727 MW which represent 5%). For the two controllers (FCC and IRPC) the proportional gain (droop in this case) is chosen in a way to be the maximum allowed value at which the system will remain stable. This choice is done to highlight the relation between the gain and the time delay.

2.1.3 Main findings

Scenario 1:

The first scenario studies the effects of the different levels of wind penetrations. It highlights the impact of converter connected resources on frequency dynamics (i.e. rate of change of frequency-ROCOF, frequency nadir and steady state value). Three different cases are investigated with different levels of wind penetration compared to the load: 0%; 25% and 90%.

Scenario 2:

In the second scenario a sensitivity analyses of the time delay is carried out. This scenario aims at highlighting the time delay importance and impact on IRPC as well as on FCC in case of different levels of double fed induction machine (DFIG) penetration. The considered time delays are pure

transport delays. The following time delay values have been considered 10ms, 50ms, 100ms and 250ms.

The controllers' gains are chosen as the maximum allowed value at which the system will remain stable. This choice is done to highlight the relation between the gain and the time delay. The gain of IRPC is smaller since it needs to limit the negative effect caused by the transport delay. The sensitivity analysis is investigated for the different levels of wind penetration (0%, 25% and 90%).

Scenario 3:

In the third scenario a performance analysis of FCC and IRPC is presented. This scenario aims at comparing the two controllers' impacts on the system frequency after the loss of a conventional generation unit corresponding to 5% of the total load. A time delay of 100 ms has been considered and only the 90% wind penetration case is considered.

2.1.4. Illustrative results

Figure 2 below illustrates the effect of applying only FCC (black line), applying only IRPC (blue line) when compared of having no cell controller active at all (red line) when the wind penetration is 90 % and time delay 100 ms.

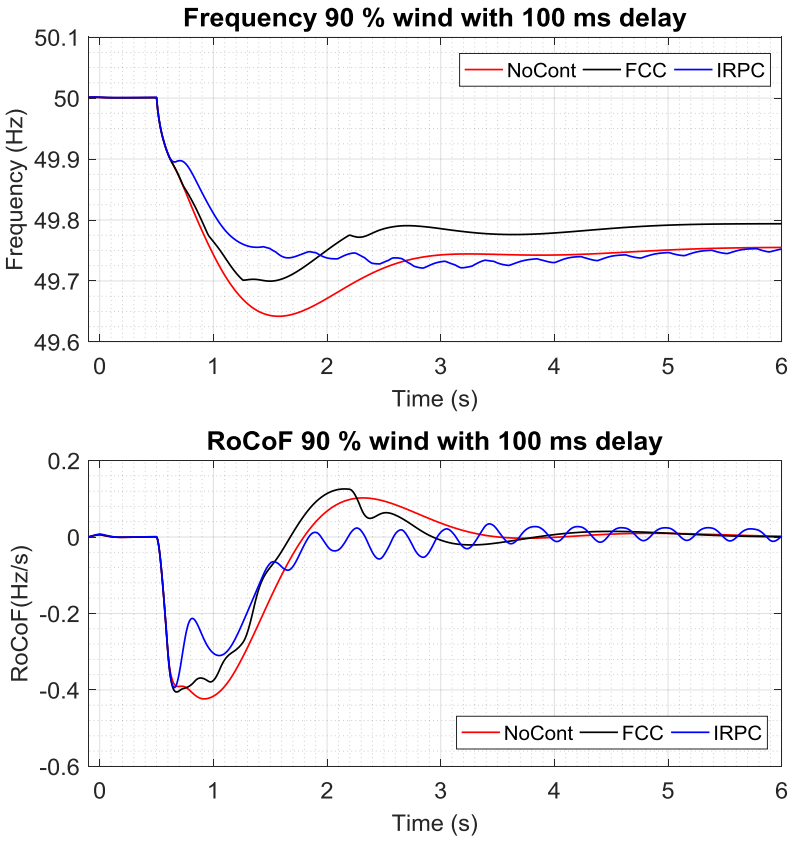

Figure 2: Simulation results when applying only frequency containment control (black line) or applying only inertia response power control (blue line) or having no cell controller (NoCont, red line) active at all

Notice that FCC and IRPC both improve the frequency behaviour. IRPC does even slightly better than FCC, but this comes at the cost of additional ringing.

2.1.5. Conclusions in general

Scenario 1:

One can notice that the case of 25% wind does not have an impact on the frequency and that´s due to the fact that all the synchronous machines were still connected. The 90% case instead presents worsen nadir, rate of change and steady frequency.

Scenario 2:

In case of no wind, the 100ms and 250ms delay creates frequency oscillations in case of IRPC. To be mentioned, this oscillation could have been limited by employing a lower gain, on the other hand, that would have led to very limited contribution or even no contribution at all.

The case with 25% wind penetration, compared to the 0% case, results to be more stable. In fact that´s due to the fact that all the synchronous machines are still connected as in the previous case plus the DFIG, which do have a certain damping effect. However, in terms of RoCoF, the 250ms has a worse behaviour compared to the no controlled case. Of course this behaviour can be limited by retuning the controller, since the larger time delay has a negative effect, but on the other hand that means reducing the controller gain and therefore reducing its effects.

Compared to the previous cases, the negative effect of the time delay is much higher due to the lower damping effect present in the grid in 90% case. In the IRPC case, the ROCOF is limited to lower values compared to the FCC case. The frequency nadir is slightly better also in the case of IRPC. These results are very much influenced by the penetration of DFIG, which deliver a certain damping effect. The results would have been more oscillating in case of fully converter wind turbines or PV generations. Larger delays in the IRPC case become critical in term of system stability.

Scenario 3:

The IRPC is limiting the ROCOF and even the frequency nadir to better values compared to the FCC. However, one can notice that IRPC imposes frequency oscillation on the system which can be reduced using a lower gain or/and a low-pass filter. On the other hand, the FCC has a better performance in terms of frequency steady state value. A steeper droop in case of FCC can be used which will improve the frequency nadir values.

2.1.6. Conclusion for WoC concept

It was shown that the implementation of IRPC or FCC employing single phase electric vehicles can enhance the frequency behaviour of the power system:

1. IRPC limits the ROCOF more than the FCC and due to the steeper droop it limits more the frequency nadir imposing also frequency oscillations.
2. The FCC has a better performance on the frequency steady state value as expected.

However, one of the main challenges is that many of the rotating synchronous machines, wind turbines and load shedding devices are connected to the grid by means of ROCOF relays. Therefore, likely a combination between IRPC and FCC needs to be present.

2.2 Frequency Containment Control - FCC

2.2.1 Setup

SRPS	Modified Cigré MV grid
Monitor	Frequency, cell power import/export
Flexible resource	Resources connected to the grid

2.2.2 Characterization of scenario

The Frequency Containment Control (FCC) has been tested on the European CIGRÉ MV grid modified with distributed energy resources (DER) in two separated simulation scenarios and with different assumptions.

- In the first group of simulation the Adaptive-FCC control function was implemented using fuzzy logic. Also, in this first scenario the reference grid topology was properly modified.
- In the second group of tests, the main scenario assumption is the following: as soon as an imbalance is detected, a step load disturbance in this case, the second version of the FCC control function uses resources from all cells to immediately mitigate the problem. After having the frequency stabilized, the contribution from healthy cells ceases and only resources from the faulty cell are used to contain the frequency deviation.

2.2.3 Main findings

In both cases the tested UC proved to be effective. More in detail:

- In the first implementation, it is shown that A-FCC can effectively detect the imbalance location and, as a result, curtail the activation of the FCC reserves if the imbalance took place outside its cell. The controller proved to be effective both under normal operation with all cells not in balance due to the uncertainty of forecasts, and in case of a step load disturbance.

- In the second implementation, the UCs proved to be effective as it was capable of stabilizing frequency by only using the cell's own resources.

2.2.4 Illustrative results

The figures below illustrate that indeed only or mainly the affected cell is taking care of the FCC action. In the reference case without any cell controller active (blue line) all the cells are responding to an event in cell 3. In presence of FCC controllers in each cell (red line) practically only the affected cell is taking an action, see figure 3.

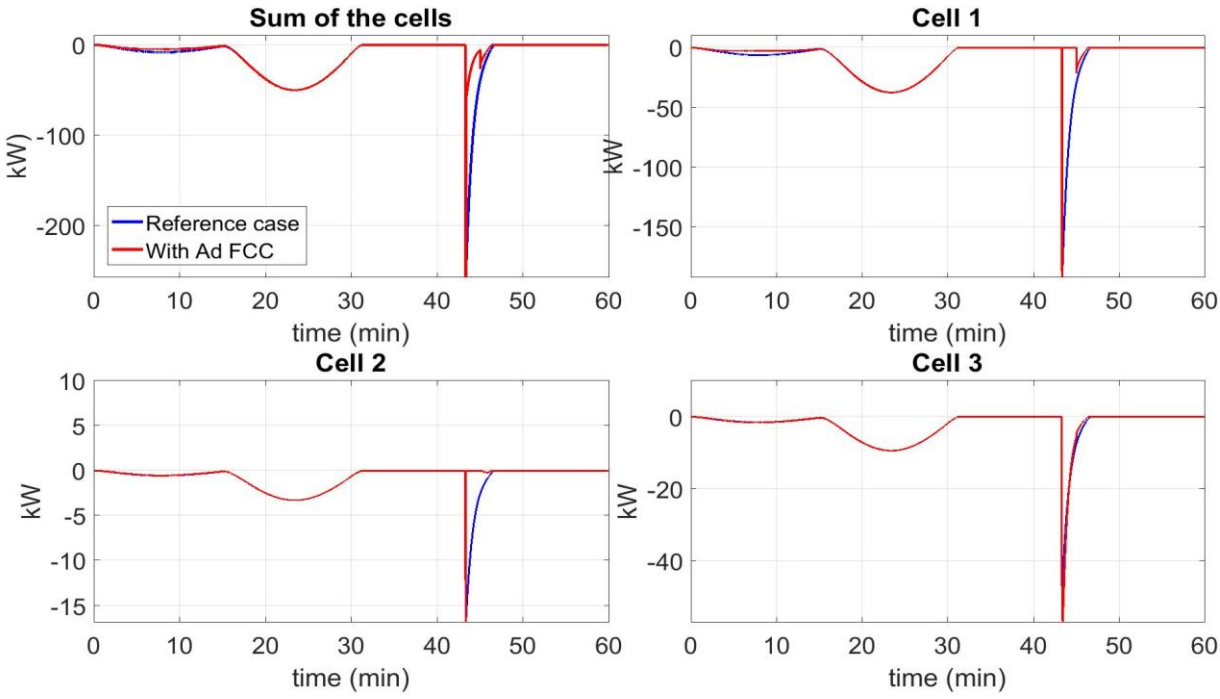

Figure 3: Variation of the power generated by photovoltaics and wind generations due to adaptive frequency containment control

2.2.5 Conclusions in general

The implementation of the adaptive logic proved to be effective when used as a standalone function (without any restoration actions by BRC) or even combined with a simplified BRC version. Overall, the use of both fuzzy and binary logics in each of the two implementations seems to be an effective solution in order not only to modify the activation of the FCC reserves, but also to provide the correct location information with regard to the imbalance. In all test cases, the system stability was not jeopardised by the deactivation of FCC reserves in neighbouring cells. In overall, with the proper design approach, especially in the case of fuzzy logic, it is possible to obtain the exact same result in terms of stability and, at the same time, confine the activations of FCC reserves only to the vicinity of the imbalance.

2.2.6 Conclusion for WoC concept

One of the most important benefits of using A-FCC control in a WoC is the fact that it prioritises the FCC reserves' activation in the cell of imbalance. This aspect is fully in line with the WoC operating premise, which dictates that imbalance problems should be solved locally, and the propagation of imbalances to other cells should be avoided. This way, the same amount of reserves can be more efficiently used, since the FCC power is consumed locally to the area of imbalance and no extreme amounts of power are necessary to be transmitted from distant cells. By doing so, the controller avoids potential voltage or capacity limits' problems across the grid lines. The reduced activation of FCC reserves in neighbouring cells makes the latter available to be used for other services (e.g. IRPC or BRC). In other words, when multiple controllers use a resource at the same time A-FCC reduces the risk of control conflicts. Last but not least, when it comes to RES (renewable energy resources) providing FCC control, the use of A-FCC is beneficial because it reduces the curtailment of power provided by RES, which is the curtailment of useful green energy, in the neighbouring cells. Thus, PV plants or wind farms that would curtail their power in case of over-frequency, maintain an output power level above the power obtained by fixed droop.

2.3 Balance Restoration Control - BRC

2.3.1 Setup

SRPS	Pan-European network
Monitor	Frequency, Power Imbalance
Flexible resource	Aggregated controllable loads and RES

2.3.2 Characterization of scenario

In order to test the functionality of the BRC controller, three cells were separately equipped with the BRC controller. The frequency response and other control signals were monitored for active power imbalances within each of the three cells in question. The imbalance event in each scenario is a load step of +150 MW, causing an instantaneous active power deficit in the cell.

For providing the fast-acting active power reserve required for the BRC control, an AC source was added to each of the three cells, to which an active power demand signal was sent from the controller. This is comparable to the way that the Automatic Generation Control (AGC) component of the controller provides active power setpoints to the synchronous generators. The AC source emulates the behaviour of aggregated renewable generation, batteries or demand response at the speed set by the fast-acting control loop of the BRC algorithm.

Two dispatch scenarios were used in the testing, to demonstrate the functionality of the controller with both a lower (25%) and higher (50%) Renewable Energy Sources (RES) penetration. Furthermore, a reduced proportion of synchronous generation is assumed for the 50% RES scenario. These scenarios have been split up into three further sub-scenarios where the load step has been applied in each of the three cells in turn.

For each sub-scenario, tests were run in which the fast-acting response was deactivated or activated. This allowed a comparison between the traditional (slow) control of reserves and the improved frequency control, which includes fast-acting reserves and location awareness.

2.3.3 Main findings

With the use of BRC the time to recover the frequency after an imbalance is highly reduced if enough fast-acting resources are available in the system. The ability of the BRC controller to successfully identify the circumstances under which the fast-acting reserves should be activated or remain inactive is also shown. The activation or deactivation depends on whether the event is within the cell or external to it. It proves one of the main characteristics of the Web of Cells, which is to solve local problems locally. The controller has exhibited full functionality under a number of scenarios with different amounts of DER penetration within the system, showing its resilience under more dynamic power system scenarios.

2.3.4 Illustrative results

The figure 4 below illustrates that adding a BRC cell controller indeed improves frequency behaviour (green line) greatly over the case where only classic AGC is active (red line)

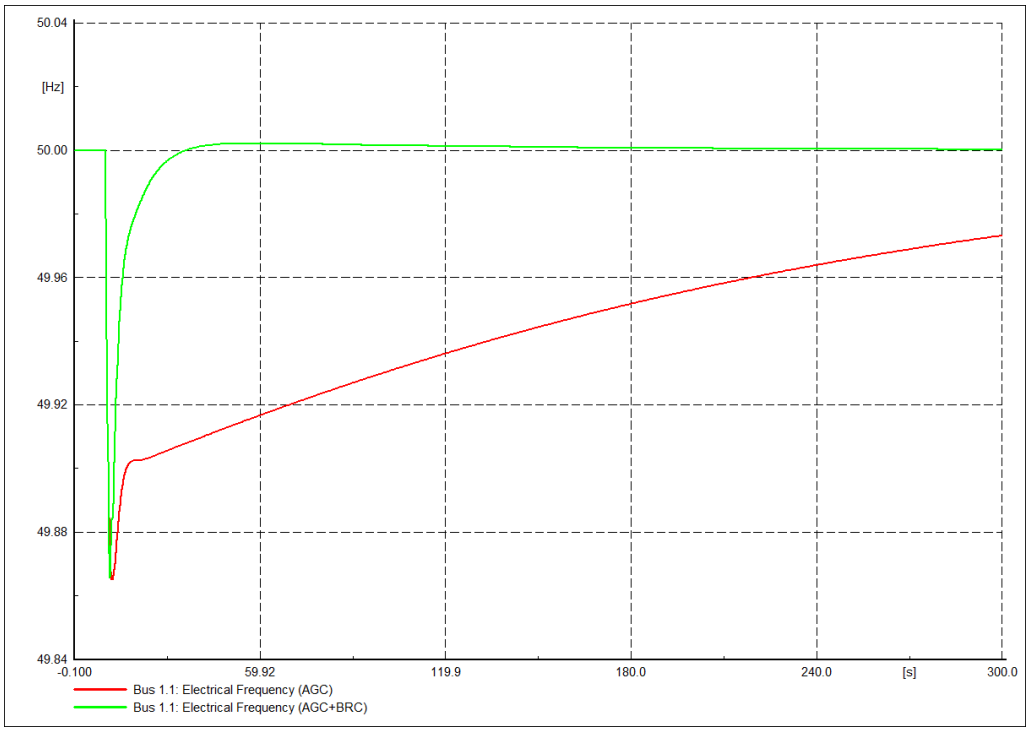

Figure 4: Frequency response of automatic generation control and automatic generation control + balance restoration control with imbalance in Cell 1

Moreover, BRC is obviously able to restrict power response to the cell where the imbalance occurs (i.e. cell 1) as is clear from the next figure 5.

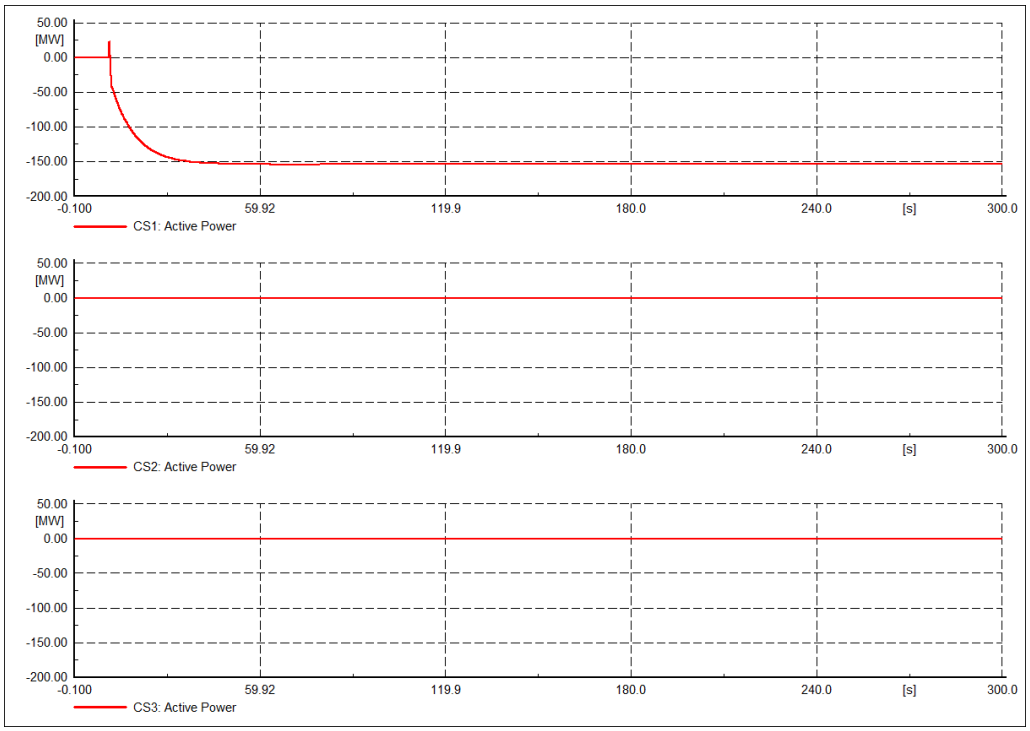

Figure 5: Active power of current source in each cell, with imbalance event located in Cell 1

2.3.5 Conclusions in general

The BRC controller successfully achieves improved frequency restoration under a range of test scenarios and imbalance events in the test system. By splitting the reserve control signal between slow-acting AGC control and fast-acting BRC control, and actuating an AC source to emulate fast

reserves, the improvement in the speed of frequency recovery is notable. The BRC controller's ability to successfully identify the circumstances under which the fast-acting reserves should be activated or remain inactive has been shown.

2.3.6 Conclusion for WoC concept

The simulation of BRC demonstrates an improved frequency response by localizing the response of the fast-acting assets and by activating the resources unilaterally only within the cell where the disturbance has occurred. The utilization of the cell imbalance for activation of fast acting devices eliminates any potential deterioration in performance of the control due to miscalculation of bias factor. This restoration controller will not only restore the frequency but also help to arrest the frequency nadir for a more resilient future low inertia networks. These characteristics are compelling reasons in support of the Web-of-Cells "solve local problems locally" concept developed within the ELECTRA project.

2.4Balance Steering Control - BSC

2.4.1 Setup

SRPS	CIGRE MV reference grid
Monitor	Frequency, Net tie-line power deviation, Imbalance Correction output, Cell Setpoint Adjusting output
Flexible resource	Photovoltaics, Wind Generator (WG), CHPs, Fuel Cells and Battery storage units

2.4.2 Characterization of scenario

The main functionality investigated in these simulation tests was the deactivation of BRC resources (corrective BSC) after imbalances that take place in different, adjacent cells of the system. The goal of these tests is to show that the involved control functions, namely CellSetpointAdjusting and TieLineLimits, are able to effectively cope with the imbalances happening in the system and change the setpoints of the tie-lines in order to reduce the amount of the activated BRC reserves, without compromising the stability and the balance of the cell. Among different tests carried out for the validation, the most important one is the response of the controllers to equal and unequal power imbalances in two adjacent cells. In these scenarios, two adjacent cells undergo equal or unequal imbalances of the opposite sign and the system's response is examined in terms of negotiation, deactivation of reserves and frequency stability. In addition, the case of violation of one selected tie-line's capacity is also investigated. The scope of this test is the investigation of the negotiation result and whether this would lead to a tie-line capacity violation or not. Finally, in an additional test the response of the system is examined when the setpoint of the tie-lines is adjusted with some delay between two cells. Evidently, despite the fact that these tests refer to a standalone investigation of the UC, it was necessary to assume the presence of at least rudimentary version of BRC and FCC in the system because BSC is a UC that can only be used in combination with the other two. In implementation terms, the selected power system was the CIGRE MV reference grid in which assumes the existence of 3 MV and 1 HV cells. In the MV part of the grid, the units that provide FCC flexibility are eight PVs, one WG, two fuel cells, two CHPs and three battery storage units.

2.4.3 Main findings

The results of the four selected tests show that the BSC control functions effectively detect the imbalances and adjust the tie-lines always towards the correct values. In some time point a tie-line may be saturated, which means that the tie-line is in its maximum allowable capacity already before the incident occurs. Even when one of the tie-lines is saturated, the controllers are able to identify the situation and avoid modifying the setpoint of the specific, saturated tie-line. The controller divides the adjustment to the non-saturated tie-lines of the cell.

In terms of BRC deactivation, by monitoring the Imbalance Correction outputs, it is evident that the whole procedure manages either completely or partially to deactivate the reserves. This works always in accordance with the implemented imbalance. On top of that, the whole process does not deteriorate the stability of the system in terms of frequency. And even when the new setpoint is asynchronously implemented to the two cells, it is possible for the BRC controllers to successfully maintain the frequency stability and, at the same time, deactivate the used BRC reserves.

2.4.4 Illustrative results

The figures 6 and 7 below illustrate that the BSC cell controller keeps frequency behaviour very stable when freeing again the reserves within the cells (small disturbance of upper trace at t=560s). The lower figure shows the deactivation of resources in cell 1 and 2 (blue and red line respectively)

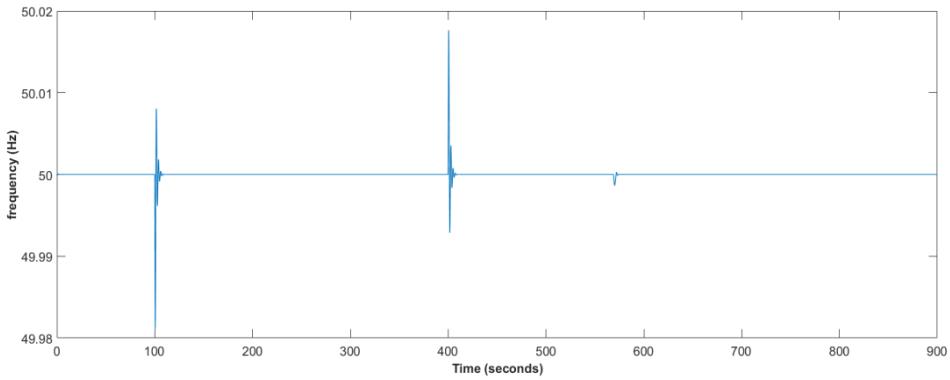

Figure 6: Frequency response of balance steering control

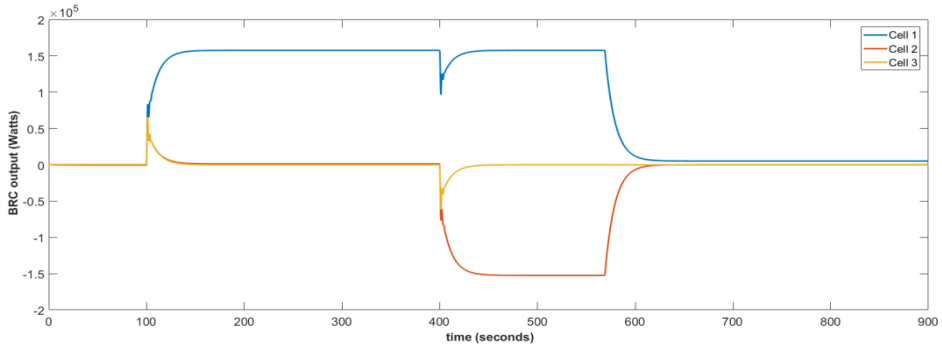

Figure 7: Balance restoration control output due to imbalances and deactivation of resources

2.4.5 Conclusions in general

Overall, the specific tests show that the implementation of the BSC logic is effective and the negotiation process leads to significant benefit from the imbalance netting of cells leading to a deactivation of the BRC reserves. The selected tests were implemented combined with some simplified versions of the BRC and FCC controllers. Therefore, one open issue for further investigation in course of the project is the performance of the controller in conjunction with the

actual ELECTRA BRC and FCC controllers. Specifically, these controllers are expected to introduce a degree of uncertainty in the system's response therefore, the analysis of the combination of the FCC+BRC+BSC UCs in course of the lab-validation (ELECTRA WP7) is of great importance. However, as a standalone implementation the results of these tests are very satisfactory.

2.4.6 Conclusion for WoC concept

In terms of the WoC proof-of-concept, the implementation and testing of BSC shows that, the assumption of potential imbalance netting exploitation as a means to save BRC reserves is a meaningful idea and can significantly improve the system's performance. The whole concept behind this can facilitate the consumption of significant amounts of RES by loads in neighbouring cells, allowing also the operators to avoid the use of restoration reserves. Additionally, having these reserves available, the operators can easily and with a higher resilience cope with continual or frequent imbalances that could appear in future power systems with high RES penetration.

2.5Primary Voltage Control - PVC

2.5.1 Setup

SRPS	Single generator – infinite bus test system
Monitor	Bus voltage, generator current
Flexible resource	Any power resource with voltage control capability

2.5.2 Characterization of scenario

Primary Voltage Control Use Case testing was performed in a simple model consisting of a generator connected via a line to a stiff network. The model allowed easy changing of the impedance between the generator and the network, which was the focus of the exercise. The assumption to be confirmed is that for networks with different proportions of resistance and reactance as seen from the generator's terminals there is a different proportion of active and reactive power that controls voltage in optimal way. For example, in a resistive network it is the active power that influences voltage more than the reactive power. The new element introduced to voltage control with PVC is the grid impedance estimation function with the main task to estimate grid impedance amplitude and angle. By knowing the R/X ratio it is possible to calculate the P/Q proportion, which will influence voltage the most. This can be used in situations where quick voltage control is more important than delivering the scheduled amount of active power.

2.5.3 Main findings

Both R/X ratio and magnitude of the grid impedance affect voltage control process. It can be noticed that for the same controller settings, different X/R ratio will result in different reactive power needed to achieve required voltage level and, in particular, extremely low values of X/R ratio will require vast amounts of reactive power, which might cause a power converter to reach its limits. In such situations adding active power to the control process facilitates it in a high degree. Even a small fraction of active power stabilises voltage in low X/R ratio conditions.

2.5.4 Conclusions in general

In grids with low X/R ratio, i.e. medium and low voltage networks, active power is an effective way to control voltage. However, using solely active power for voltage control may be adverse for frequency or balance control and also it might be expensive from the resource owner perspective. Therefore, the optimum way to control voltage in these conditions is to use a mix of active and

reactive power. The proportions of P and Q can be selected in such a way that they correspond to the resistive and reactive parts of the grid impedance or only a part of active power range can be allocated for the purpose of voltage control, like it is done for frequency control.

2.5.5 Illustrative results

The figure 8 below illustrates that the PVC cell controller restores the voltage at the whole range of line-impedances (blue, red and yellow lines in the upper graph) at 1 p.u. after a major step in grid voltages (dashed line I upper graph). The required active and reactive power from the cell resources is presented in the lower two graphs. Colours indicate again line impedances (blue: high X/R, red: equal X and R, yellow: low X/R).

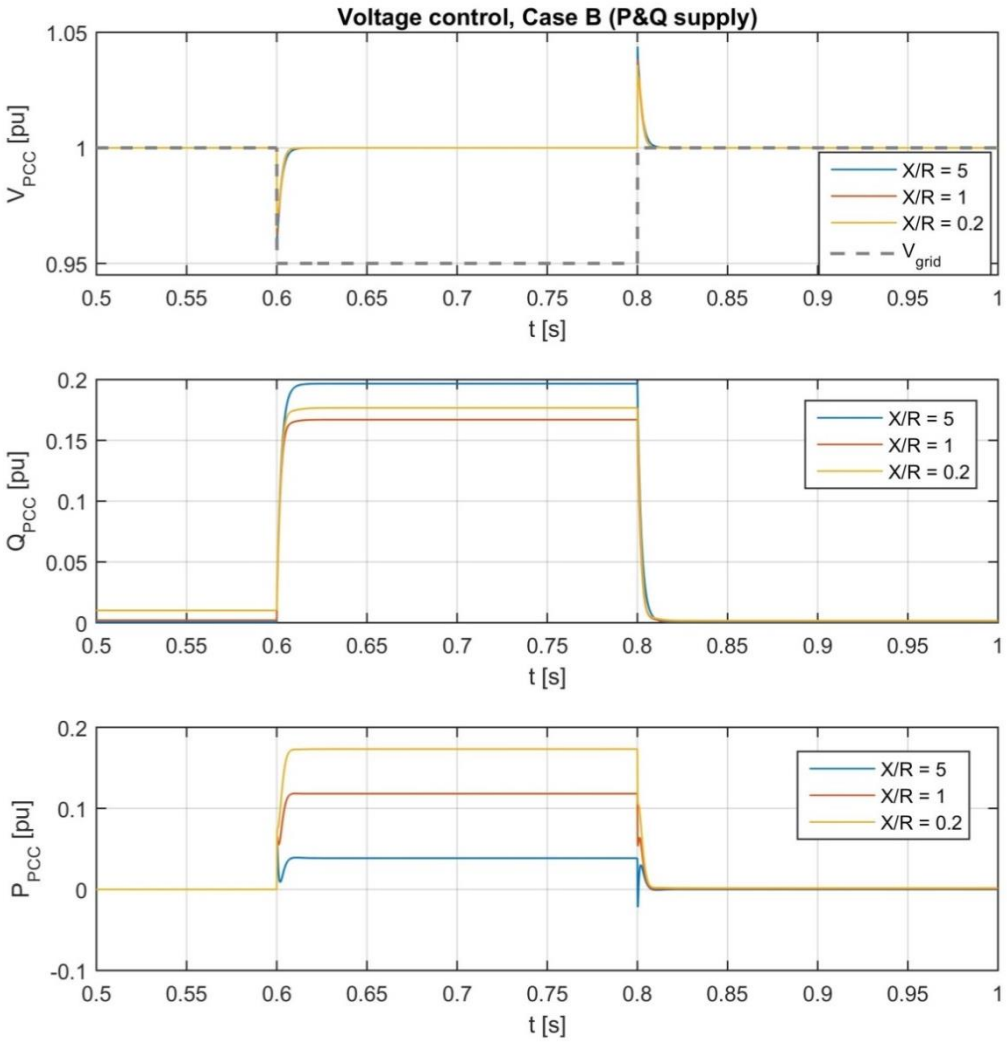

Figure 8: Local (cell) voltages, active and reactive power after steps in grid voltage

2.5.6 Conclusion for WoC concept

PVC as a fast-acting voltage control is indispensable in any power system, including the one based on the Web-of-Cell concept. A novel concept here consists in using also active power as a means for controlling voltage. It is intended to be used primarily whenever classic voltage control employing reactive power is not enough, i.e. in low X/R conditions, but can also help in case of disturbances or in the parts of the system where it is essential to stabilize voltage rather than control balance. For a decentralised power system with high degree of autonomy lying in cells, PVC, particularly operating in “combined mode”, in which P and Q take part, will help to stabilise voltage where no other control means are present.

2.6Post-Primary Voltage Control - PPVC

2.6.1 Setup

SRPS	European Cigré MV grid modified with DERs
Monitor	Voltage in the nodes
Flexible resource	PVC resources with AVR functionality and PPVC resources without AVR functionality such as transformers with on load tap changers, capacitor banks, shifting transformers or interruptible loads.

2.6.2 Characterization of scenario

The PPVC has been tested over the European CIGRÉ MV grid modified with distributed energy resources (DERs) to explore its possibilities as a feasible cell structure. It includes several types of distributed generation such as a wind turbine, PV panels, batteries or fuel cells. For any of the distributed energy resources and loads involved, generation and load profiles with a 1-min resolution (sampling ratio of the forecasts) and based on the rated powers have been created. This reference scenario has been used for the validation of the voltage control strategy under the two operation modes of the PPVC (proactive and corrective) taking into account the safe bands defined by the Regulations. Additional scenarios considering incremental load changes have been tested as well. In those scenarios, the voltage control capabilities have been assigned mainly to the transformers with on-load tap changers together with a limited reactive power control capacity coming from the PV panels.

2.6.3 Main findings

A clear reduction in active power losses is achieved for the proposed scenarios when the cell operator considers the optimal power flow algorithm in the planning phase. The calculated cutbacks are up to 5% in active power losses and up to 3% in reactive power losses. For the cell topology proposed (the CIGRE MV grid) the optimal voltage set-points can only be reached if the transformers at the header of the feeders are equipped with tap changers and they are the responsible of voltage control by properly changing their taps regardless the distributed resources. This is possible in a cell but not very realistic. It is convenient to take advantage in future power systems (2030+) of the high penetration ratio of distributed resources at MV/LV levels giving them authority to actively participate in the voltage control strategy. In this particular topology, the reactive power capabilities of the installed DER capacity is not enough to restore the voltage levels by themselves so the control of the tap changers is required in the most severe fault events.

2.6.4 Illustrative results

The figures below illustrate the improvement that van be achieved by applying PPVC. The first figure (reference case) shows the voltages without any PPVC action, the second one where a full-blown corrective PPVC is in place.

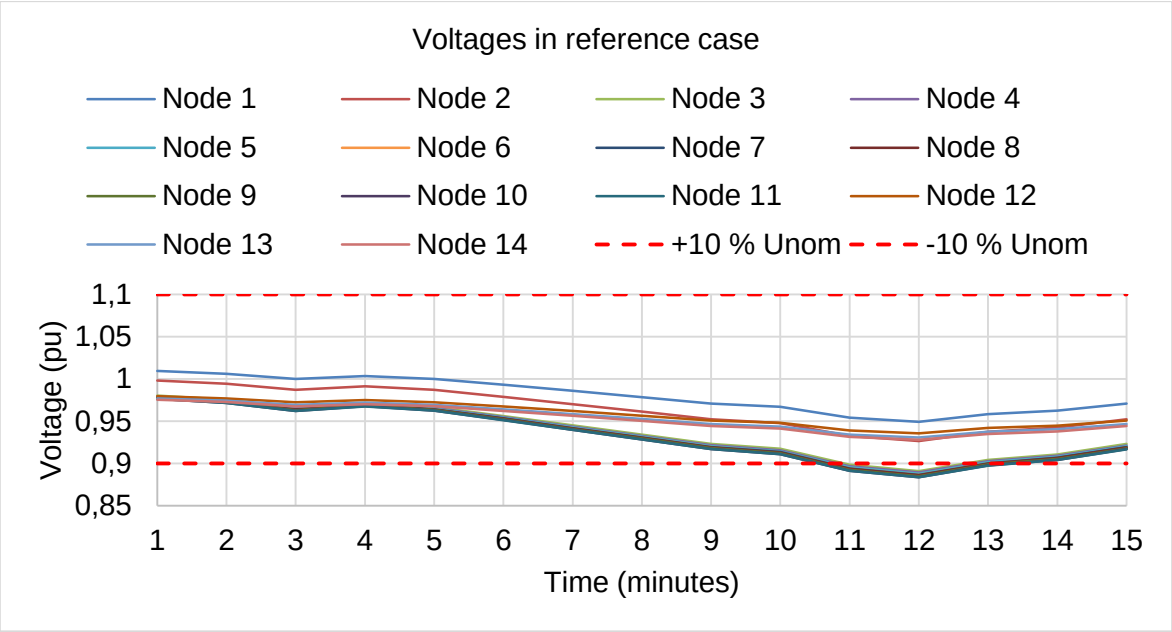

Figure 9: Voltage in reference case

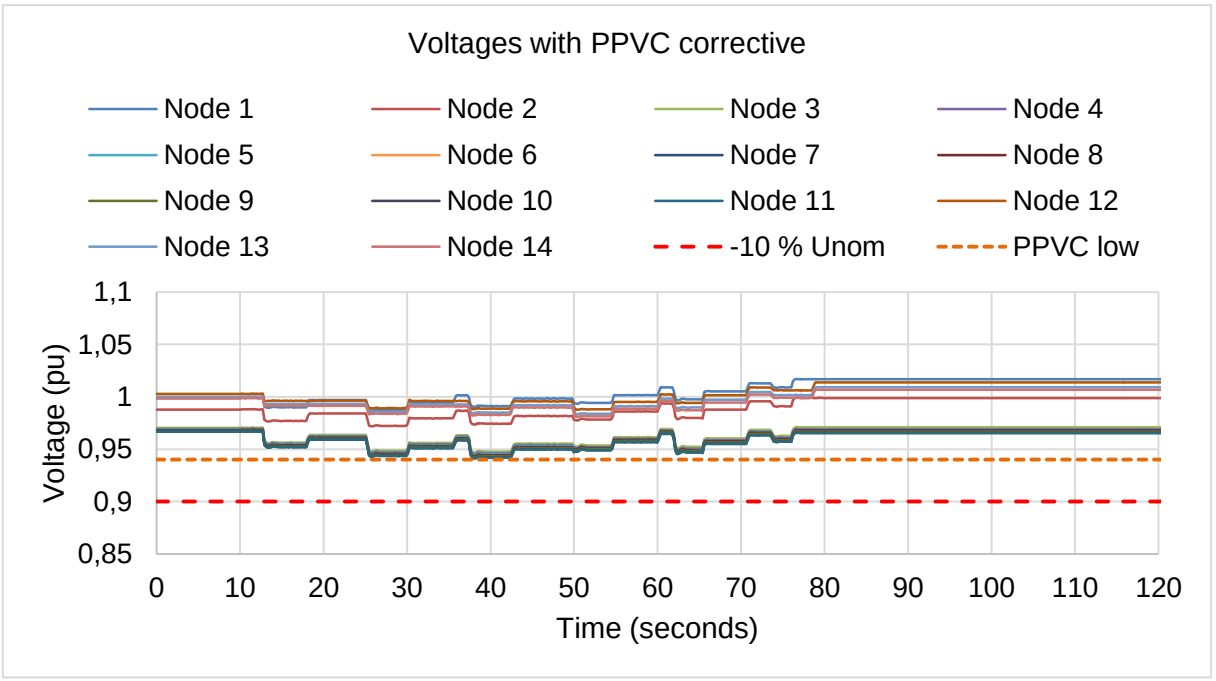

Figure 10: Post primary voltage control corrective simulation results

2.6.5 Conclusions in general

Results from the implementation of the scenarios have demonstrated the validity of the PPVC proactive mode in terms of active power losses reduction for the reference scenario. This is achieved by planning the power system operation based on optimal power flows instead of power flows, as it is done nowadays. Concerning the corrective mode, the capability to restore the voltage levels to the optimal set-points provided by the PPVC to the resources is only relying on having enough voltage control reserves within the cell. This is because the voltage control scheme is centralized at a cell level with no active contribution from neighbouring cells (even import/export reactive power flows are allowed based on tie-lines' reactive power limits).

2.6.6 Conclusion for WoC concept

The implementation of the PPVC that leads to a more efficient operation of the power system is possible due to the increase in observability and communication capabilities that are provided in the framework of the WoC. The advantages of the PPVC Proactive mode have been clearly addressed by a comparison of the active power losses in the WoC with regards to the current procedures in power systems. The Corrective mode is relying on the wide spread of the distributed energy resources expected in the WoC.

3. Discussion and outlook

The simulation results reported in this deliverable are a world première for the six control schemes featuring on the stage of the Web-of-Cells. The main conclusion is that the control schemes on their own are performing according to the expectations.

It turned out that in some cases the control schemes cannot perform in isolation, but need an affined control scheme as in the case of the BSC and the BRC. This is of course a natural dependency and indeed a sign that the concept as a whole is coherent.

Widespread fast responding distributed renewable resources is a feature of the future grid. IRPC, FCC and BRC exploit these resources. By giving higher responsiveness of units within the cells where the imbalances occur, the effectiveness of the WoC concept is illustrated: demand or supply changes are dealt with locally (on cell level) and so a propagation to the surrounding cells is kept to a minimum.

The BSC is more about interaction of cells. It turned out that BSC performs well in this interaction and effectively makes free BRC reserves on cell level. This makes the cells on their own again prepared for the next local imbalance and makes the cells as a web robust against disturbances in general.

For PVC the autonomy of the cell control scheme turned out to be beneficial for the voltage stability. Such an autonomy is an inherent feature of the WoC concept. The ability to control locally both P and Q stabilizes the voltage without the need of other controls or resources elsewhere.

The PPVC exploits two essential features of the WoC concept: first the higher observability and secondly the widespread presence of the distributed energy resources. The related flexibility option allows optimizing the voltages within each cell.

The interaction of the cells comes predominantly into play in the BSC case. Both voltage control schemes (PVC and PPVC) are by physical nature more local tasks. To have these control schemes active at cell level has turned out to be a good approach. BRC, FCC and IRPC are control schemes that act on the frequency and the balance, which is by its physical nature a more global task. However, the WoC concept transforms these tasks into more local ones, and keeps the effects of disturbances restricted to the cells where they occur or to their immediate neighbours.

The general conclusion of the investigation is that the six WoC Use Cases and related control function apparently strike the balance of doing locally what can be done locally and do more globally which need a more global approach. This is a feature of the WoC concept that is conducive, if not crucial for a renewable energy society. In such a renewable energy society the paradigm of centralized energy supply has been replaced by a new one: local supply for local demand. It is therefore paramount that local demand is indeed supplied by resources nearby or otherwise stated in the cell where the demand occurs or its immediate neighbours. The reports in this deliverable obviously show that this is feasible.

The validation has been done on basis of simulation of stand-alone Use Cases. This allows for a zooming in on the specific properties of each Use Case and allow for a meaningful discussion on improvement and interference with other Use Cases. It is beneficial to have evidence of the behaviour of each Use Case on its own.

There are however further steps to be taken before a full declaration of the qualities of the WoC concept can be given. But the first essential steps are taken in this document.

4. References

[1] ELECTRA deliverable D3.1 “Specification of Smart Grids high level functional architecture for frequency and voltage control”, 2015, Caerts, C., D’hulst, R., De Breucker, S., Rikos, E., Kolodziej, D., Merino, J., Rodríguez, E., Heussen, K., Kok, K., Geibel, D., Tornelli, C.,Temiz, A., 112 p.

[2] ELECTRA deliverable D4.2 “Description of the detailed Functional Architecture of the Frequency and Voltage control solution(functional and information layer)”, 2017, Caerts, C., Rikos, E., Syed, M., Guillo Sansano, E., Merino Fernandez, J., Rodriguez Seco, E., Evenblij, B., Rezkalla, M., Kosmecki, M., Temiz, A., Cabiati, M., Tornelli, C., Uslar, M., Heussen, K., Marinelli, M. 115 p.

[3] ELECTRA deliverable “Core functions of the Web-of-Cells control scheme”, 2018, Evenblij, B., Rikos, E., Heussen, K., Hu, J., Rezkalla, M., Marinelli, M., Löf, A., Pasonen, R., Hänninen, S., Merino, J., Rodríguez, E., Sansano, G., Mazher, S., Johnstone, K., Kosmecki, M., 50 p.

[4] ELECTRA deliverable “Functional specification of the control functions for the control of flexibility across the different control boundaries”, 2015, Visscher, K., Heussen, K., Hu, J., Hänninen, S., Rezkalla, M., D’hulst, R., Merino, J., Rodríguez, E., Rikos, E., Kosmecki, M.,. 85 p + Appendix 1, 46 p. and Appendix 2, 42 p.

[5] http://www.electrairp.eu (ELECTRA IRP web site)

5. Disclaimer

The ELECTRA project is co-funded by the European Commission under the 7th Framework Programme 2013.

ANNEX 1: Inertia Response Power Control (IPRC) and Frequency Containment Control (FCC)

1 Introduction

The increasing share of converter connected energy sources reduces the available rotational inertia in the power system leading to faster frequency dynamics, which may cause more critical frequency excursions. Both, IRPC and FCC could serve as a solution to improve frequency stability.

In this study, two different techniques have been implemented and investigated to enhance the frequency dynamics after a power imbalance. Both IRPC and FCC have been implemented and analyzed using the power system simulation software PowerFactory. Exemplarily, the controllers employ the EVs as flexibility resources since it is foreseen as widespread distributed energy resource. The most cost effective solution is taken in consideration and therefore the EVs are not equipped with vehicle to grid (V2G) capability. In fact, the controllers can only modulate the charging current between 6 and 16 A as imposed by the standards IEC 61851 [1].

The overarching research question addressed here is: Is synthetic inertia (IRPC) really needed or can or is the frequency containment control (FCC) delivered from fast resources, e.g. from batteries, EVs, sufficient?

2 Methodology

The pan-European power system has been used for this study as shown in Figure 4 [2], [3].

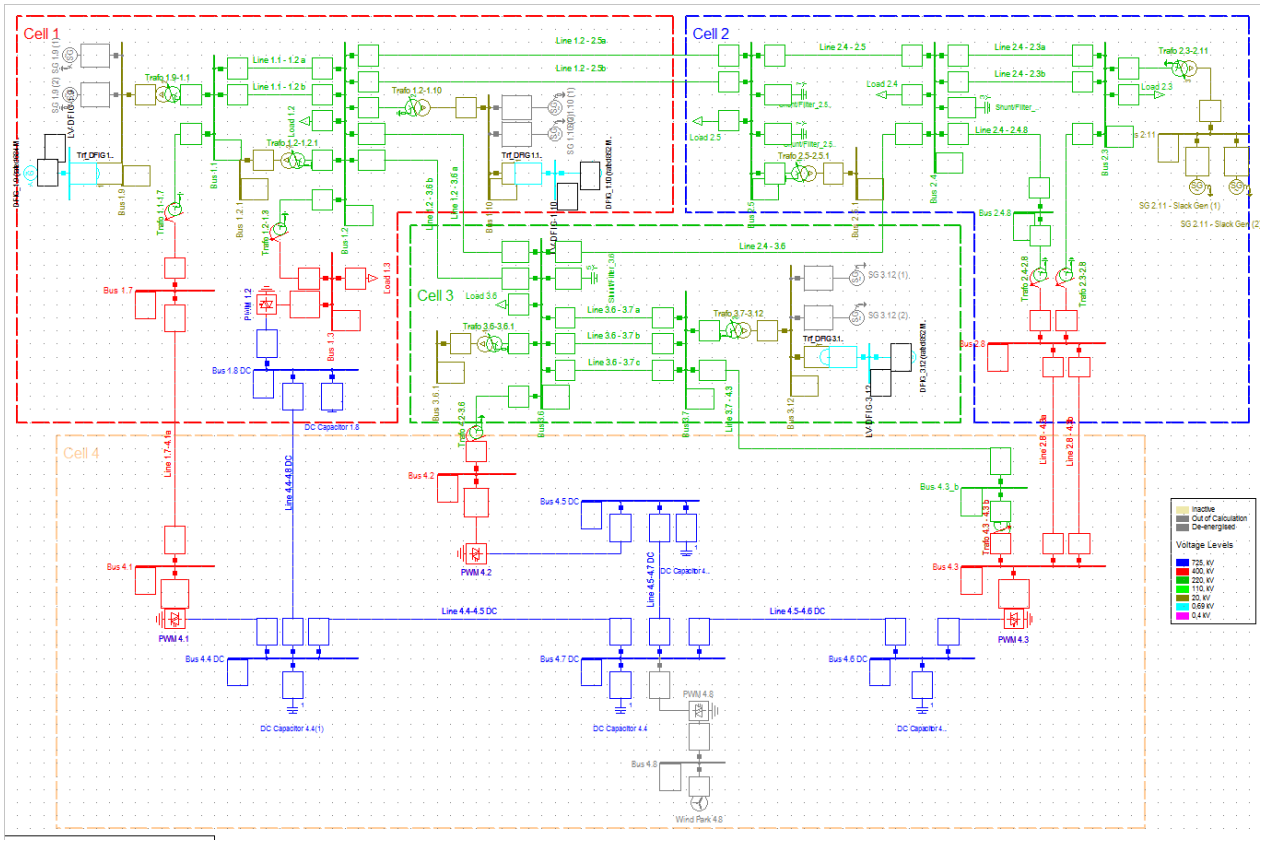

Figure 4: Pan European network

The total number of unidirectional charge EVs is equal to 50000 (126 MW at 11A per phase). This allows the total EVs flexibility to be equal to ±57.5 MW. In the three scenarios the system response is triggered by the loss of one of the slack machines (Ploss=136MW versus Pload=2727 MW which represents 5%). For the two controllers (FCC and IRPC) the droop-based proportional gain is chosen in a way to be the maximum allowed value at which the system will remain stable. This choice is done to stress the importance between the gain and the time delay.

The FCC and IRPC controllers are presented in Figure 5 and more detailed in [4] [5], [6].

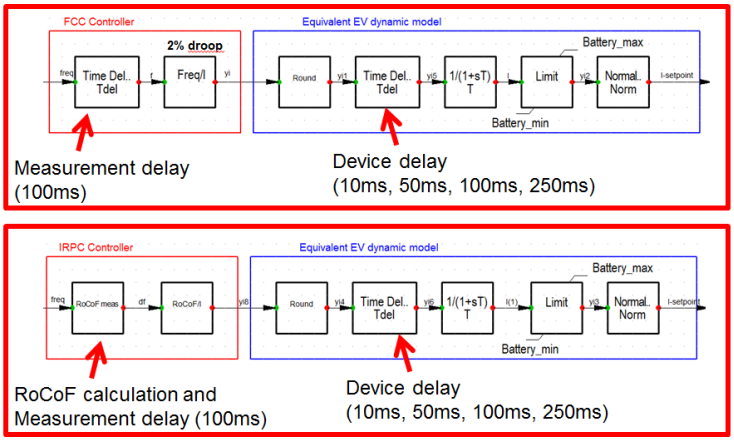

Figure 5: FCC and IRPC controllers

The 2% droop present in Figure 3 is used for FCC while the droop presented in Figure 4 is used for the IRPC.

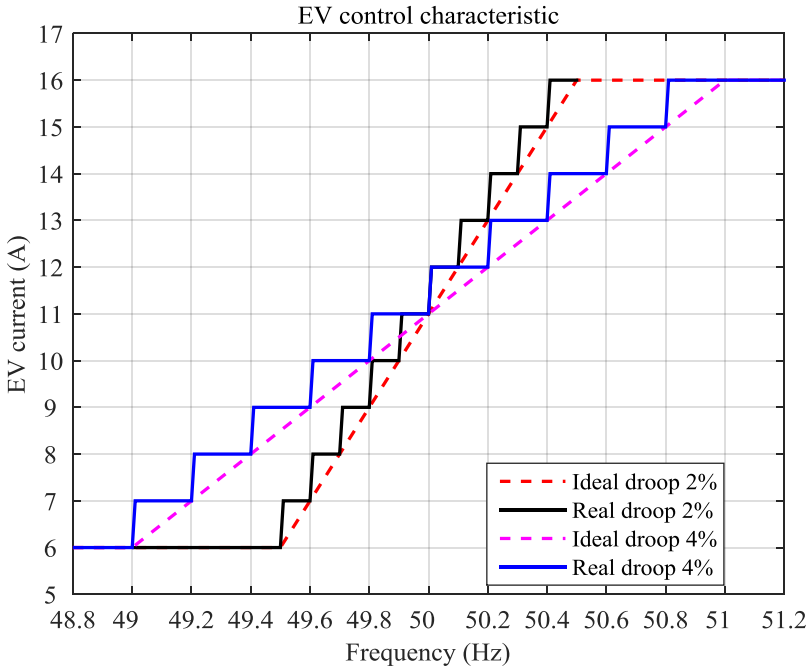

Figure 6: FCC droop

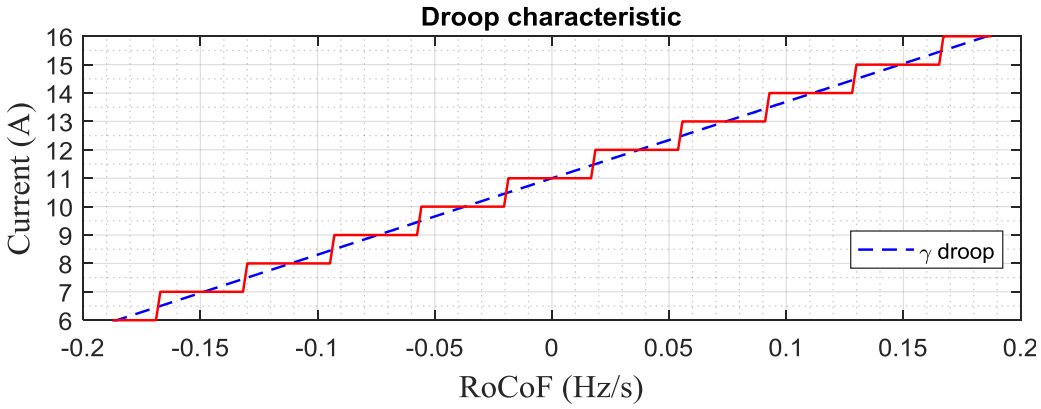

Figure 7: IRPC droop

3 Simulation results

Three different scenarios are investigated with different levels of wind penetration:

1. 0% Wind generation of the total load
2. 25% Wind generation of the total load
3. 90% Wind generation of the total load

3.1 Scenario 1

The first scenario studies the effects of the different levels of wind penetrations. It highlights the impact of converter connected resources on frequency dynamics (i.e. ROCOF, frequency nadir and steady state value). The results are shown in Figure 8.

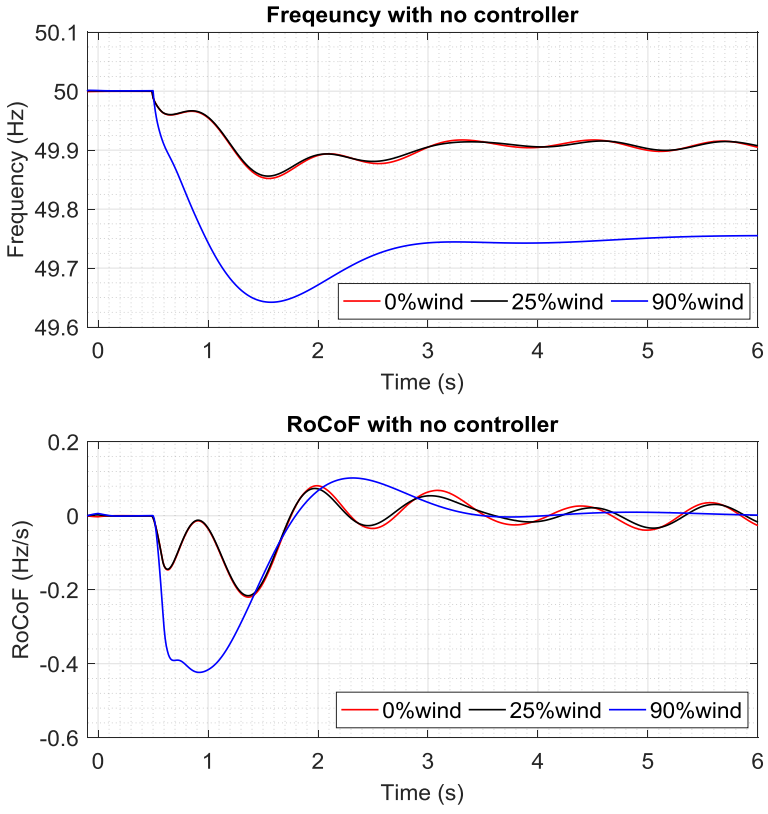

Figure 8: Frequency and RoCoF behaviors – no additional controllers

One can notice that the case of 25%wind does not have an impact on the frequency and that´s due at the fact that all the synchronous machines were still connected.

3.2 Scenario 2

In the second scenario a sensitivity analyses of the time delay is carried out. This scenario aims at highlighting the time delay importance and impact on IRPC as well as on FCC in case of different levels of DFIG penetration. The considered time delays are pure transport delays. The following time delay values have been considered 10ms, 50ms, 100ms and 250ms.
The controllers' gains are chosen as the maximum allowed value at which the system will remain stable. This choice is done to highlight the relation between the gain and the time delay. The gain of IRPC is smaller since it needs to limit the negative effect caused by the transport delay.
The sensitivity analysis is investigated for the different levels of wind penetration, shown in figures 9-11.

Case 1: 0% wind generation of the total load

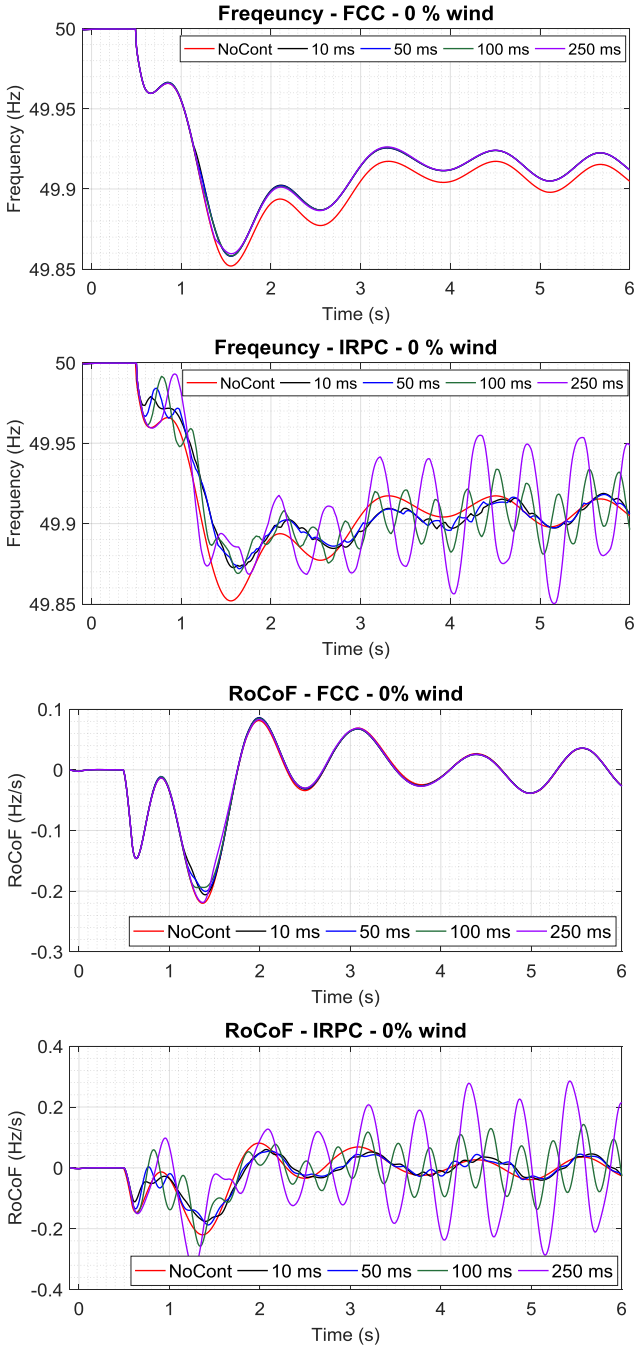

Figure 9: Left plots: Frequency behavior for FCC and IRPC in case of 0% wind. Right plots: RoCoF behavior for FCC and IRPC in case of 0% wind

As it can be seen in Figure 9Figure the 100ms and 250ms delay creates frequency oscillations in case of IRPC. To be mention, this oscillation could have been limited by employing a lower gain, on the other hand, that would have led to very limited contribution or even no contribution at all.

Case 2: The 25% wind generation of the total load.

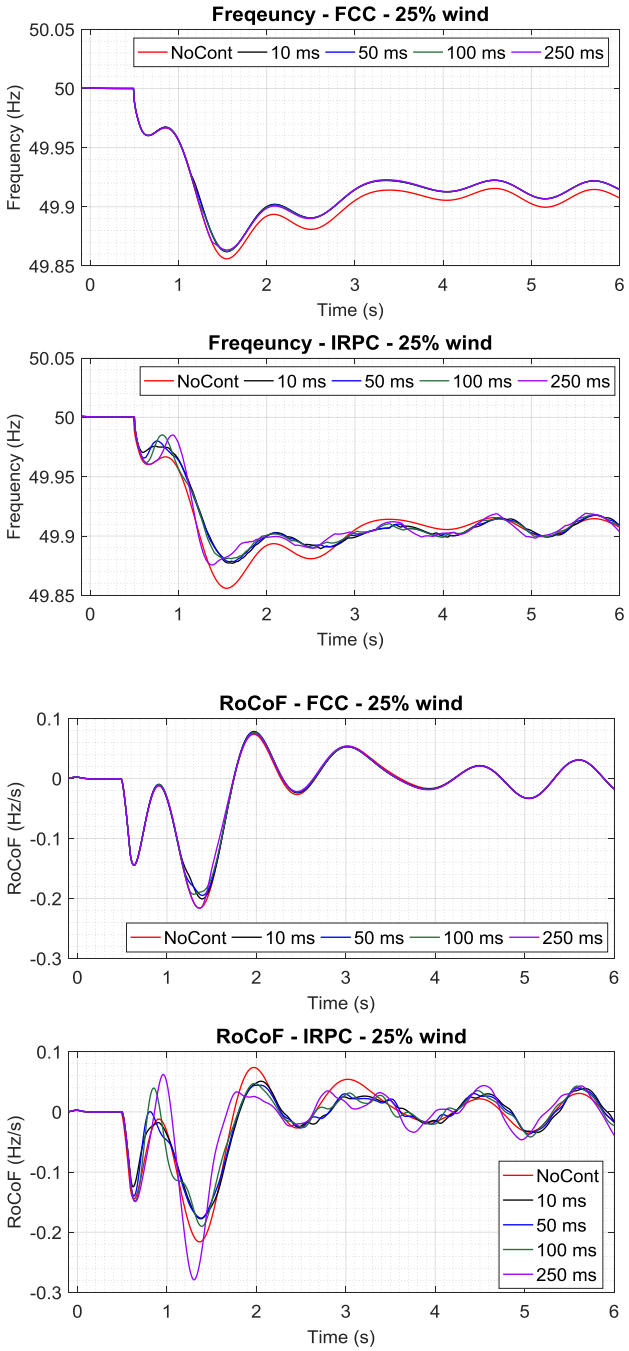

Figure 10: Left plots: Frequency behavior for FCC and IRPC in case of 25% wind. Right plots: RoCoF behavior for FCC and IRPC in case of 25% wind

Compared to the 0% wind penetration, the 25% case is more stable. In fact that´s due to the fact that all the synchronous machines are still connected as in the previous case plus the DFIG, which do have a certain damping effect. However, in terms of ROCOF, the 250ms has a worse behavior compared to the no controlled case. Of course, this behavior can be limited by retuning the controller since the larger time delay has a negative effect but on the other hand that means reducing the controller gain and therefore reducing its effects.

Case 3: 90% wind generation of the total load

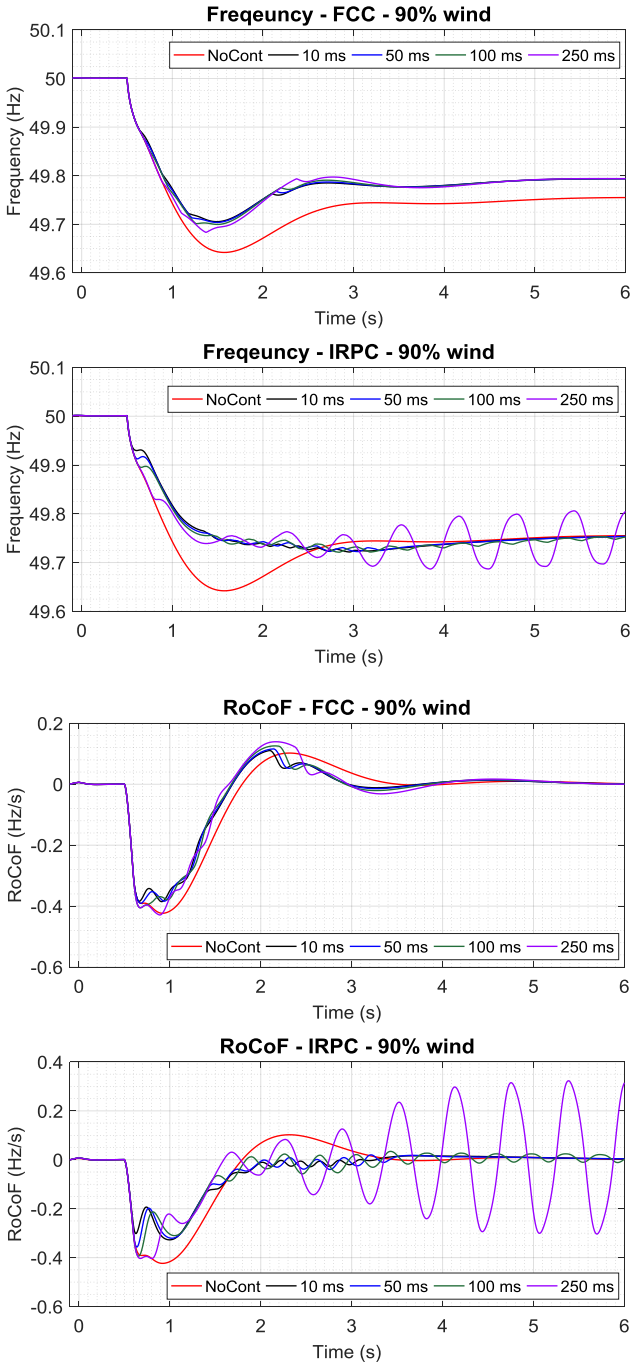

Figure 11: Left plots: Frequency behavior for FCC and IRPC in case of 90% wind. Right plots: RoCoF behavior for FCC and IRPC in case of 90% wind

Compared to the previous cases, the negative effect of the time delay is much higher due to the lower damping effect present in the grid in 90% case. In the IRPC case, the ROCOF is limited to lower values compared to the FCC case. The frequency nadir is slightly better also in the case of IRPC. These results are very influenced from the penetration of DFIG which deliver a certain damping effect and the results would have been more oscillating in case of fully converter wind turbines or PV generations. Larger delays in the IRPC case become critical in term of system stability.

3.3 Scenario 3

In the third scenario a performance analysis of FCC and IRPC is presented. This scenario aims at comparing the two controllers' impacts on the system frequency after the loss of a conventional generation unit corresponding to 5% of the total load. A time delay of 100 ms has been considered and only the 90% wind penetration case is considered.

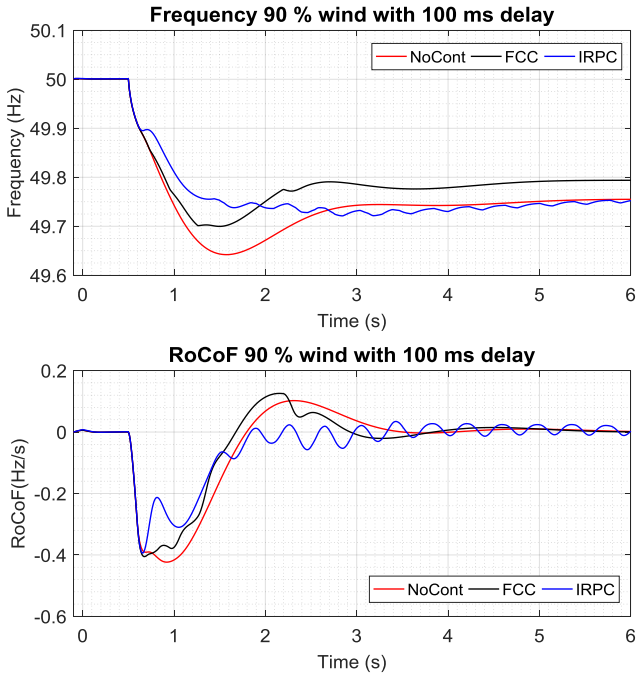

Figure 12: Frequency and RoCoF in case of 90% wind

It can be seen that the IRPC is limiting the RoCoF and even the frequency nadir to better values compared to the FCC. However, one can notice that IRPC imposes frequency oscillation on the system which can be reduced using a lower gain or/and a low-pass filter. On the other hand the FCC has a better performance in terms of frequency steady state value. A steeper droop in case of FCC can be used which will improve the frequency nadir values.

4 Summary and Conclusion

It was shown that the implementation of IRPC or FCC employing single phase electric vehicles can enhance the frequency behavior of the power system:

1. IRPC limits the RoCoF more than the FCC and due to the steeper droop it limits more the frequency nadir imposing also frequency oscillations.

2. The FCC has a better performance on the frequency steady state value than expected.

However, one of the main challenges is that many of the rotating synchronous machines, wind turbines and load shedding devices are connected to the grid by means of RoCoF relays. Therefore, likely a combination between IRPC and FCC needs to be present.

The work here presented laid the foundation for the experimental work reported in ELECTRA D7.1 and in the following publication [4] and [7].

References

[1] M. Marinelli, S. Martinenas, K. Knezović, and P. B. Andersen, “Validating a centralized approach to primary frequency control with series-produced electric vehicles,” J. of Energy Storage, vol. 7, pp.63-73, Aug. 2016.

[2] M. Marinelli, M. Pertl, M. Rezkalla, M. Kosmecki, S. Canevese, A. Obushevs, and A. Morch, “The Pan-European Reference Grid Developed in the ELECTRA Project for Deriving Innovative Observability Concepts in the Web-of-Cells Framework,” *Universities Power Engineering Conference (UPEC),* 2016 Proceedings of the 51st International, pp. 1-6, Coimbra, 6-9 Sep. 2016.

[3] V. T. Sæmundsson, M. Rezkalla, A. Zecchino, M. Marinelli, “Aggregation of Single-phase Electric Vehicles for Frequency Control Provision Based on Unidirectional Charging,” Universities Power Engineering Conference (UPEC), 2017 Proceedings of the 52nd International, pp. 1-6, Heraklion, 29 Aug. – 1st Sep. 2017

[4] M. Rezkalla, M. Marinelli, A. Zecchino, S. Martinenas, A. M. Prostejovsky, “Comparison between Synthetic Inertia and Fast Frequency Containment Control on Single Phase EVs in a Microgrid,” *Applied Energy,* vol. 210, pp. 764-775, Jan 2018.

[5] M. Rezkalla, S. Martinenas, A. Zecchino, M. Marinelli, E. Rikos, “Implementation and Validation of Synthetic Inertia Support Employing Series Produced Electric Vehicles,” CIRED, Open Access Proc. J., vol. 2017, Iss. 1, pp. 1197-1201, 2017.

[6] M. Rezkalla, M. Marinelli, M. Pertl, and K. Heussen, “Trade-off Analysis of Virtual Inertia and Fast Primary Frequency Control During Frequency Transients in a Converter Dominated Network,” *Innovative Smart Grid Technologies (ISGT Asia), 2016 IEEE PES International Conference and Exhibition on*, pp.1-6, Melbourne, 28 Nov - 01 Dec 2016.

[7] A. Zecchino, S. D’Arco, A. G. Endegnanew, M. Korpås, M. Marinelli, “Aggregated Response Time and Granularity as Key Enablers for EVs Providing Fast Frequency Control,” *Transportation Electrification, IEEE Transaction on*, under revision (submitted in Dec 2017)

ANNEX 2: Frequency Containment Control (FCC)

1 Introduction

This annex presents the results of the simulations run to evaluate the Frequency Containment Control (FCC) adaptive function behavior. In these simulations, the FCC has been tested on the European CIGRÉ MV grid (Task Force C6.04.02) modified with distributed energy resources (DER) in two separated scenarios and with different assumptions.

- In **"simulation case" A,** the Adaptive-FCC control function was implemented using fuzzy logic. Also, in this first scenario the reference grid topology was properly modified.
- In **"simulation case" B,** the main assumption is the following: as soon as an imbalance is detected, a step load disturbance in this case, the second version of the FCC control function uses resources from all cells to immediately mitigate the problem. After having the frequency stabilized, the contribution from healthy cells ceases and only resources from the faulty cell are used to contain the frequency deviation.

Thus, the main difference between the two cases is the operation of the function Adaptive Cell Power Frequency Characteristic (CPFC) Determination, which will be explained in the following sections. Figure 1 shows the network topology and the cell subdivision adopted.

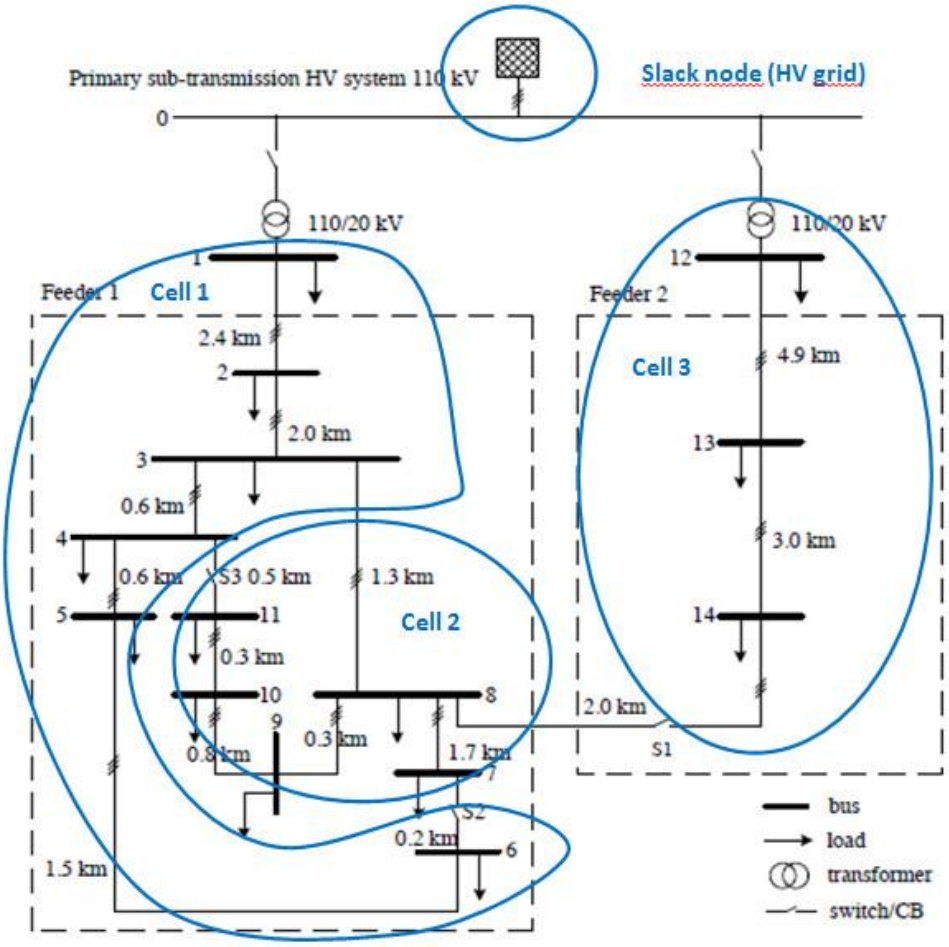

Figure 1: Reference network and cell subdivision

The following sections present the methodology implemented for the simulations, the results achieved and the main conclusions drawn.

2 Methodology

2.1 Reference model descriptions

In order to simulate the use case under test we have made some critical assumptions on the network depicted in figure 1.The assumptions are briefly presented below and are valid for **simulation cases A and B.**

- all circuit breakers were considered closed in order to have a meshed network topology
- the "slack node" that represents the HV grid and is responsible for frequency dynamics is modelled as an equivalent generator through a first order transfer function (considering an inertia constant H = 5 s) and equipped with primary (R = 0.1) and secondary frequency control (Ki_{Sec} = 0.3) as shown in Figure 2. The model presented in the picture is in per unit, the nominal power of this equivalent generator is 50 MW, this in order to observe a significant impact of imbalances that occurs at MV level on frequency dynamics and better evaluate the effect of the UCs under test.

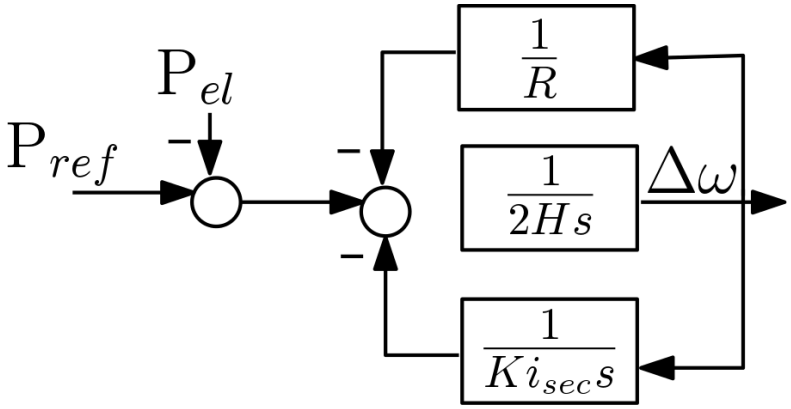

Figure 2: "slack node" model

3 Simulation results

3.1 Simulation scenario for case A

The following Figure 3 illustrates the displacement of renewable generators and loads. Generators are: photovoltaics, wind turbines and combined heat power plants (CHP). There are also storage units. Both generators and loads are modelled as power sources.

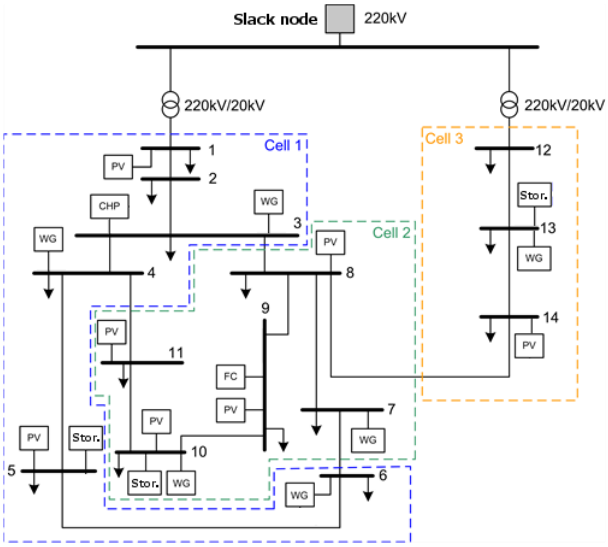

Figure 3: Load and generation displacement

In table 1 a summary of the nominal power of generators, divided by type, and cells loads is reported. A high penetration of Photovoltaics (PV) and Wind Generators (WG) is introduced, especially in cell 1.

Table 1: Nominal power of generators and loads

Generation				
[MW]	Cell 1	Cell 2	Cell 3	*Total*
PV	7.5	0.495	0.775	*8.77*
WG	9.5	1	3.5	*14*
Storage	0.8	0.2	0.6	*1.6*
CHP	9	1	0	*10*
Total	*26.8*	*2.695*	*4.875*	*34.37*
Load				
[MW+jMVAr]	Cell 1	Cell 2	Cell 3	*Total*
Load	22 + j5.2	2.1 + j0.8	20 + j5	44.1 + j11

Each generator connected to MV grid has to contribute to frequency control but not all of them in the same manner. CHP and storage units are considered as fully dispatchable generators and they contribute to the primary frequency control in both directions (negative and positive frequency deviations). Also the slack node has a full droop characteristic. PVs and WGs are following the Maximum Power Point Tracking Strategy (MPPT), and so they can only reduce their power output.

The simulations have been done considering a variable load and generation profile and a two load step disturbances of 1 MW, one at t=35 min (step load increase) and one at t=43 min (step load decrease). In the following graphs show the inputs for the simulation summarized on cell basis. Load and generator forecasts for each time window (15 min.) are used to compute the tie-line set-points, and the actual load and generation profiles. The variability in generation is due to the wind and solar power variation.

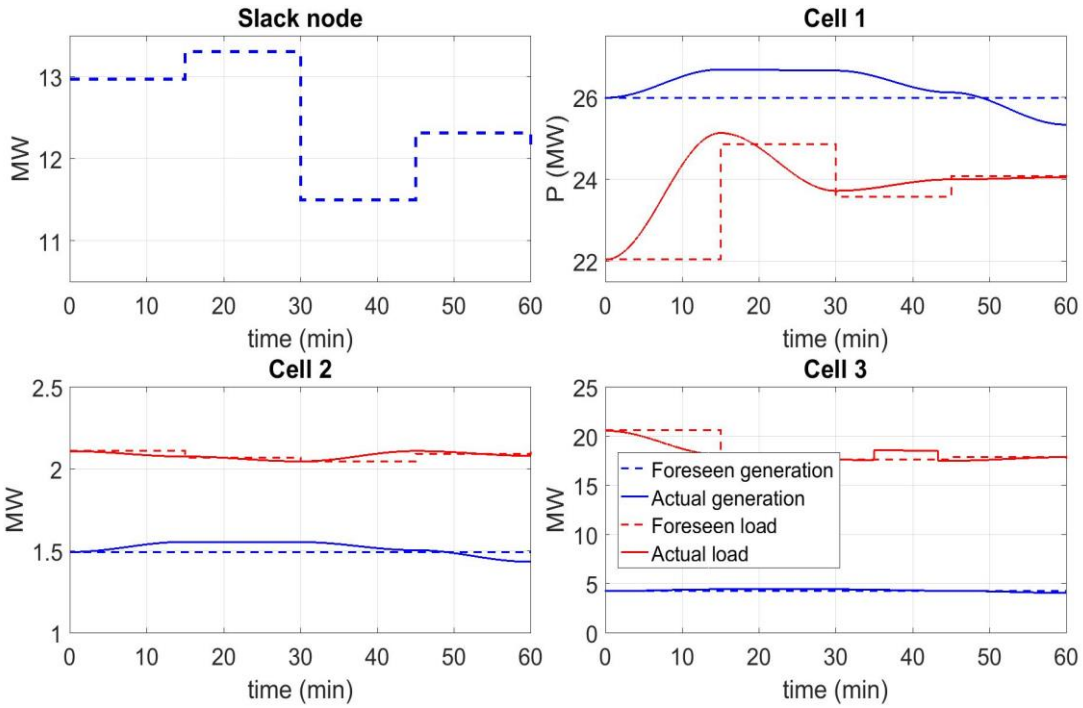

Figure 4: Total cell load and generation

It has been considered to devote the resources that are following the MPPT strategy (in our case PV and WG) to the Adaptive functionality of the FCC Use Case. This is because, among DG resources, these are units that can obtain a great benefit from the adaptiveness of the FCC. In a traditional approach, where these resources are equipped with a droop control for positive frequency deviations, they will curtail their generation if the frequency is higher that the nominal. The Adaptive FCC allows them to avoid curtailment of power output in case that the disturbance took place outside the boundaries of their cell. In this way they are able to better follow the MPPT. Other resources such as storage systems and CHP have a constant droop characteristic both for positive and negative frequency deviation.

The A-FCC control function has been implemented with a fuzzy logic, and simulations of the system with and without it have been performed in order to compare results. Figure 5 illustrates the frequency of the system, the scheduled export and the actual export power for each cell. Scheduled and actual power exports are much different in some cases because the control devoted to adjust cell power exports (the BRC) is not in place since here since the aim was to test only the A-FCC.

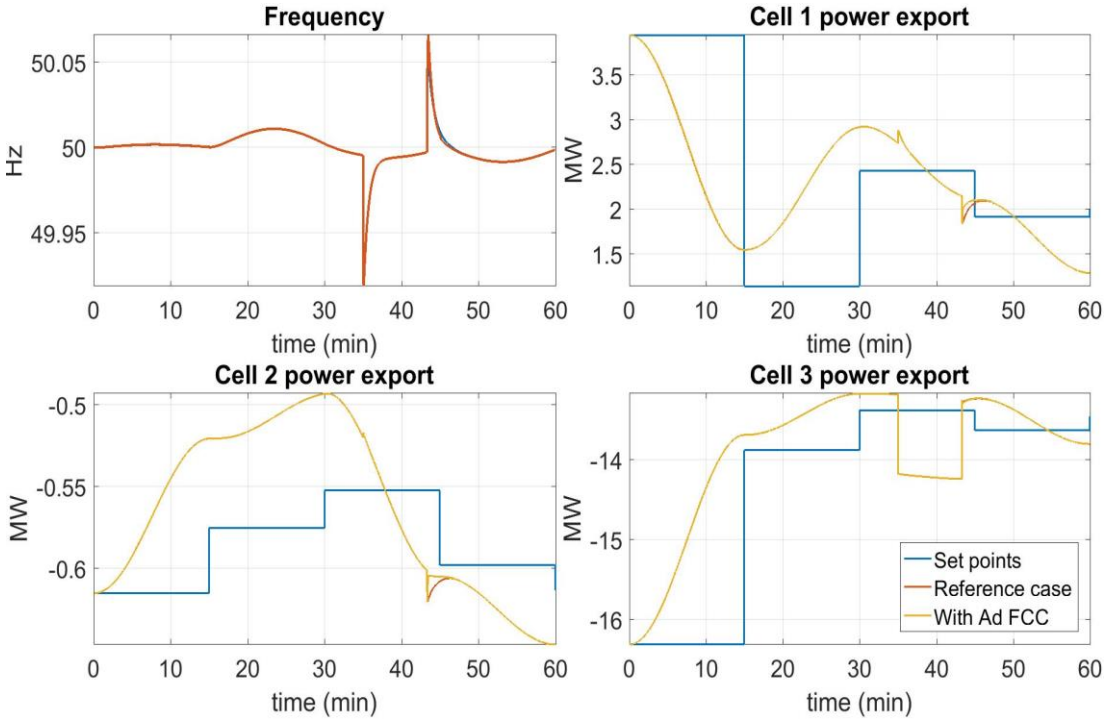

Figure 5: Ad FCC inputs (frequency and the cell import/export power)

In figure 6 the action of the Adaptive FCC on the power variation due to the primary frequency control of PVs and WGs is presented. Except for a very short interval, a few seconds after the disturbance at 43 minutes, the power output curtailment due to the primary control action is restored to 0 in the cells 1 and 2 where the disturbance is not happening. In this case the A-FCC efficiently locates the load imbalance.

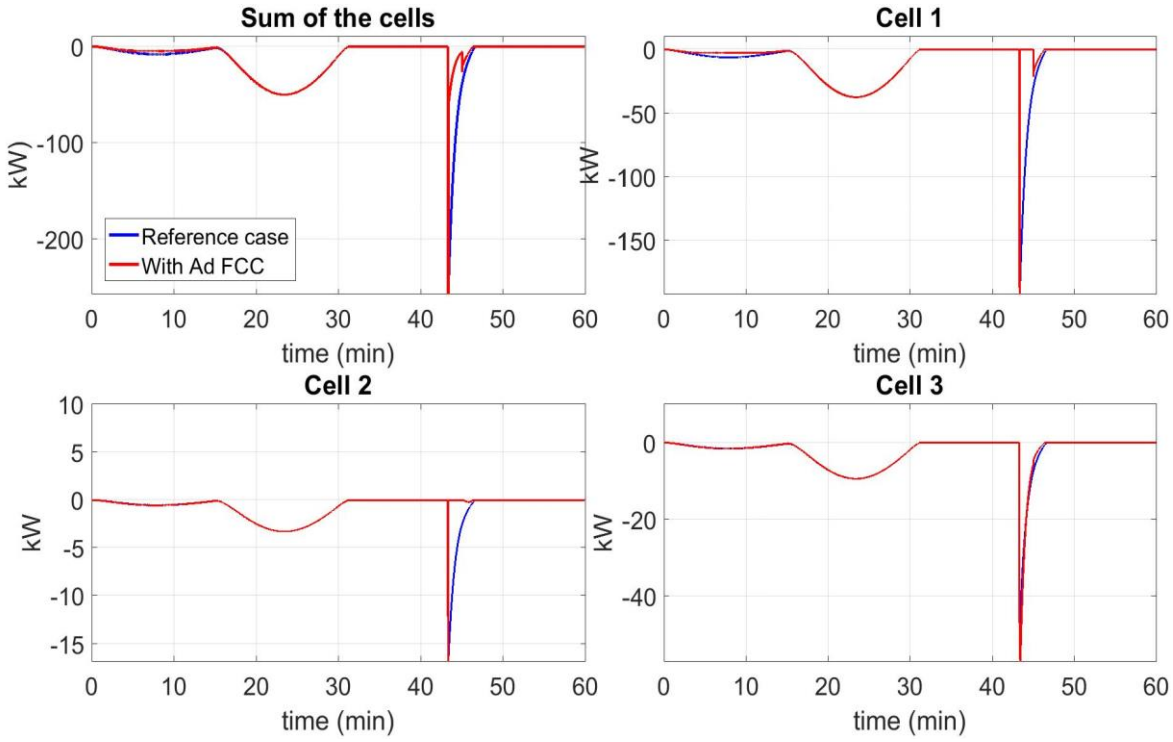

Figure 6: Variation of the power generated by PVs and WGs due to Adaptive FCC

Moreover (again in Figure 6), it is shown that in cell 1 in the first time window the A-FCC is acting and reducing the contribution of cell 1 PVs and WG since it detects a positive frequency deviation and an excessive power export.

Two indices have been computed in order to evaluate the effectiveness of the Adaptive FCC function: the total energy used by the FCC control of PVs and WGs equation (1) and a cost function based on the squared values of the power deviations for primary RES control actions described by equation (2). In table 2 we can see the results. All cells see reduction in the usage of RES primary reserves, but cell 1 and 2 see in terms of percentage a lot more reduction since the load step disturbance happened in cell 3.

$$\int_0^{\infty}\left[\left|\Delta P_{droop,1}\right|+\cdots+\left|\Delta P_{droop,n}\right|\right]dt \qquad (1)$$

$$\int_0^{\infty}\left[\left(\Delta P_{droop,1}\right)^2+\cdots+\left(\Delta P_{droop,n}\right)^2\right]dt \qquad (2)$$

Table 2: A-FCC indices

Total energy – equation (1)				
[MWs]	Cell 1	Cell 2	Cell 3	*Total*
Ref. case	35,6	3,1	9,0	29,8
Ad FCC	25,1	2,3	9,0	18,4
Saving	29,6 %	26,5 %	0,4 %	38,3 %
Cost function – equation (2)				
[MW²s]	Cell 1	Cell 2	Cell 3	*Total*
Ref. case	1722	13	109	1845
Ad FCC	789	6	126	921
Saving	54 %	54 %	16 %	50 %

3.2 Simulation scenarios for case B

The main difference of the case A to case B is the development of the function Adaptive CPFC Determination. In this case, the value of the CPFC for each cell will consider if the incident occurred in its cell or in another cell. If the incident occurred in another cell, the value of the CPFC is equal to 0, meaning that the cell will stop contributing to mitigate the problem. Otherwise, the CPFC will keep the value previously defined and this cell will be the only one contributing to mitigate the problem.

To test the functions two scenarios were created:

1. In the first scenario, there is an increase of the load in bus 6 (Cell 1) by 1 MW, at t=30 s;
2. In the second scenario, there is a loss of the load in bus 6 (Cell 1), by 1 MW at t=30 s.

In the following, the main results obtained from the simulations performed are presented. The frequency of the system and the active power output of the generators and batteries are the most important parameters and through them it is possible to evaluate the performance of the models created and the differences between the analysed scenarios. The reactive power of the machines and the buses voltages are always kept within admissible limits.

Scenario 1

In this scenario, the behaviour of the models is tested by simulating a problem in Cell 1. The results obtained for the frequency are shown in the following figure:

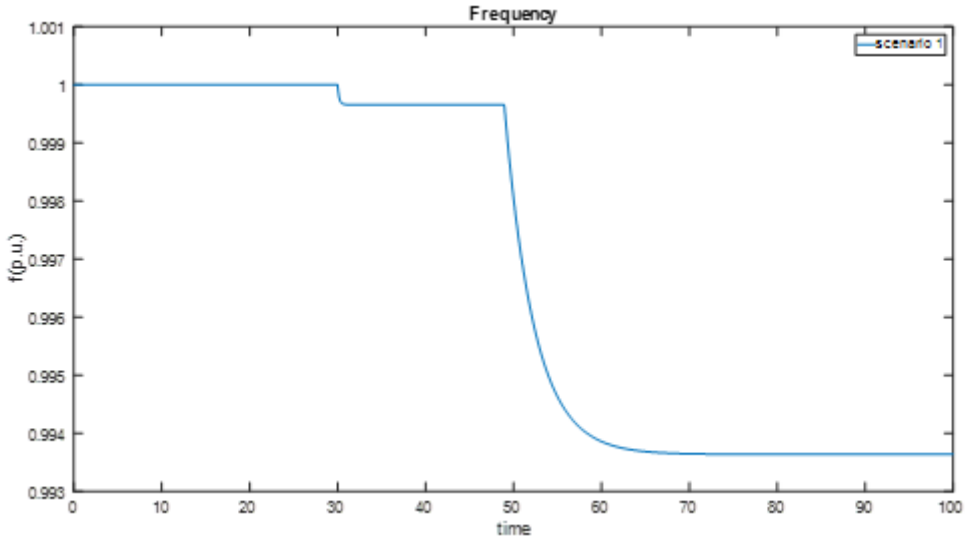

Figure 7: Frequency of the system

As it is shown, the frequency is constant until the problem occurs (at 30s). After the incident, the frequency drops due to the increase of the load in bus 6. When the frequency reaches a steady state, the frequency drops even more as the other cells stop contributing to mitigate the problem and the cell where the problem occurred has to assume the frequency control alone. After this last drop, the frequency ends up stabilizing again, meaning that the area had enough reserve capacity to respond to the problem. The following figure shows the results obtained for the active power output of Wind Turbine 4 and Battery 5 in Cell 1:

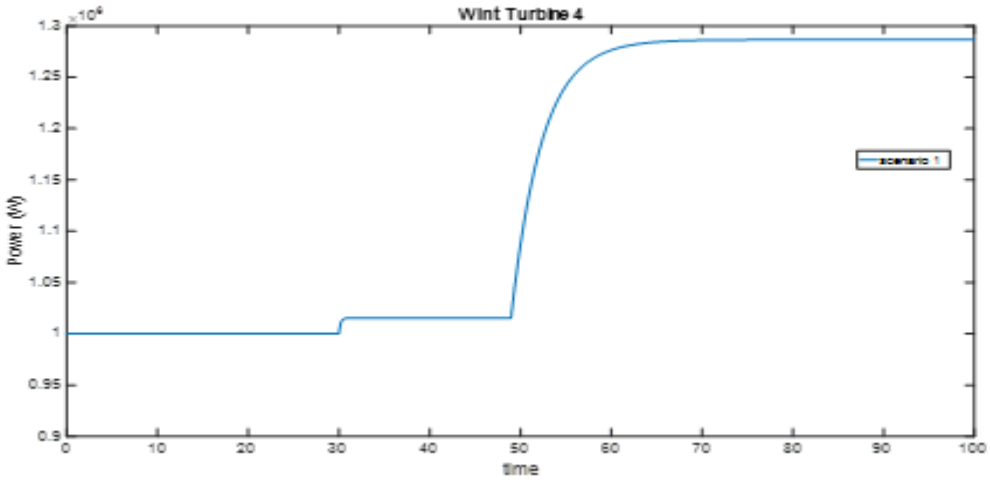

Figure 8: Active Power of Wind Turbine 4 (Cell 1)

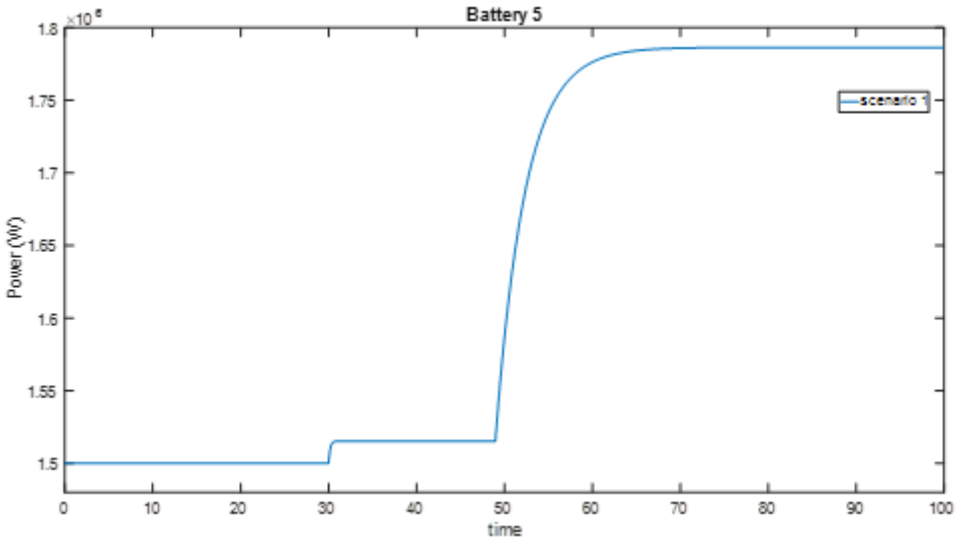

Figure 9: Active Power of Battery 5 (Cell 1)

The active power stays constant until the problem occurs and then the generators increase their power output in order to mitigate the frequency drop. After reaching the steady state, the generators increase their power output again. This is due to the fault location, which occurred in the cell where these generators are located.

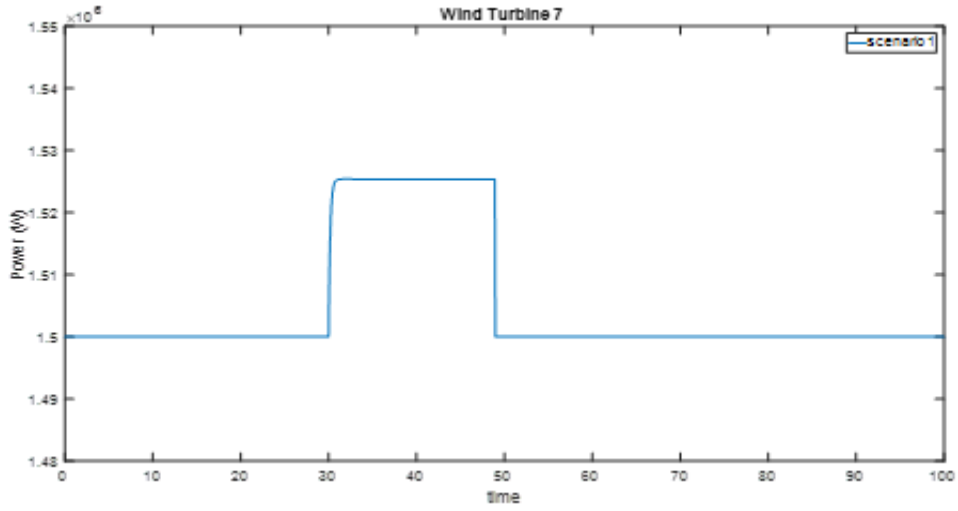

Figure 10: Active Power of Wind Turbine 7 (Cell 2)

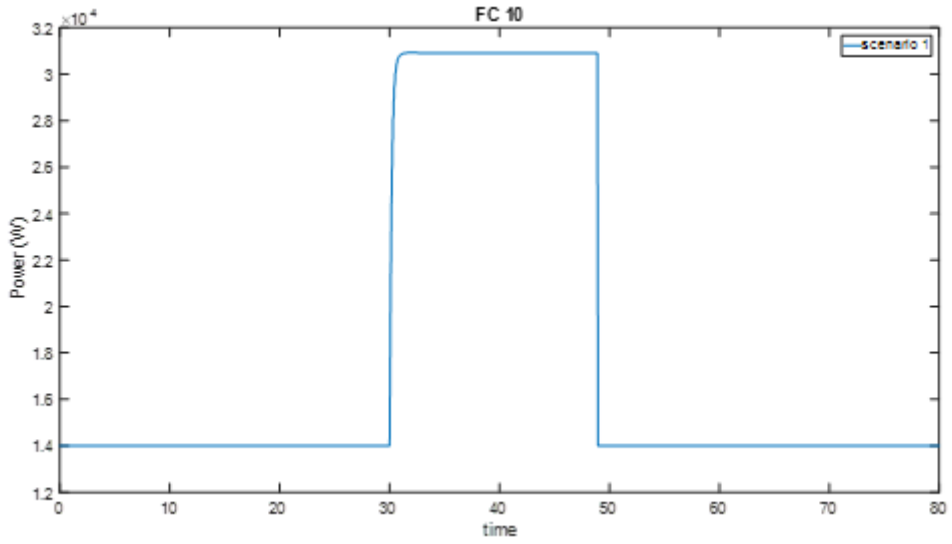

Figure 11: Active Power of FC 10 (Cell 2)

The generators in Cell 2 present a different behavior. After the increase of active power due to the imbalance and afterwards reaching the steady state, the power output returns to its initial value because the problem did not occur in this cell.

Scenario 2

In this scenario the loss of a load in bus 6 (Cell 1) was simulated. The results obtained for the frequency are shown in the following figure:

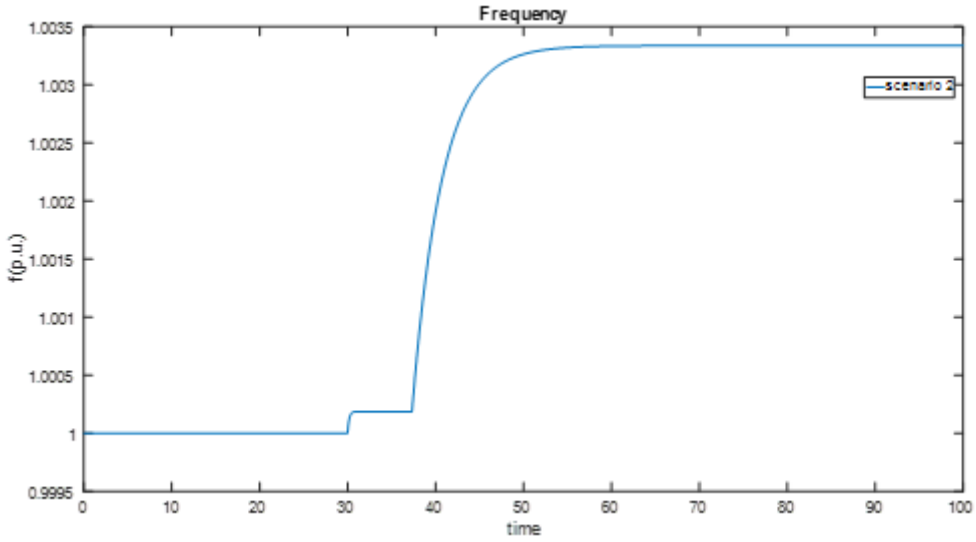

Figure 12: Frequency of the system

The frequency is constant until the problem occurs (t=30 s). Then the frequency increases due to the excessive generation. When the frequency reaches a steady state, there is another increase in the frequency of the system since in this case, only the cell where the problem occurred contributes to solve the problem. The frequency ends up stabilizing again, what means that the cell had enough downward reserve capacity to mitigate the problem.

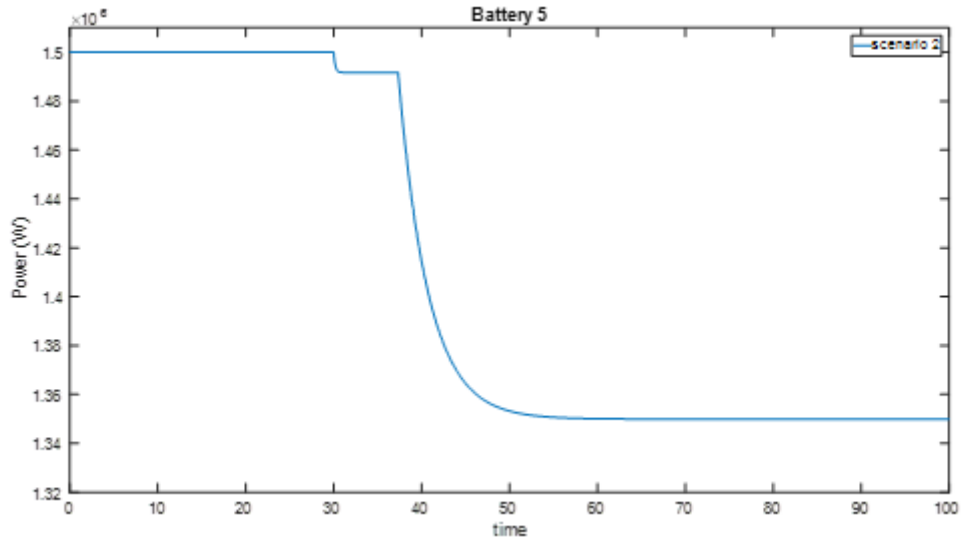

Figure 13: Active Power of Battery 5 (Cell 1)

In figure 13 it is possible to observe the active power generated by Battery 5. When the imbalance occurs, the battery decrease its power output in order to compensate the frequency rise. Then, when the steady state is reached, the battery decreases its power output again because it is located in the cell where the problem occurred.

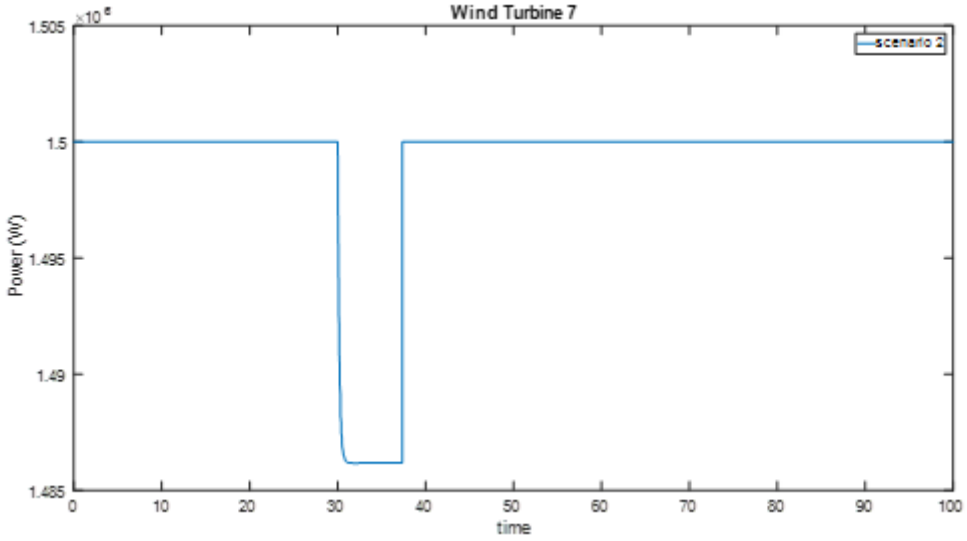

Figure 14: Active Power of Wind Turbine 7 (Cell 2)

The power output of Wind turbine 7, which is located in cell 2, returns to its initial value after the incident because it is not in the cell where the problem occurred and thus it does not contribute to the problem mitigation.

4 Summary and Conclusion

The simulation tests of case A show that the A-FCC control function, that was implemented using a fuzzy logic, can effectively detect the imbalance location and, as a result, curtail the FCC reserve if the imbalance took place outside its cell. The controller proved to be effective both under normal operation with all cell is not in balance due to the uncertainty of forecasts, both in case of a step load disturbance.

In the simulations of case B, it is possible to observe that when the FCC reserves from the neighboring cells are deactivated, the reserves of the cell where the problem occurred are able to confine the problem on their own and the frequency stabilized. It is then possible to conclude that the implementation of the controls developed proved to be effective in stabilizing the frequency by using only the cell's own resources.

ANNEX 3: Balance Restoration Control (BRC)

1 Introduction

For the purpose of testing the developed Balance Restoration Control (BRC) within a realistic environment, a reference grid based on the CIGRE benchmark grid for High Voltage (HV) [1], has been used. This has been previously presented within the Deliverable 5.4 “Functional description of the monitoring and observability detailed concepts for the Pan-European Control Schemes” within the ELECTRA IRP project. Figure 13 shows the developed reference power system model, named “Pan-European” network model, which represents future grid characteristics, including different voltage levels, AC and DC sections, and is composed of four cells with different properties in terms of generation portfolio (including a variety of renewable energy resources) and load (including demand-side response). The key features of the model are summarized in Table 1. More information on this model is available in public Deliverable 5.4.

According to the BRC algorithm, each cell should address deviations originating within itself i.e. solving local problems locally. The division of the system into four cells allows for analysing the unbalance (its location identification and size) and the corresponding activation of BRC. The performance of all the cells is analysed to show that the BRC controller performs as expected and to ensure correct local activation.

A robust optimization approach to schedule the power and allocate the frequency reserves on a day-ahead basis, considering the uncertain energy content of two types of regulation signals, i.e., fast regulation signal and slow regulation signal, and the energy constrained property of batteries has been developed and separately tested within the project. Therefore, having taken into account that this algorithm is performing a scheduling task prior to the real-time control, the reserve allocation of the different cells is assumed to be known at the time of the unbalance for each of the scenarios in this document.

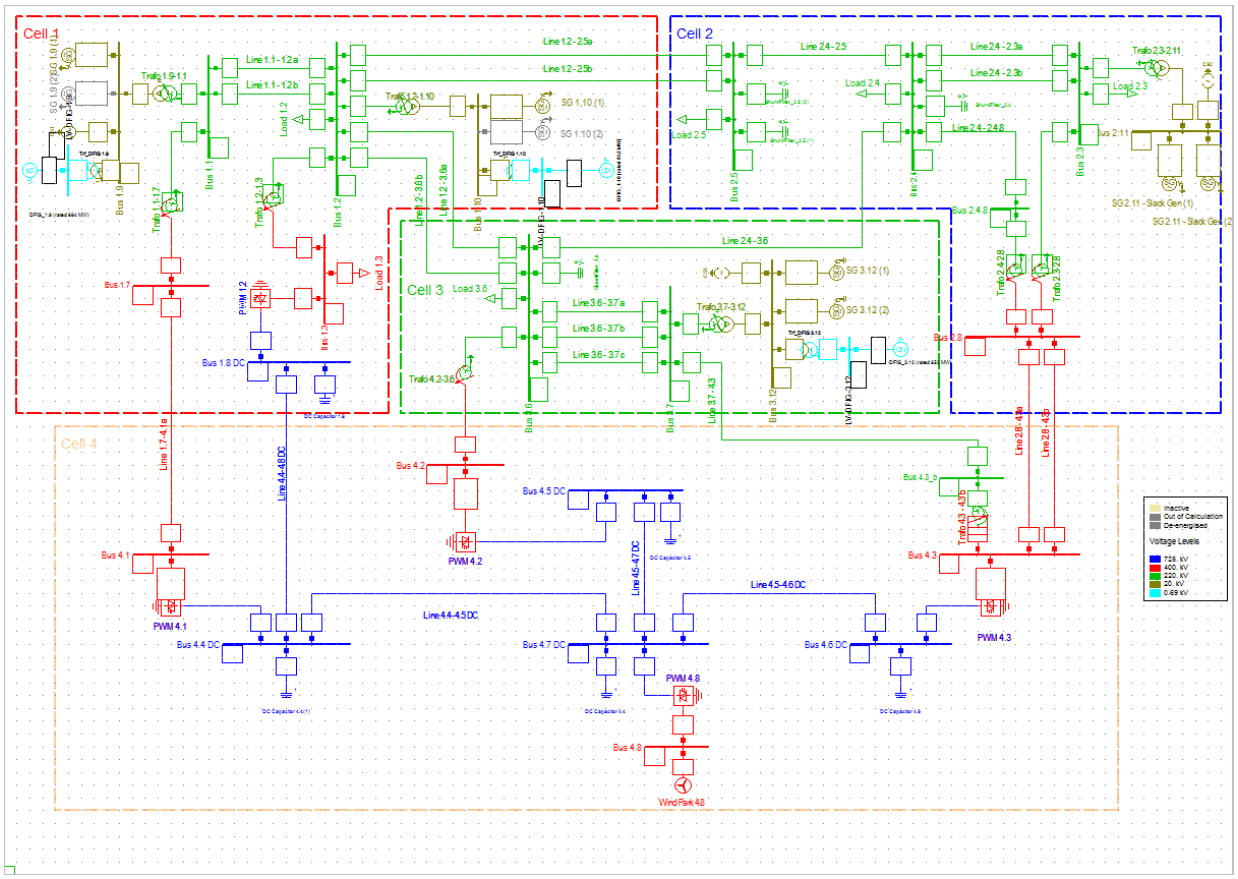

Figure 13: The Pan-European model used to test the BRC controller

Table 1: Test system data

	Cell 1	Cell 2	Cell 3	Cell 4
Voltage levels (kV)	20; 220; 400; 725	20; 220; 400	20; 220	400; 725
AC/DC	AC and DC	AC	AC	AC and DC
Nominal generation power	2x400 MVA 2x500 MVA synchronous machines (gas turbine governor) 100x6 MW (type 3 wind turbines) 100x6 MW (type 3 wind turbines)	1x700 MVA synchronous machine (gas turbine governor) note: this machine is used as slack for LF calculations	2x500 MVA synchronous machines (hydraulic governor) 100x6 MW (type 3 wind turbines)	1x600 MVA equivalent wind generation (type 4)
Nominal consumption power	2x1000 MW + 2x165 MVAr loads (load P consumption is linearly dependent on voltage and constant on frequency; load Q is quadratically	3x400 MW + 3x130 MVAr loads	1x400 MW + 1x130 MVAr loads	no load

	Cell 1	Cell 2	Cell 3	Cell 4
	dependent on V and constant on frequency)			
Number of tie-lines	Cell 1-2: 2 AC 220 kV tie lines Cell 1-3: 2 AC 220 kV tie lines Cell 1-4: 1 AC 400 kV tie line; Cell 1-4: 1 DC 725 kV tie line	Cell 2-1: 2 AC 220 kV tie lines; Cell 2-4: 2 AC 400 kV tie lines; Cell 2-3: 1 AC 220 kV tie line	Cell 3-2: 1 AC 220 kV tie line; Cell 3-4: 1 220/400 kV transformer 1 tie line Cell 3-4: 1 AC 220 kV tie line;	Cell 4-1: 1 AC 400 kV tie line; Cell 4-1: 1 DC 725 kV tie line; Cell 4-2: 2 AC 400 kV tie lines; Cell 4-3: 1 220/400 kV transformer Cell 3-4: 1 AC 220 kV tie line
Number of internal lines	2x220 kV line	4x220 kV lines	3x220 kV line	3x725 kV lines
Nominal HVDC capacity	1x500 MVA PWM converter	no PWM	no PWM	3x500 MVA PWM converters

2 Methodology

In order to test the functionality of the BRC controller, a simulation with the presented model in Figure 1 is performed with DIgSILENT PowerFactory software. For each of the scenarios to be tested, an unbalance will be triggered and data recorded during 300 seconds for analysing the behaviour of the controller.

Three cells are separately equipped with the BRC controller and the frequency response and other control signals are monitored for active power imbalances within each of the three cells in question. The imbalance event in each scenario is a load step of +150 MW, causing an instantaneous active power deficit in the cell.

For providing the fast-acting active power reserve required for the BRC control, an AC Current Source was added to each of the three cells, to which an active power demand signal was sent from the controller in the same way that the Automatic Generation Control (AGC) component of the controller provides active power setpoints to the synchronous generators. The AC current source emulates the behaviour of aggregated renewable generation, batteries or demand response at the speed set by the fast acting control loop of the BRC algorithm.

Two dispatch scenarios were used in the testing, to demonstrate the functionality of the controller with both a lower (25%) and higher (50%) Renewable Energy Sources (RES) penetration. Furthermore, a reduced proportion of synchronous generation is assumed for the 50% RES scenario. These scenarios have been split up into three further sub-scenarios where the load step has been applied in each of the three cells in turn.

For each sub-scenario, tests were run in which the fast-acting response was deactivated (business as usual scenario, labelled AGC in the following plots) or activated (labelled AGC+BRC). This allowed a comparison between the traditional (slow) control of reserves and the improved frequency control which includes fast-acting reserves and location awareness. Only three cells were equipped with the BRC controller as one of the four cells in the test system was not

energised for the first test scenario (lower RES penetration). For consistency, a fourth cell controller was not included in the other test scenario and that cell acted only to provide power from the RES.

3 Simulation Results

3.1 Scenario 1 – 25% RES, 8 Synchronous Generators

Scenario 1 examines a dispatch where all eight of the synchronous generators in the system are in service – four in Cell 1 and two in each of Cell 2 and Cell 3. In this scenario, 25% of the active power demand is met by renewable energy sources in the form of wind turbine models.

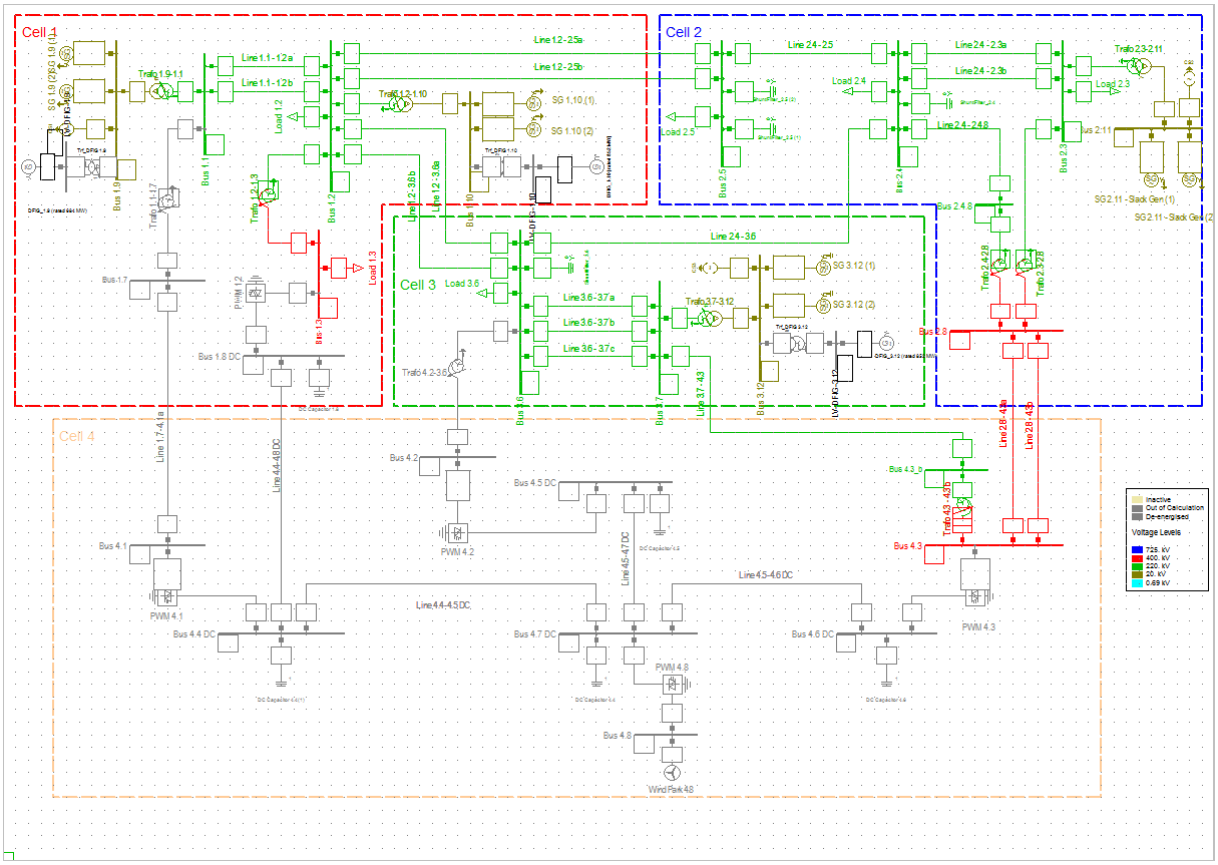

Figure 14: Test system with Cell 4 de-energised for Scenario 1

3.2 Scenario 1.1 – 150 MW Imbalance located in Cell 1

Under this scenario, it can be seen from Figure 15 that the AGC control takes several minutes to restore frequency to the nominal value, while the introduction of the fast-acting BRC control significantly reduces the time taken for nominal frequency to be reached. A slight overshoot in frequency is experienced in the BRC case, which would be addressed by the appropriate tuning of the controller parameters in further work. Table 2 shows the selected controller gains for the simulations.

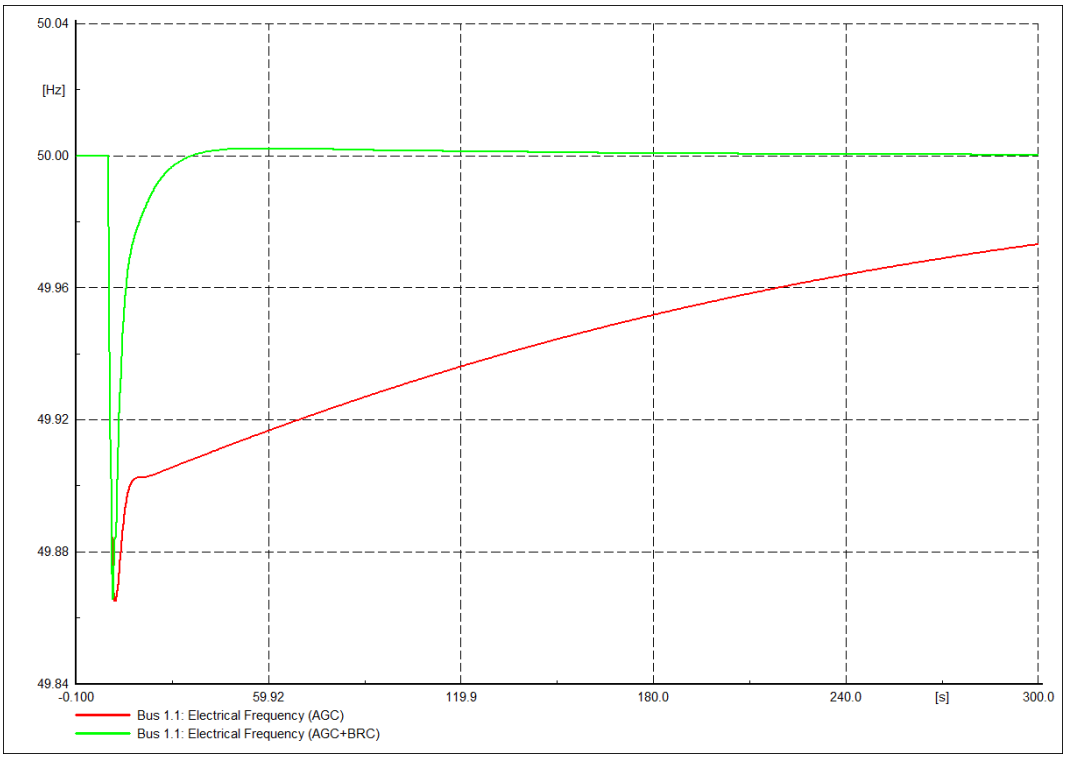

Figure 15: Frequency response of AGC and AGC+BRC with imbalance in Cell 1

Table 2: BRC Controller gains selected for simulations (controller description can be found in White Box description)

	AGC	BRC
Proportional Gain (Kp)	0.1	0
Time Constant (Ti)	50	2

Figure 16 and Figure 17 highlight that the controllers (in each cell) were successful in only sending a reserve activation signal to the fast-acting active power reserves in the affected cell, thereby activating the Cell 1 fast-acting current sources in this case. This minimizes controller conflicts between the fast-acting reserves in multiple cells and ensures that the affected cell will provide the entirety of the fast-acting reserve for the power imbalance event. Note that the convention for active power from the current source is negative for active power injection to the system within the DIgSILENT PowerFactory software.

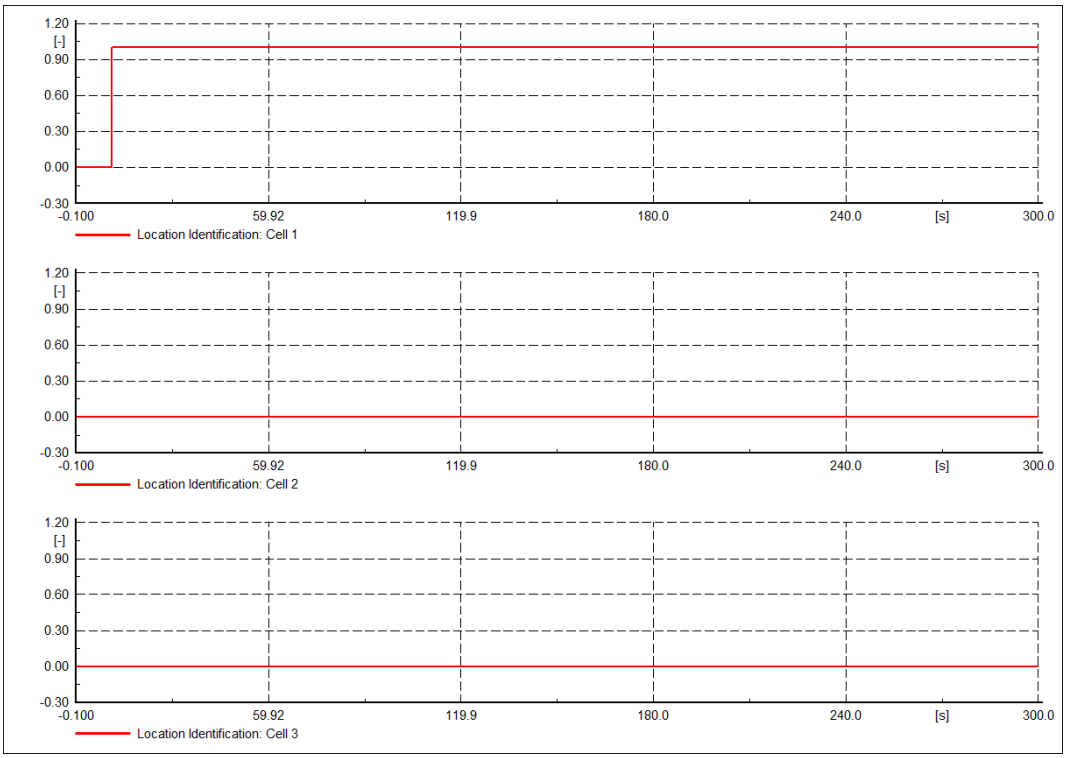

Figure 16: Location identification. A signal with magnitude = 1 indicates the imbalance is in the relevant cell

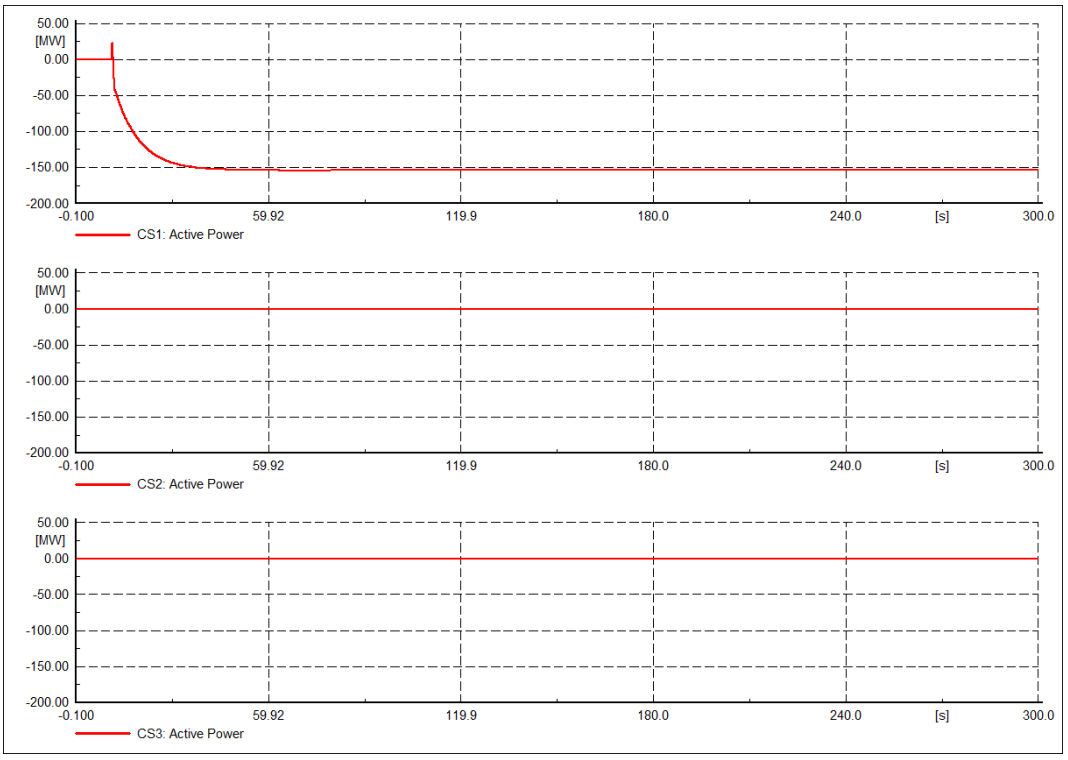

Figure 17: Active power of current source in each cell, with imbalance event located in Cell 1

In Figure 18, the active power imbalance calculated within each cell (dPnet) by the BRC cell controller is shown. The BRC control logic calculates the location of the fault making use of the dPnet signal, which shows whether a cell has a surplus or deficit of active power in the wake of an event, and the sign of the rate-of-change of system frequency. It follows that there is only activation of fast-acting BRC control within the affected cell and none of the others – a key objective of the controller functionality.

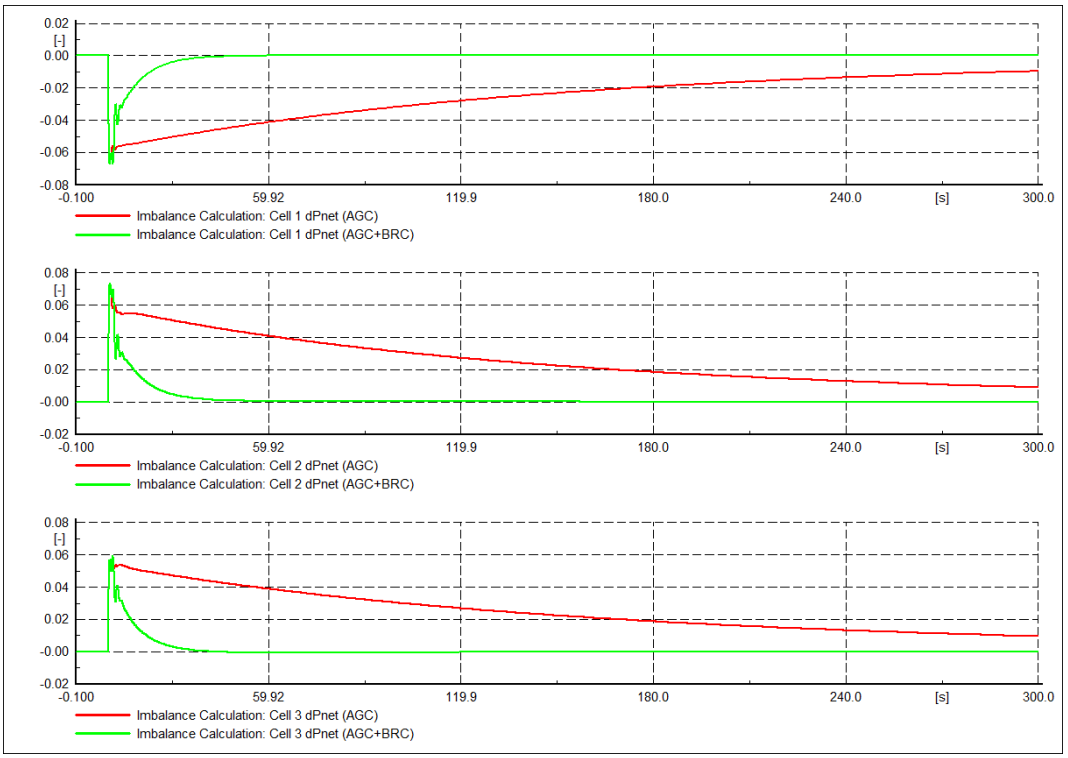

Figure 18: dPnet signals (in p.u.) of three controllers with imbalance in Cell 1

The Area Control Error (ACE) signal within the controller is calculated using the dPnet signal and the frequency deviation, and is used as the control signal for the slow-acting AGC component of the reserve activations (i.e. the synchronous generators). It can be seen from Figure 19 that when the BRC is activated there is little active power demand sent to the synchronous generators after several seconds and that the cell with the original imbalance event contributes much more in slow-acting AGC reserves than the other two cells, therefore responding as local as possible to any unbalance.

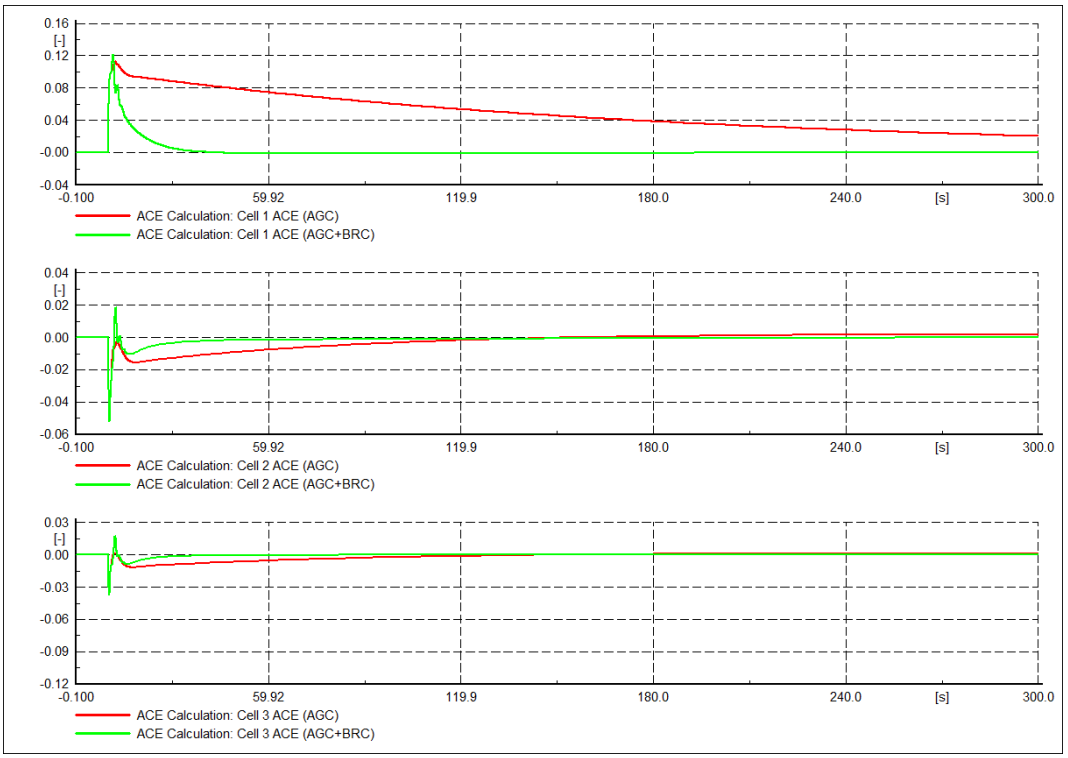

Figure 19: ACE signals (in p.u.) of three controllers with imbalance in Cell 1

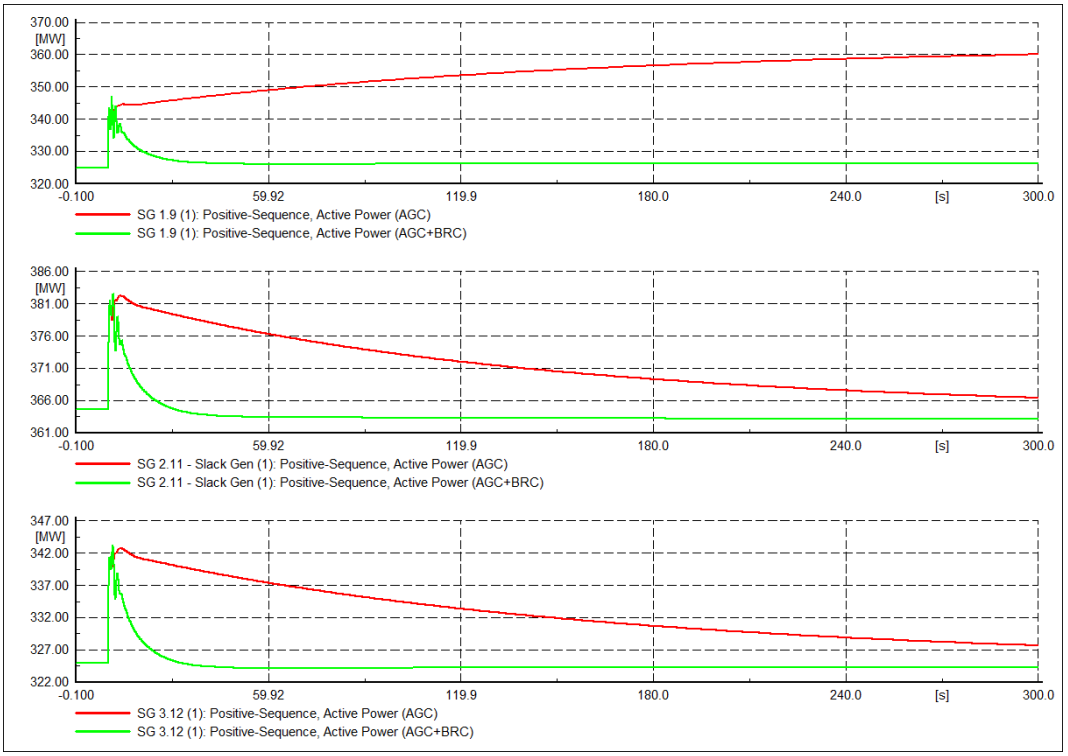

Figure 20: Active power response of generators in three areas to imbalance in Cell 1

Figure 20 shows the active power response of a synchronous generator located in each of the three cells to an imbalance within Cell 1. It can be seen that without the BRC function activated, the synchronous generators in Cell 1 are responsible for providing the entire reserve and the synchronous generators in the other cells return to their pre-fault generation levels after some time. When the BRC function is implemented, the active power of the synchronous generators in all three cells returns to the pre-fault level very quickly, as the fast-acting reserve in Cell 1 is responsible for the entire reserve activation in this scenario (as can be seen in Figure).

The remaining sub-scenarios exhibit the same behaviours in terms of the accurate identification of the fault location and activation of fast-acting reserves in the AGC+BRC case, therefore only the frequency and control signals (dPnet, ACE) are shown to prove the functionality across the scenarios.

3.3 Scenario 1.2 – 150 MW Imbalance located in Cell 2

In this scenario, similar to Scenario 1 when BRC is activated and enough reserves are added in the form of a current source in Cell 2, the cell responds much faster than AGC, whilst maintaining the stability of the network. With the selected reference grid parameters of the generators, under this scenario the generators are unable to provide sufficient active power reserves to fully restore the frequency, however the slower recovery compared to BRC can be observed and a final recovery of the frequency can be assumed if enough reserves were available from the conventional generation providing AGC. This fast reaction of BRC control also helps to marginally reduce the nadir point of the frequency, therefore contributing to maintain a more stable grid and reducing the risk of possible tripping of under-frequency relays that could increase the magnitude of the imbalance event.

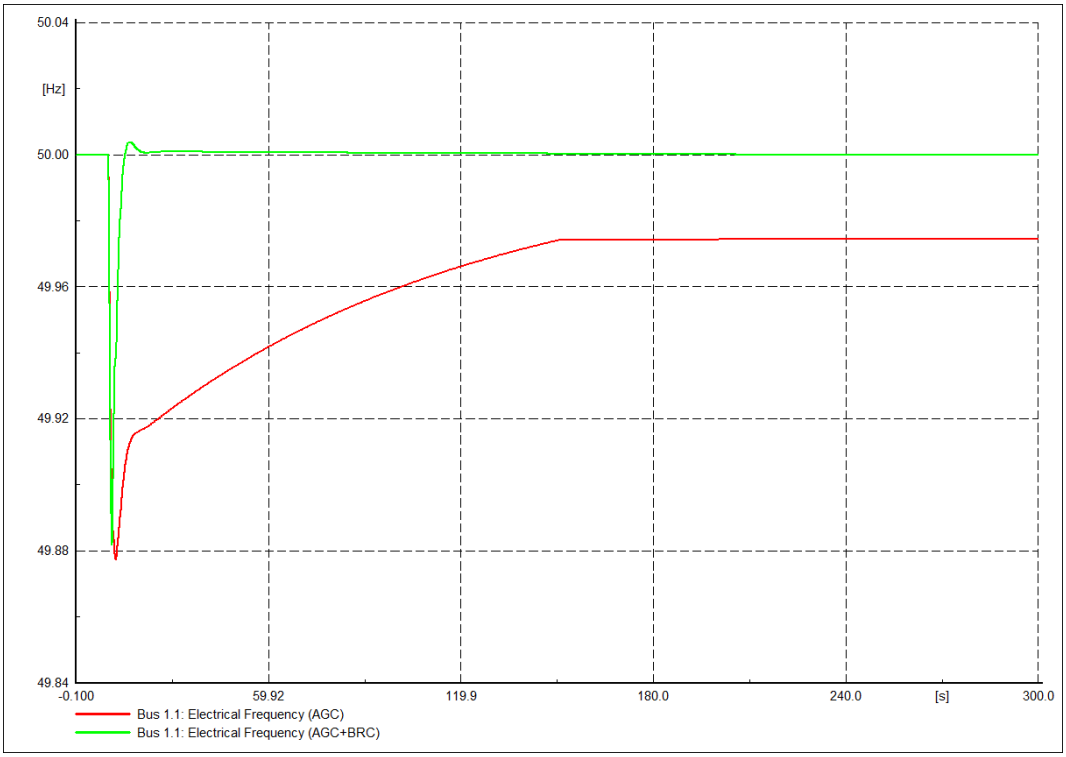

Figure 21: Frequency response of AGC and AGC+BRC with imbalance in Cell 2

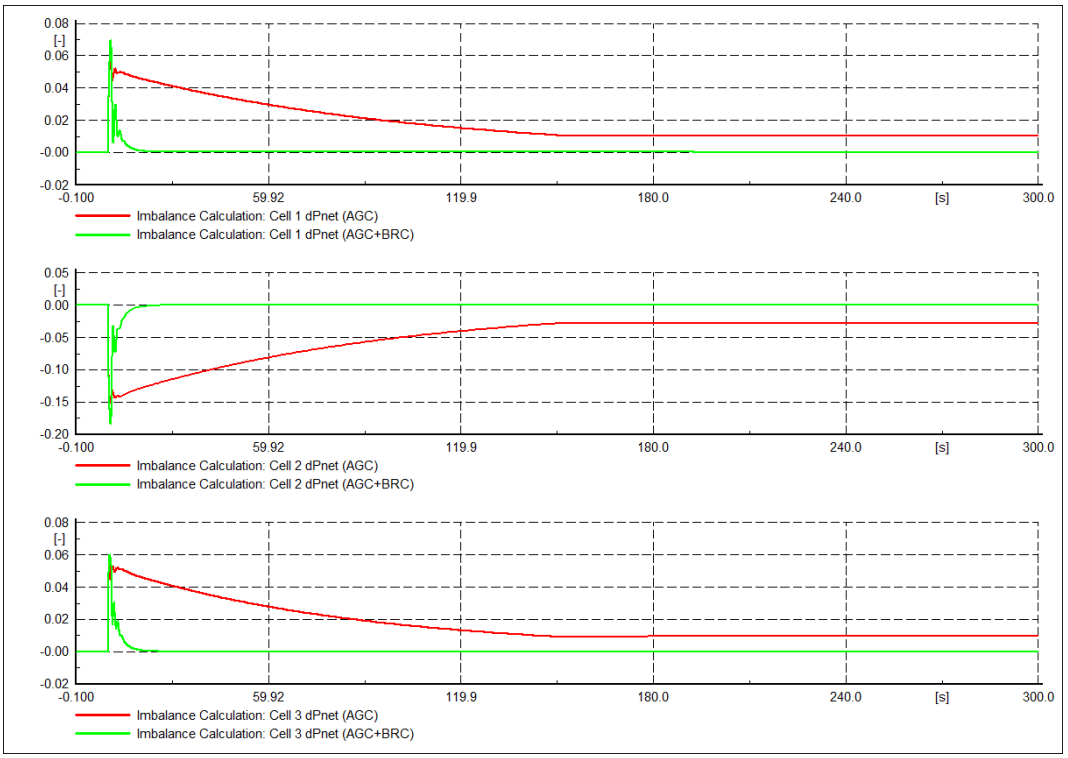

Figure 22: dPnet signals (in p.u.) of three controllers with imbalance in Cell 2

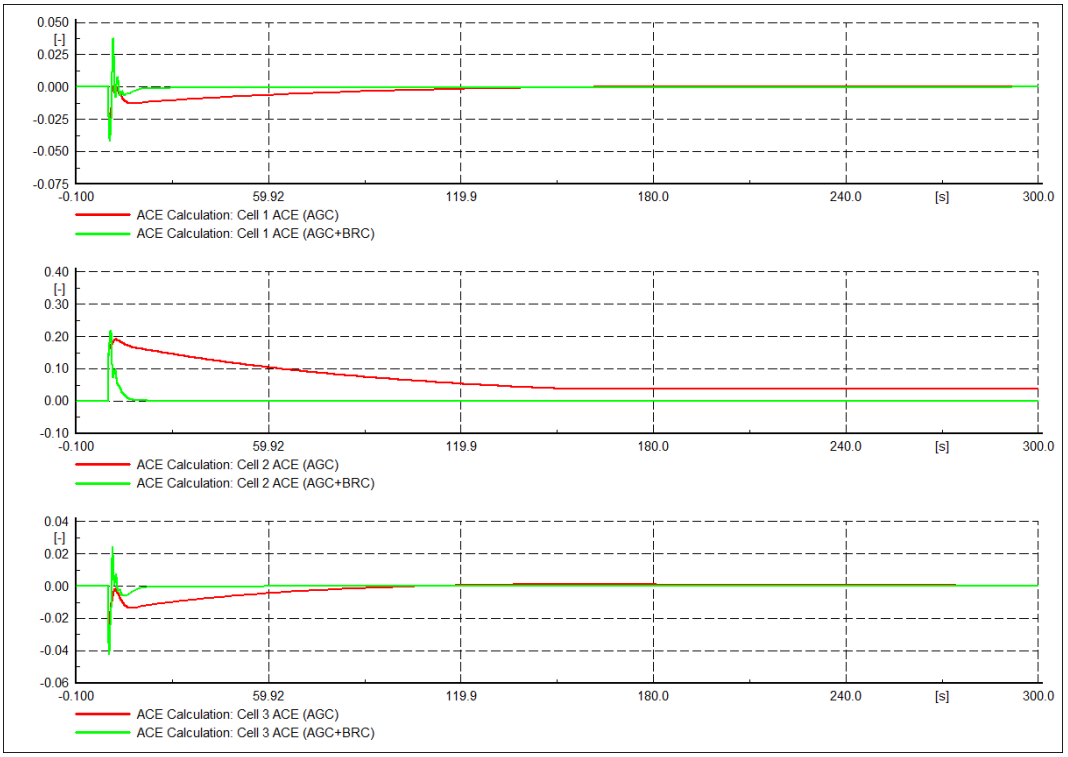

Figure 23: ACE signals (in p.u.) of three controllers with imbalance in Cell 2

3.4 Scenario 1.3 – 150 MW Imbalance located in Cell 3

The Figures shown under this scenario reinforce the robust operation of BRC for an event located in Cell 3. Therefore, it can be concluded that, independent of the area where the event takes place, the controller is capable of correctly detecting the imbalance and activating a local response – taking advantage of fast-acting RES and demand-side resources – which enables the grid to rapidly return to steady state conditions.

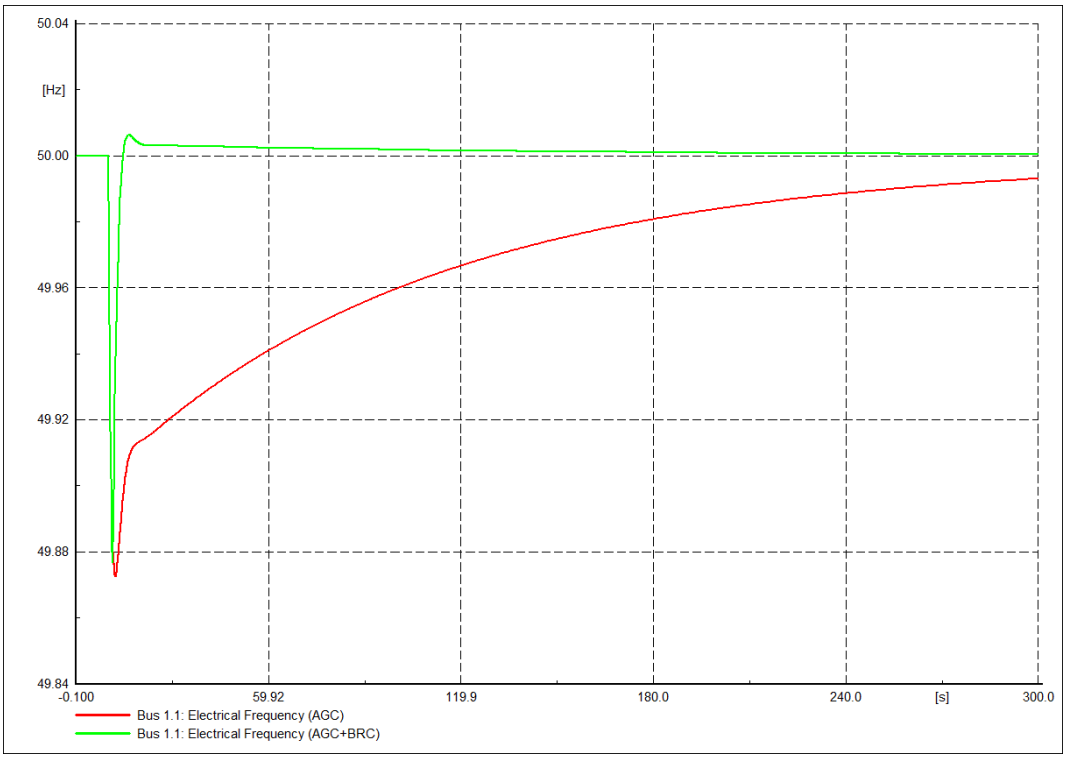

Figure 24: Frequency response of AGC and AGC+BRC with imbalance in Cell 3

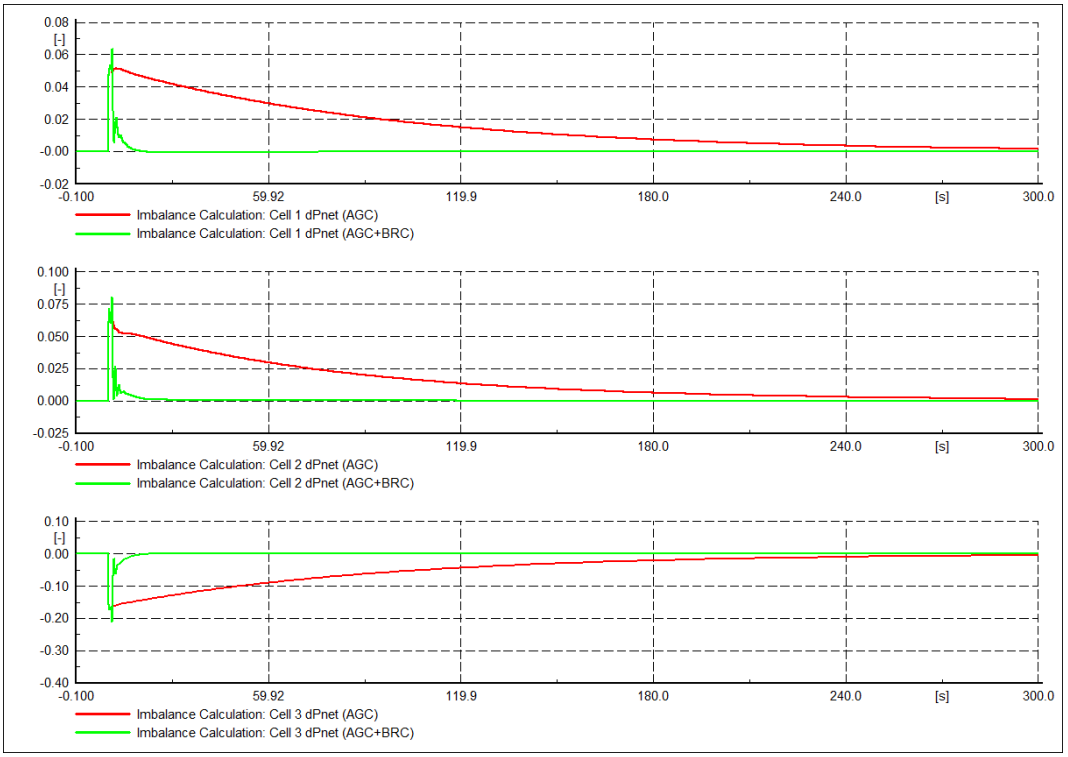

Figure 25: dPnet signals (in p.u.) of three controllers with imbalance in Cell 3

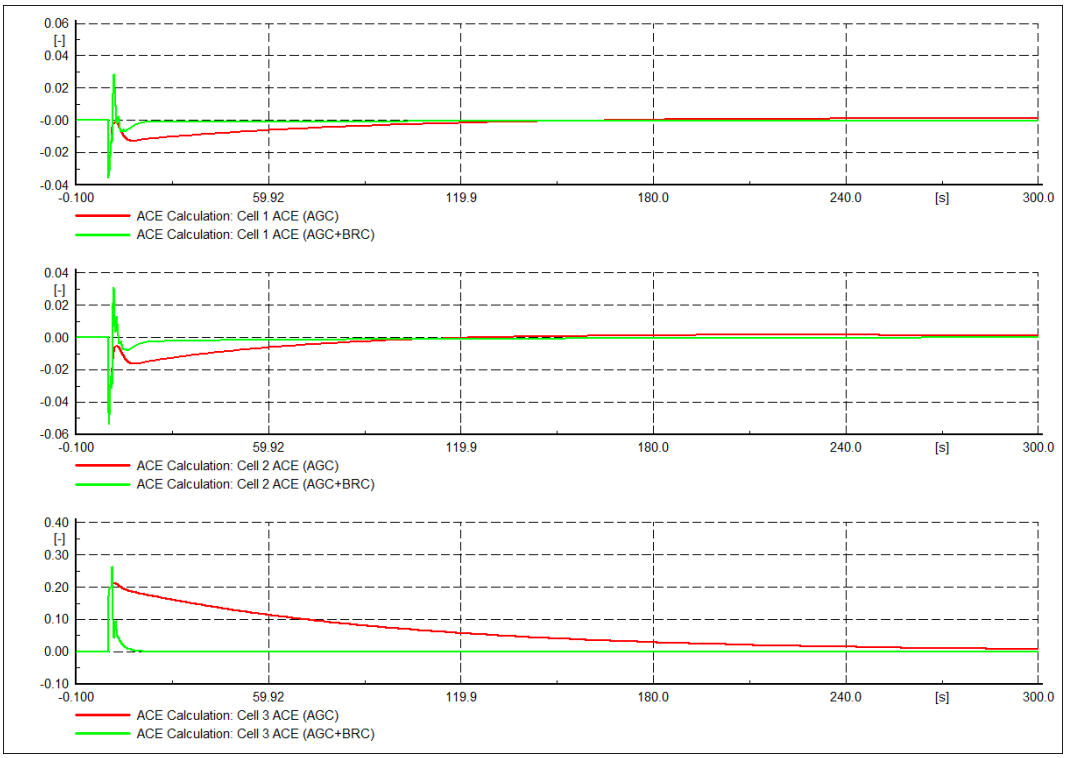

Figure 26: ACE signals (in p.u.) of three controllers with imbalance in Cell 3

3.5 Scenario 2 – 50% RES, 6 Synchronous Generators

In this case a future-oriented scenario has been tested where faster dynamics are expected and therefore more challenging conditions for the controller are expected. Therefore, two of the synchronous generators in Cell 1 are switched out of service – leaving two synchronous generators in each of Cell 1, Cell 2 and Cell 3. In this scenario, 50% of the active power demand is met by renewable energy sources in the form of wind turbines models. The complete test system is shown in Figure .

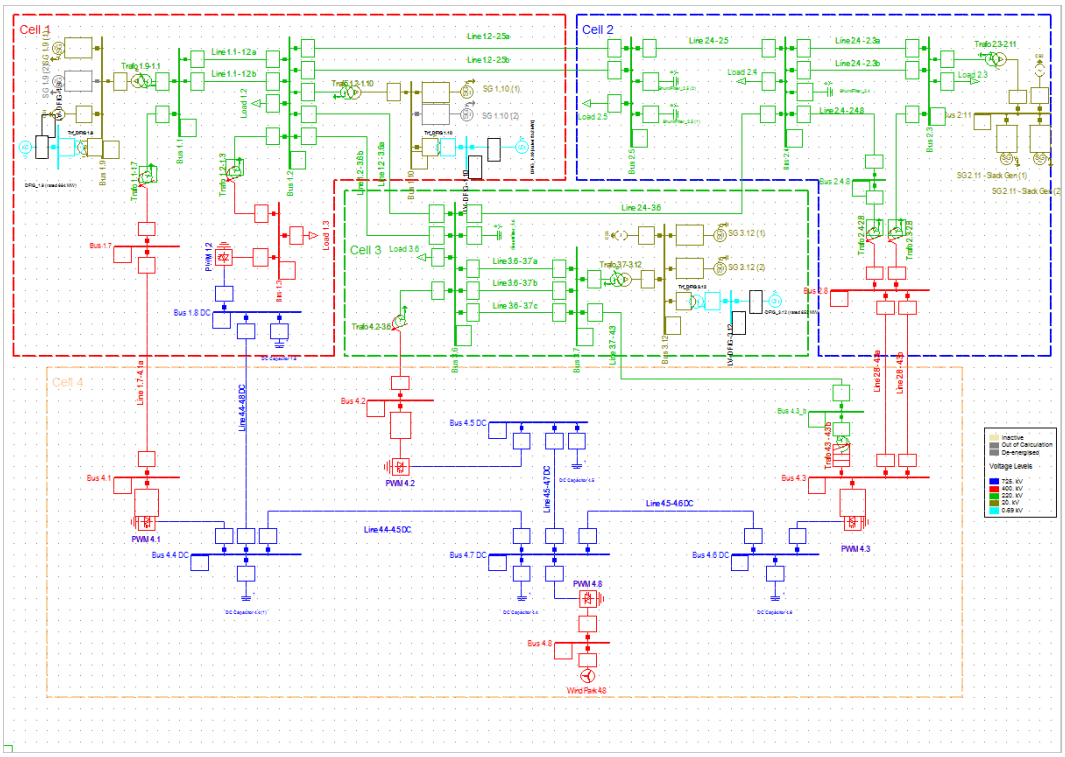

Figure 27: Test system with Cell 4 energised and two synchronous generators out of service for Scenario 2

3.6 Scenario 2.1 – 150 MW Imbalance located in Cell 1

In comparison with Scenario 1 it can be observed from Figure that the maximum frequency deviation is larger in this case due to the reduced inertia of this scenario caused by the increased RES penetration. Even with these characteristics, the BRC algorithm appears to perform as expected, reducing the maximum frequency deviation (nadir) as a result of the fast event location and activation of fast-acting resources, and accordingly rapidly recovering the system frequency to its nominal value.

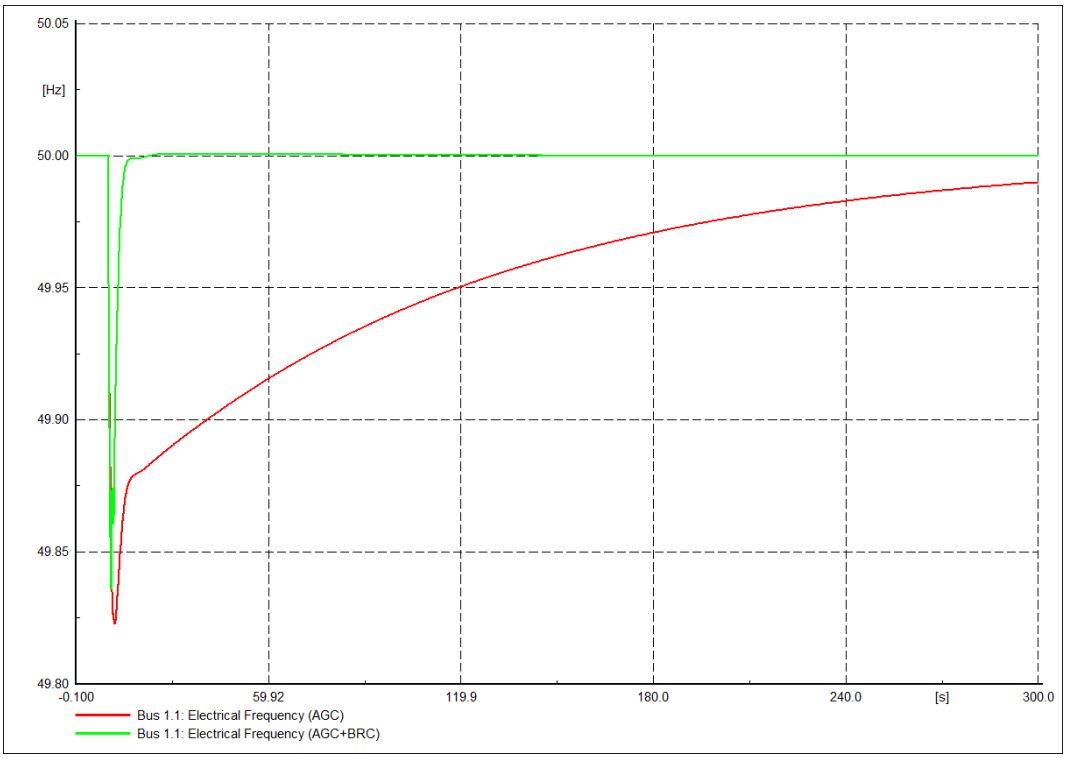

Figure 28: Frequency response of AGC and AGC+BRC with imbalance in Cell 1

Figure and Figure show the behaviour of the area and controller as for Scenario 1, in this case the location is correctly located and appropriately only the area with the imbalance responds to the event.

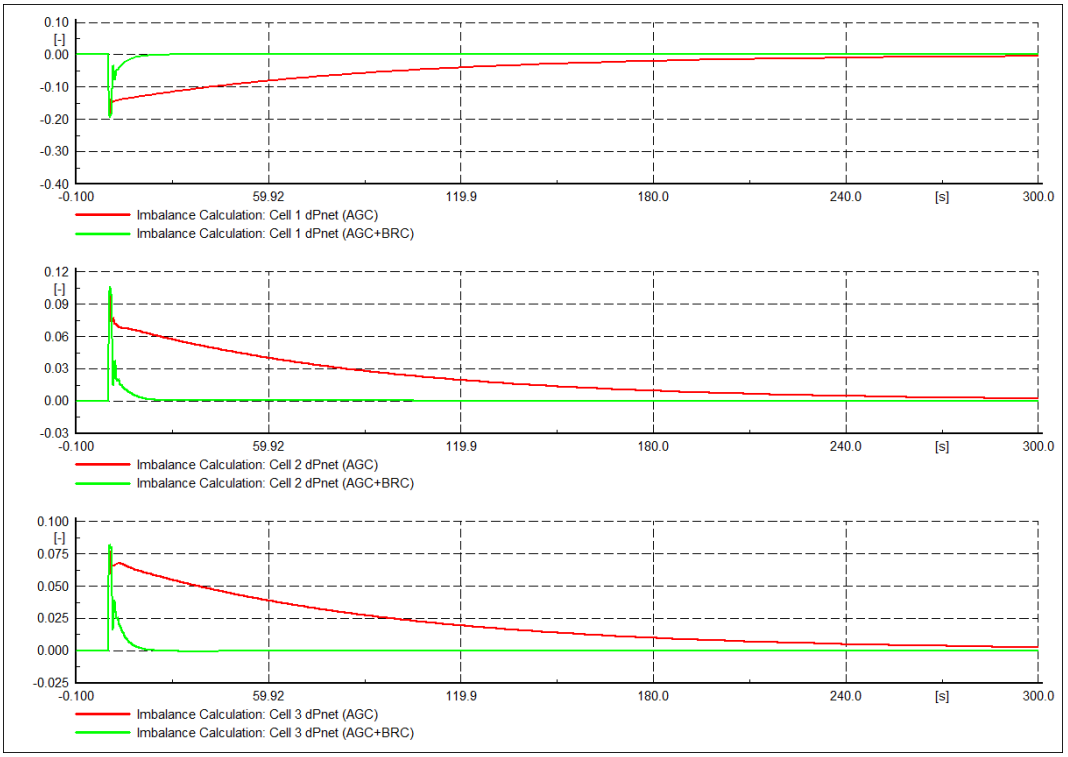

Figure 29: dPnet signals (in p.u.) of three controllers with imbalance in Cell 1

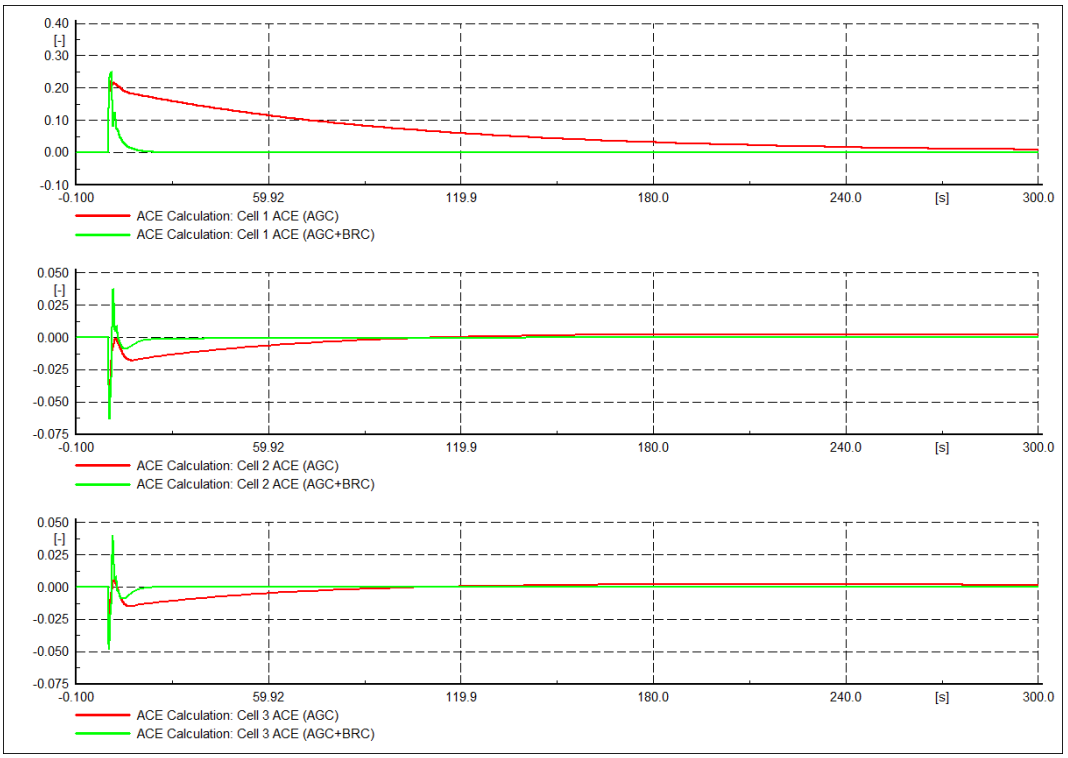

Figure 30: ACE signals (in p.u.) of three controllers with imbalance in Cell 1

3.7 Scenario 2.2 – 150 MW Imbalance located in Cell 2

The imbalance experienced at Cell 2 has also been successfully located and corrected with the BRC control in a faster manner compared with conventional AGC as shown on the following Figures.

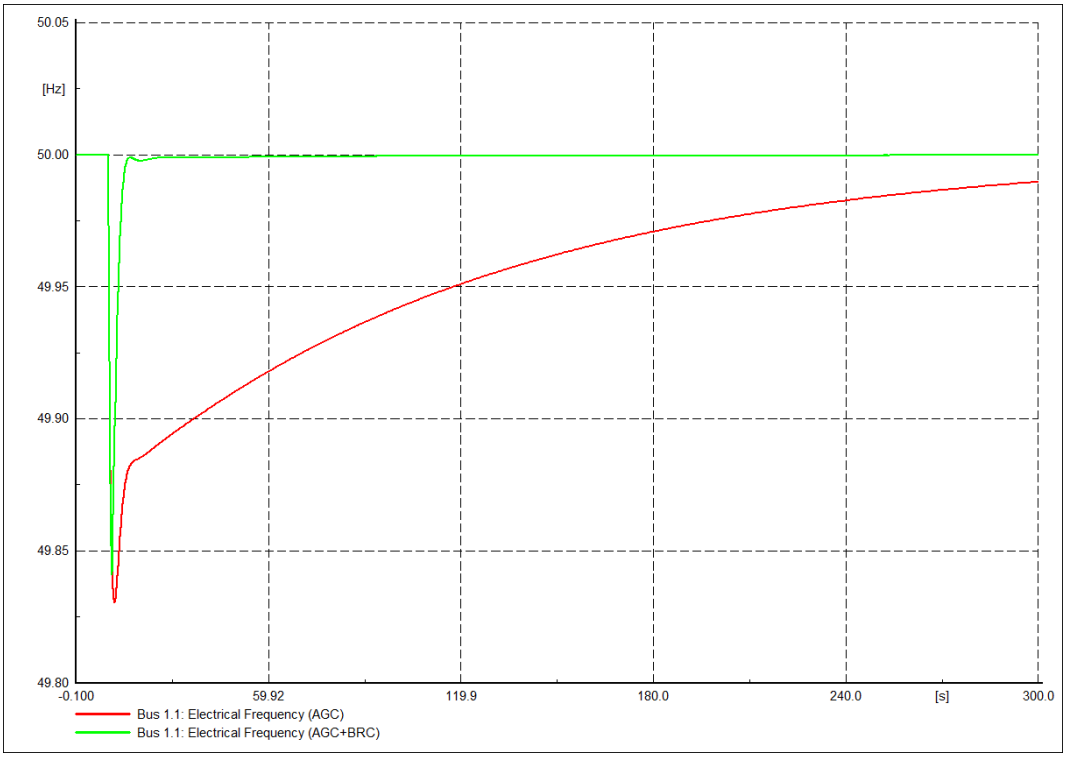

Figure 31: Frequency response of AGC and AGC+BRC with imbalance in Cell 2

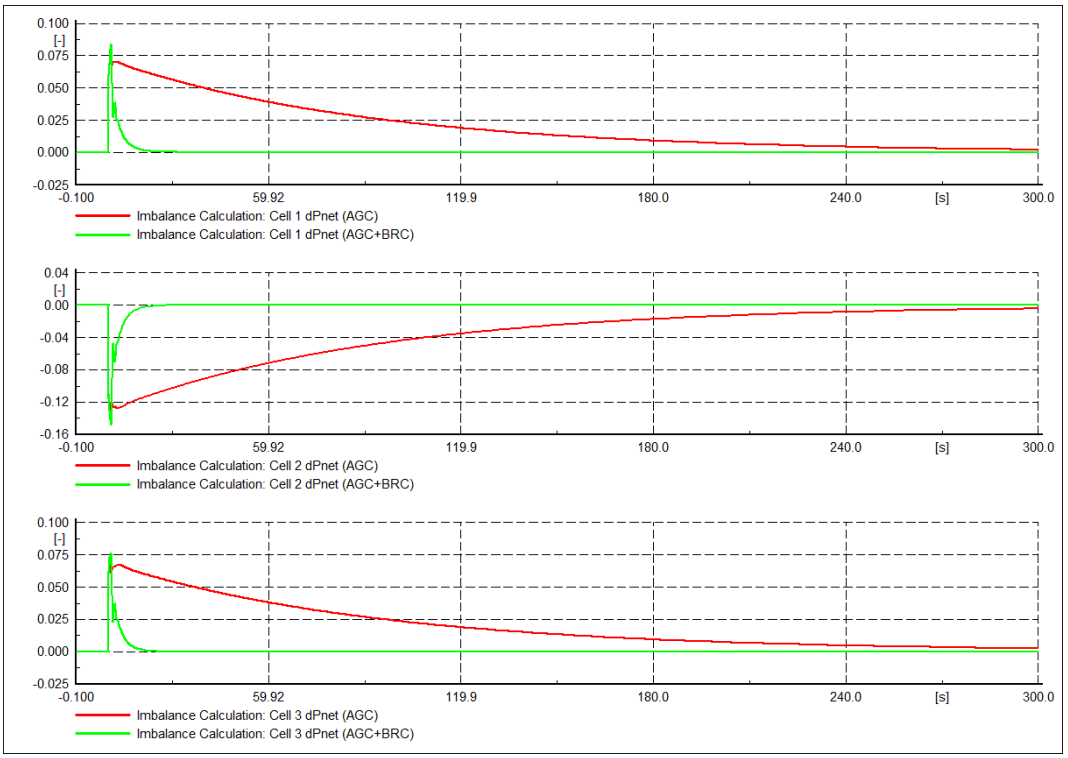

Figure 32: dPnet signals (in p.u.) of three controllers with imbalance in Cell 2

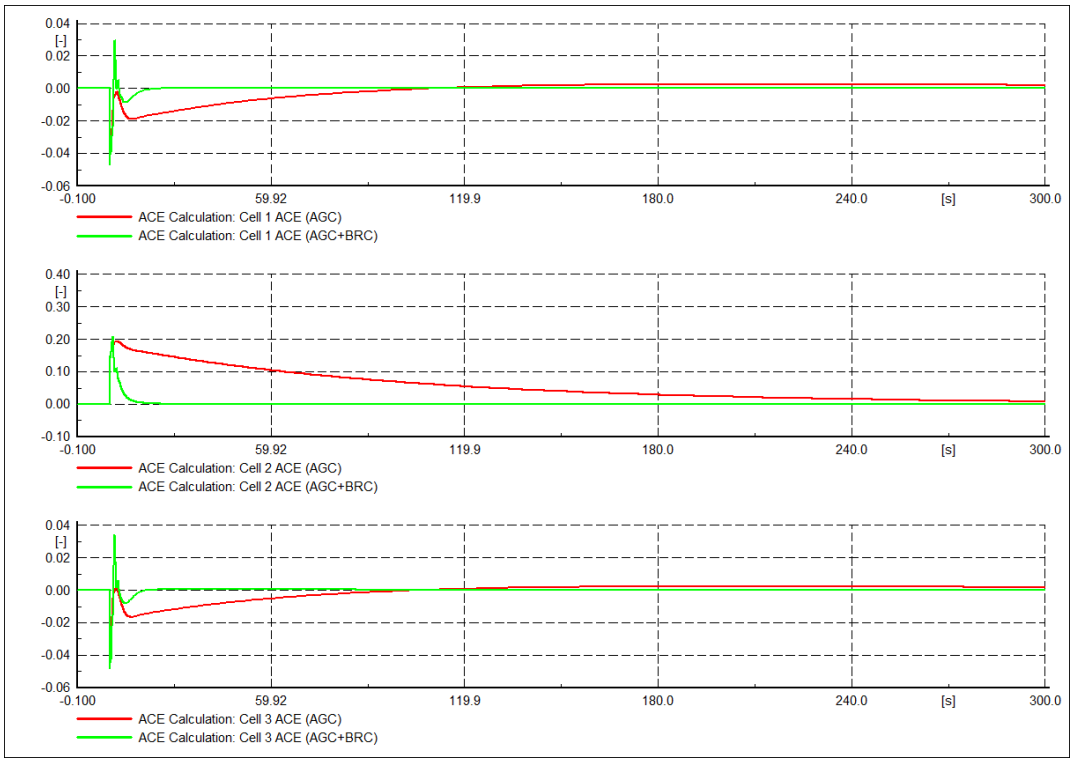

Figure 33: ACE signals (in p.u.) of three controllers with imbalance in Cell 2

3.8 Scenario 2.3 – 150 MW Imbalance located in Cell 3

Similarly to Scenario 2.2, the imbalance experienced at Cell 3 in this case has also been successfully located and corrected with the BRC control in a faster manner compared with conventional AGC as shown on the following Figures.

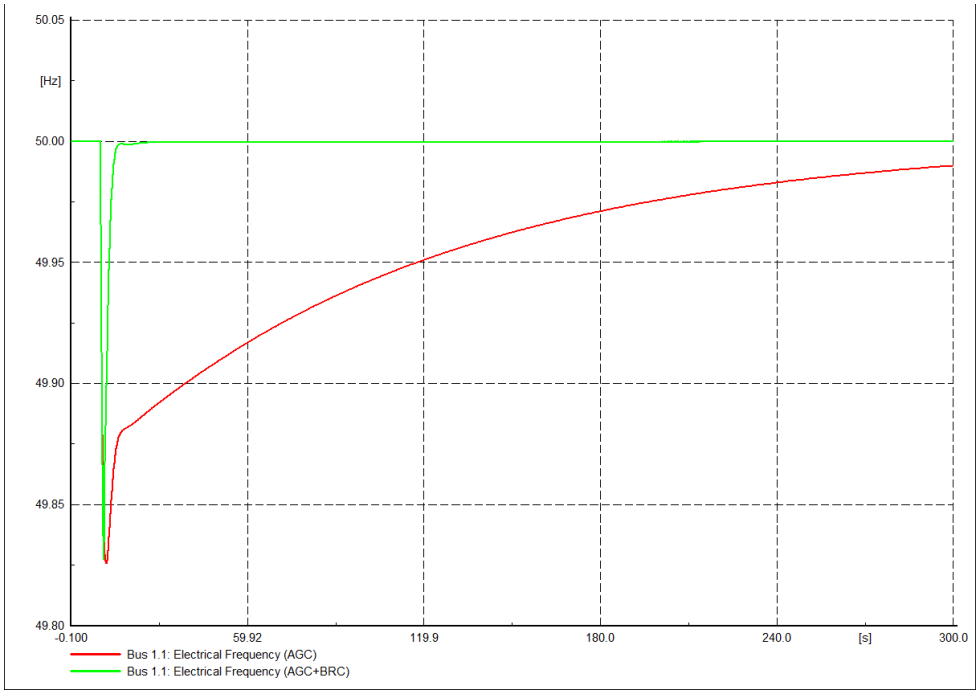

Figure 34: Frequency response of AGC and AGC+BRC with imbalance in Cell 3

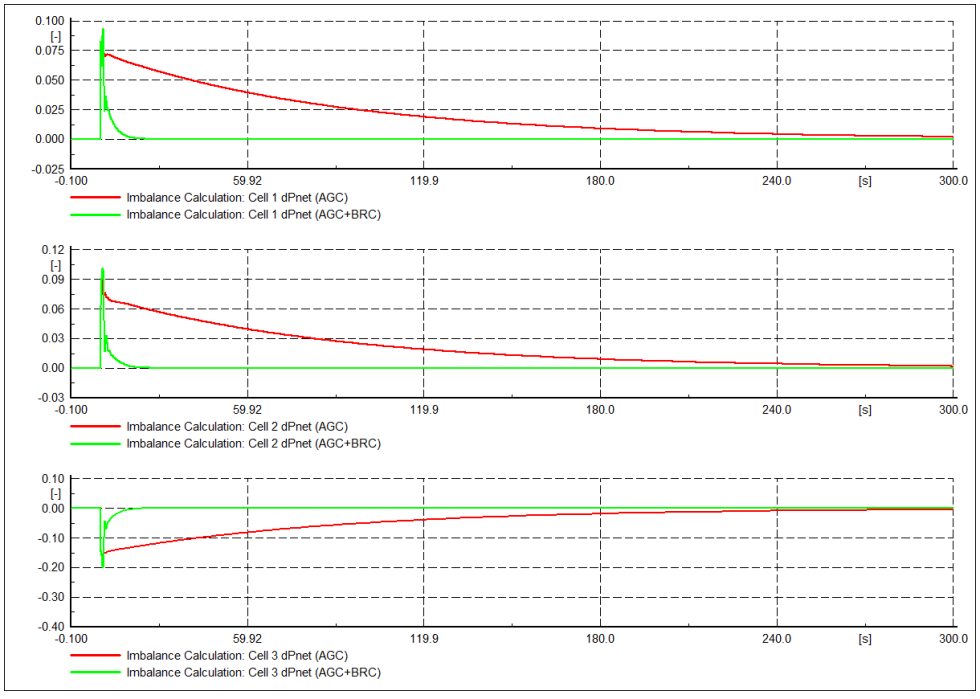

Figure 35: dPnet signals (in p.u.) of three controllers with imbalance in Cell 3

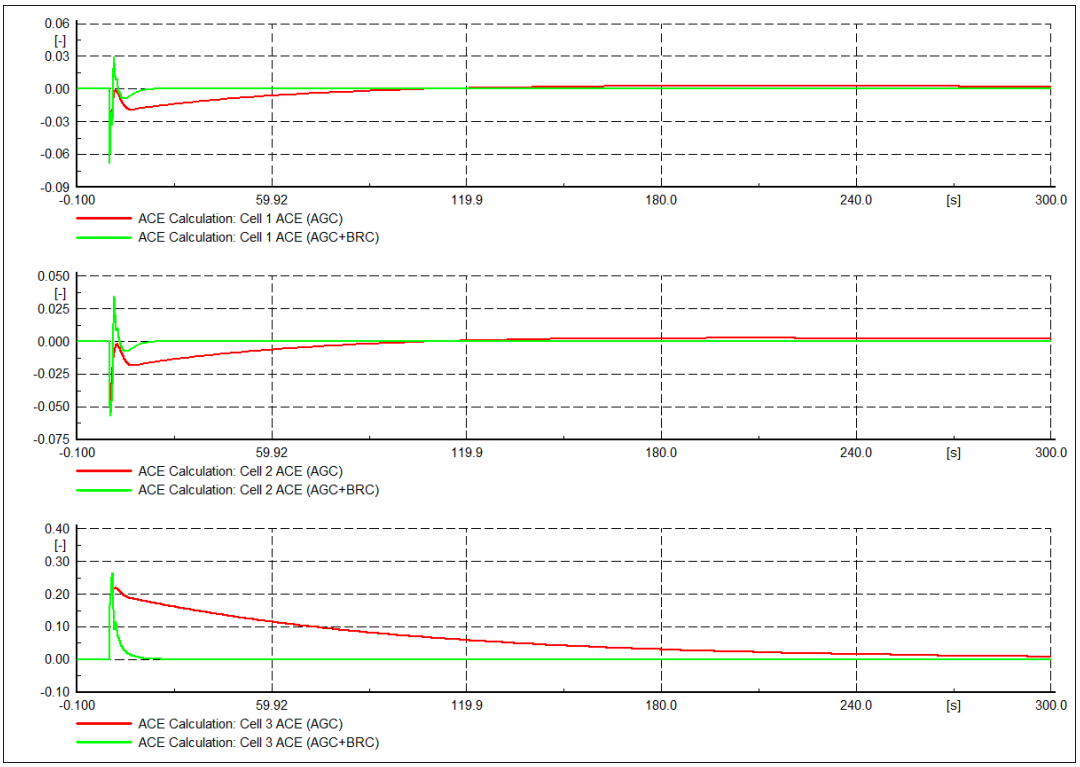

Figure 36: ACE signals (in p.u.) of three controllers with imbalance in Cell 3

4. Summary and Conclusion

The results presented in this annex show how the BRC controller successfully achieves improved frequency recovery under a range of test scenarios and imbalance events in the test system. By splitting the reserve control signal between slow-acting AGC control and fast-acting BRC control, and actuating an AC current source to emulate fast reserves, the improvement in the speed of frequency recovery is notable. The BRC controller's ability to successfully identify the circumstances under which the fast-acting reserves should be activated or remain inactive has been shown. The key benefits of BRC which have been demonstrated, including improved frequency response and the ability to leverage a multitude of distributed RESs, are compelling reasons in support of the Web-of-Cells "solve local problems locally" concept developed within the ELECTRA project.

References

[1] CIGRÉ Working Group 14.07 / IEEE Working Group 15.05.05, Guide for Planning DC Links Terminating at AC System Locations Having Low Short-circuit Capacities I, CIGRÉ Report 68, 1992.

ANNEX 4: Balance Steering Control (BSC)

1 Introduction

This report describes the validation of the Balance Steering Control (BSC) Use Case (UC) as a stand-alone implementation. The implementation and testing of the BSC Use Case was done by using the CIGRE MV reference grid, which was selected among the ELECTRA partners as one of the two main Single-Reference Power Systems (SRPS). The main functionality investigated in these simulation tests can be summarised in the deactivation of BRC resources (corrective BSC) after imbalances that take place in different cells of the system. The goal of these tests is to show that the control functions involved in the UC, namely CellSetpointAdjusting (CSA) and TieLineLimits (TLL), are able to cope with the imbalances happening in the system in a secure (in terms of stability) way and effectively change the set-points of the tie-lines power in order to reduce the activation of BRC reserves. Evidently, despite the fact that these tests refer to a standalone investigation of the UC, it was necessary to assume the existence of simplified form of BRC and FCC controllers in the system because, in principle, BSC is a subset of functions related to BRC and is not a standalone control loop.

2 Methodology

For the needs of these tests the selected CIGRE MV grid was divided into areas (cells) delineated by the dashed lines as shown in figure 1. As it can be seen in this diagram the model is divided in 3 MV cells (Cell1-3) plus one HV area which can be considered as fourth cell not actively participating, however, in the BSC control. The MV cells are interconnected with each other in the configuration shown in figure 2.

The selected configuration provides sufficient complexity for the controller validation due to the number of interconnections between each two cells as well as the number of tie-lines between at least one pair of cells (cell1 and 3). Also the cells are equipped with flexible resources that all provide frequency containment control with fixed droop. For the sake of simplicity in terms of BRC usage in the tests, the only resources considered participating in the control were the storages in cell ,1 bus 5 (600kW), cell 2, bus 10 (200kW) and cell 3, bus 13 (600kW). The schedules of the tie-lines are assumed fixed for the timeframes within which the system was tested. The imbalances in all scenarios are caused by load changes in all three MV cells (buses 2, 8, and 12).

The list of loads for each bus of the system is shown in Table 1. This table is divided into three columns representing the bus number, the active power consumed at the corresponding bus as well as the reactive power injected to or absorbed from the corresponding bus. Similarly, Table 2 provides an overview of the scheduled power for each tie-line of the system as well as the maximum line capacity in terms of active power. Last but not least, Table 3 provides an overview of the Distributed Energy Resources. This information includes the bus which the DER is connected to, the type of DER the forecast/scheduled active power and the maximum power capacity of the unit.

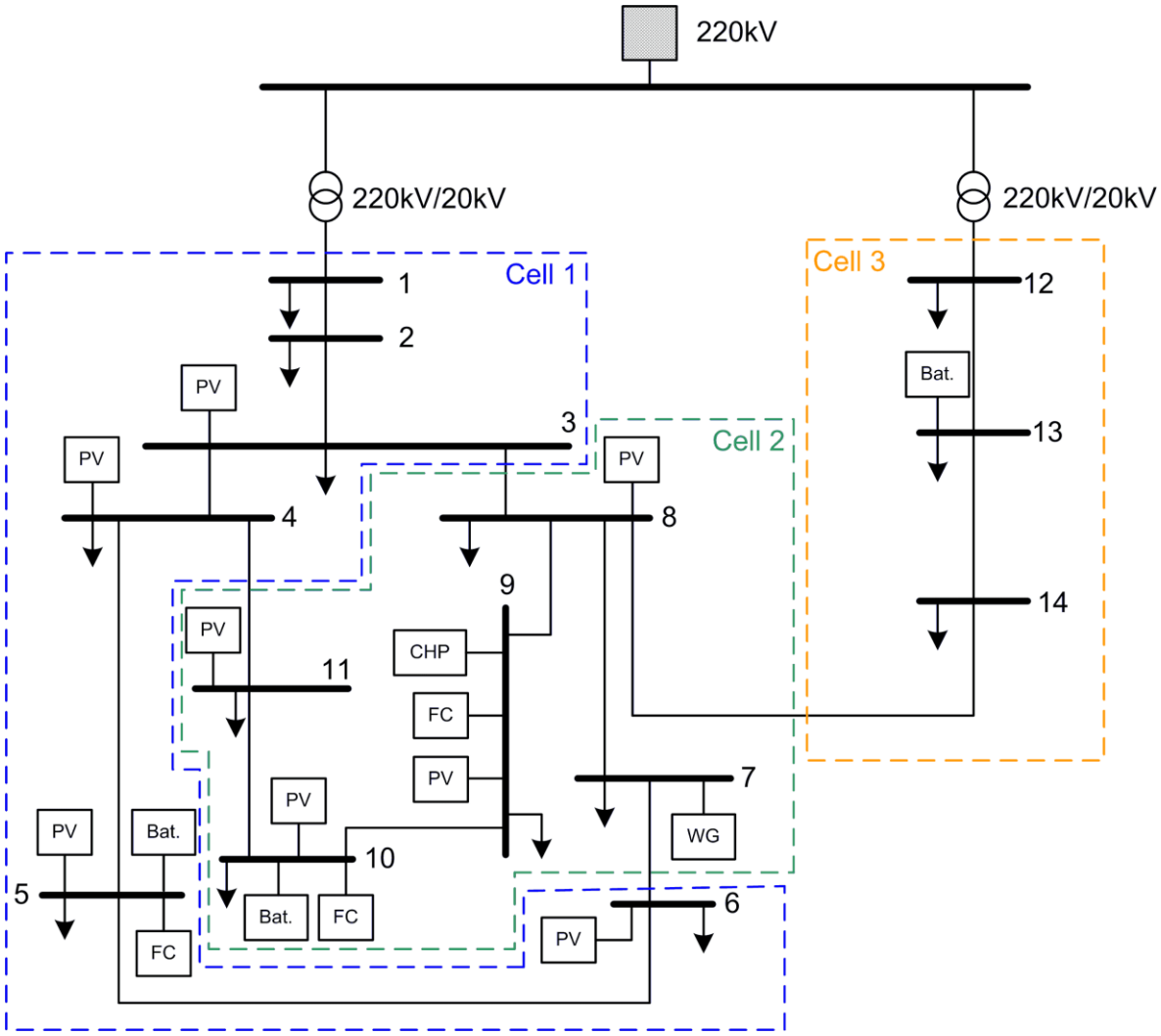

Figure 1: Selected cells' configuration for the standalone BSC validation

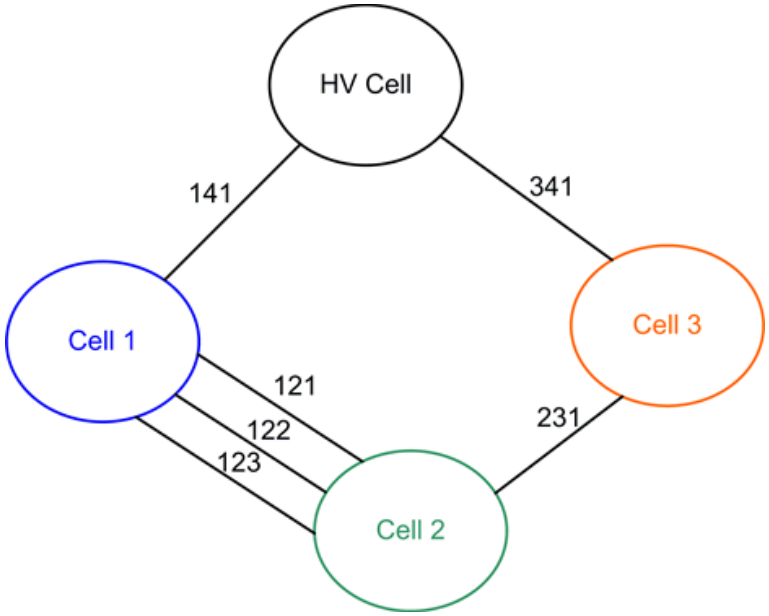

Figure 2: Interconnections between cells

Table 1: Active and reactive power load values used in the tests

Bus No.	P(kW)	Q(kVAr)
1	22,992	19,992
2	0	0
3	502	209
4	432	107
5	728	180
6	550	136
7	76.5	48
8	587	145
9	574	358
10	543	160
11	330	82
12	19,482	5,858
13	34	21
14	540	258

Table 2: Tie-line schedules and capacities

Line	Schedule (kW)	Capacity (kW)
121	200	1,000
122	375	1,000
123	-1,002	2,000
141	-24,556	40,000
231	-588	1,000
341	-20,631	40,000

Table 3: Active power of all distributed resources

Bus No.	Type	P(kW)	Capacity(kW)
3	PV	20	20
4	PV	20	20
5	PV	30	30
5	Battery	0	600
5	FC	10	33
6	PV	30	30
7	WG	1,450	1,500
8	PV	30	30
9	CHP	200	310
9	CHP-FC	100	212
9	PV	30	30
10	PV	40	40
10	Battery	0	200
10	FC	10	14
11	PV	10	10
12	Battery	0	600

3 Simulation results

The simulation tests are divided into four scenarios each of which focuses on a different aspect of the BSC functionality. Therefore, scenarios are assumed for the investigation of the controller behaviour under the influence of nearly equal imbalances (scenario 1), the response to the same imbalances when the set-point is changed with some time delay between two cells (scenario 2), the response of the controller under two different imbalances (scenario 3) and, last but not least, the response of the controller to a case where a tie-line is saturated due to utilisation of its maximum allowable capacity (scenario 4). It is worth noting that some of the scenarios were selected in order to validate the correct negotiation among the CellSetpointAdjusting (CSA) controllers of each cell (scenario 1 and 3), whereas, some scenarios (mainly, 2 and 4) were intended to highlight the impact that the controller has on the system stability, especially when it comes to frequency and power balance. Therefore, for each scenario we investigate the output of the control function, as well as the frequency/balance response of the system. In the next pages, the exact details of the selected scenarios together with the corresponding test results are presented.

3.1 Scenario 1: symmetrical imbalances

In this case two subsequent imbalances in cells 1 and 2 were examined. The size of the load changes in the cells are approximately equal, namely 160kW but of opposite sign since at t=100 s the load at bus 2 increases and, subsequently, the load in cell 2 (bus 9) decreases at t=400 s by the same amount. The sensitivity of the CSA was selected to measure the BRC output approximately after 130s from its activation. The load changes over time that cause the disturbances are depicted in figure 3. Figure 4, shows the behaviour of all three BRC controllers. It is evident that aside from any transient activation of all three controllers, only cell 1 remains steadily active after the first imbalance and the BRC controller of cell 2 is permanently activated only after the second imbalance. In terms of negotiation, after the first imbalance at t=100 s and after the delay time of approximately 130 seconds elapses cell 1 generates a request signal for its tie-lines power change corresponding to the values below:

Power Change (kW)	Tie-line ID
28.48	121
22.25	122
106.90	123
157.60	141

In other words, the cell 1 controller requests an incoming power increase by approximately 158 kW by cell 2 or the same amount by cell 4 which, of course, does not participate in the control procedure. This correction amount is equal to the imbalance happened in the cell. After the second imbalance in cell 2 and once the BRC2 output has stabilized, the controller of cell 2 responds with an acceptance for set-point changes based on the values below:

Power Change (kW)	Tie-line ID
27.55	121
21.52	122
103.40	123

The total change is approximately 153 kW and at t=570 sec the CSA of the two cells settle on the new set-point and immediately implement the values leading to complete deactivation of all BRC reserves in cell 2 and almost completely in cell 1. It is worth noting that throughout this procedure the balance of cell 3 remains unaffected and the frequency and balance of all cells (fig. 5 and 6) present no steady-state deviation from the reference values. Also, the dynamic response of both the frequency and imbalance show that the system does not present any significant deviations or oscillations that could jeopardise the dynamic stability.

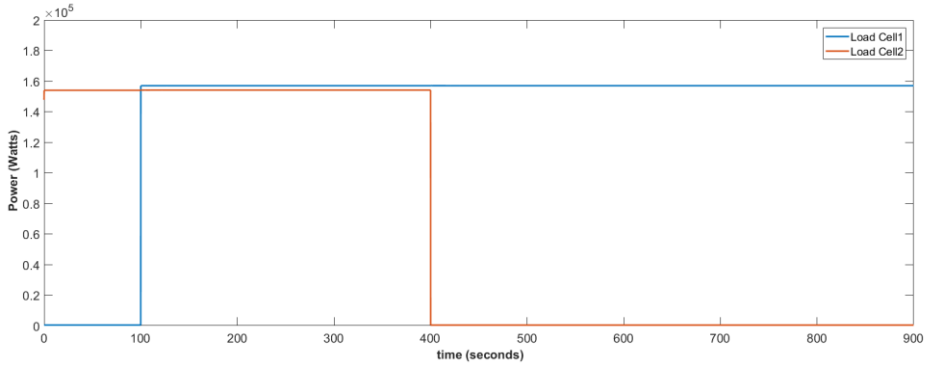

Figure 3: Load variations for scenario 1

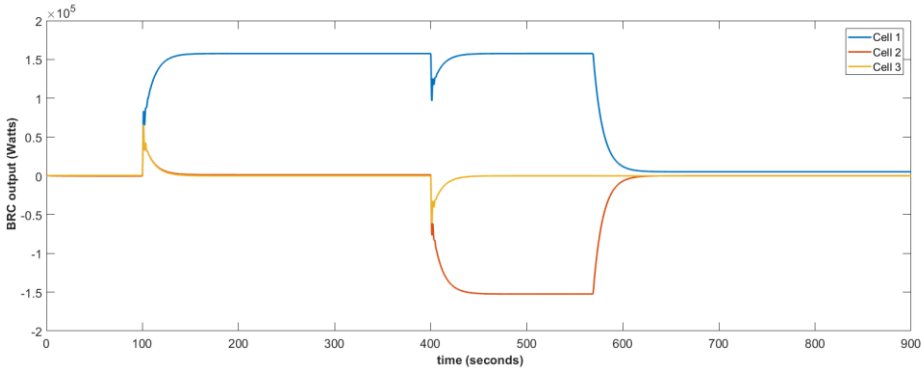

Figure 4: BRC output due to imbalances and deactivation of resources for scenario 1

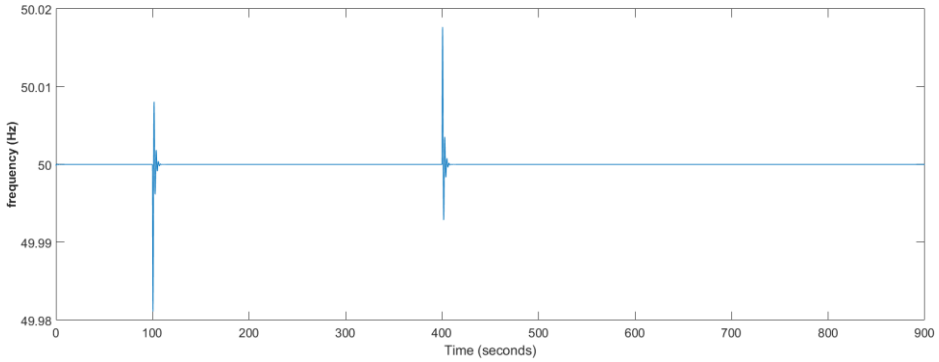

Figure 5: Frequency response for scenario 1

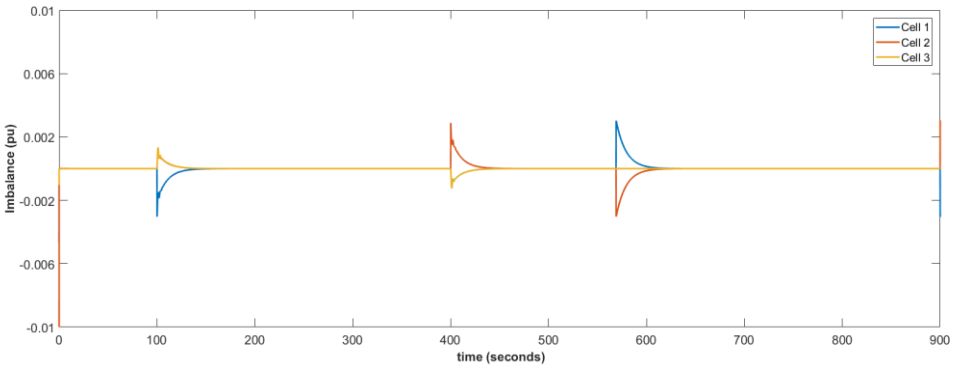

Figure 6: Imbalance response (50MW base power) for scenario 1

3.2 Scenario 2: time-delayed implementation

This scenario is a slight variation of the previous one with the only difference that the implemented set-point change takes place with a time delay of 2 seconds between the two cells. This scenario was used in order to assess the stability of the system to such a case in which synchronism of the set-point variation could be an issue. As a result, and by contrast to the frequency response shown in Figure 5, the frequency response in Figure 7 shows a small fluctuation at t=570 sec, the time when the set-points are changed. However, this deviation is rather insignificant and shortly afterwards the frequency is restored back to its nominal value while the BRC outputs as shown in figure 8 are deactivated as expected.

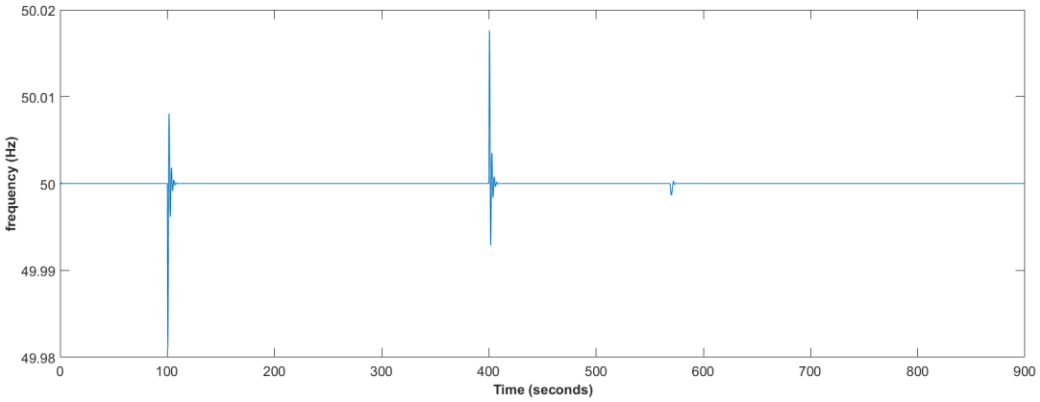

Figure 7: Frequency response for scenario 2

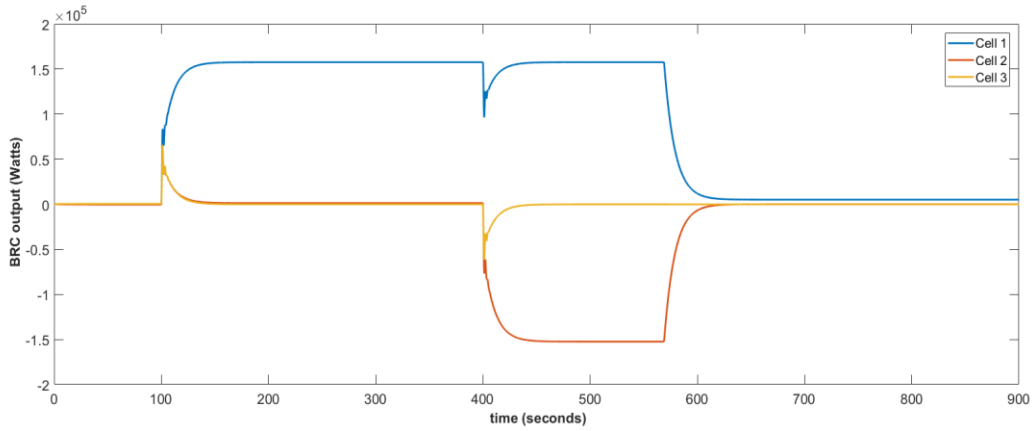

Figure 8: BRC output due to imbalances and deactivation of resources for scenario 2

3.3 Scenario 3: Asymmetrical imbalances

This scenario shows the behaviour of the system under asymmetrical imbalances that lead to partial deactivation of BRC resources. In fact, asymmetries were also noticed in Scenario 1 but the difference between imbalances was rather negligible. In this case the initial imbalance caused in cell 1 is 300 kW and the subsequent one is cell 2 is remains the same (160kW) as shown in Figure 9. As a result of a similar to Scenario 1 procedure, after t=570 seconds there is a complete deactivation in the BRC reserves of cell 2 and partial deactivation of those in cell 1 (Figure 10). Also, the frequency remains stable at 50Hz after the correction (Figure 11).

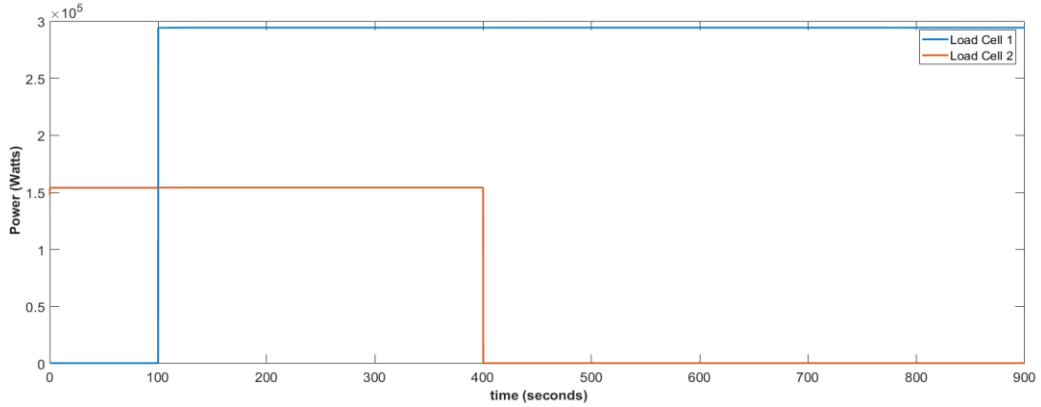

Figure 9: Load variations for scenario 3

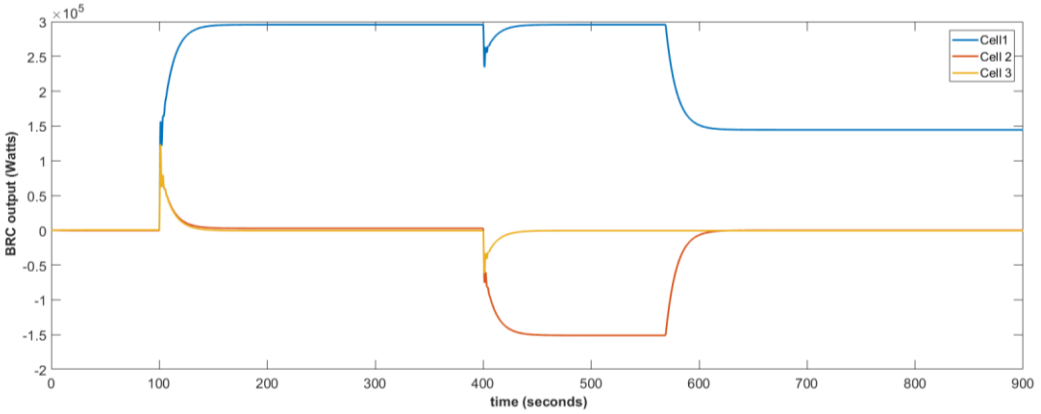

Figure 10: BRC output due to imbalances and deactivation of resources for scenario 3

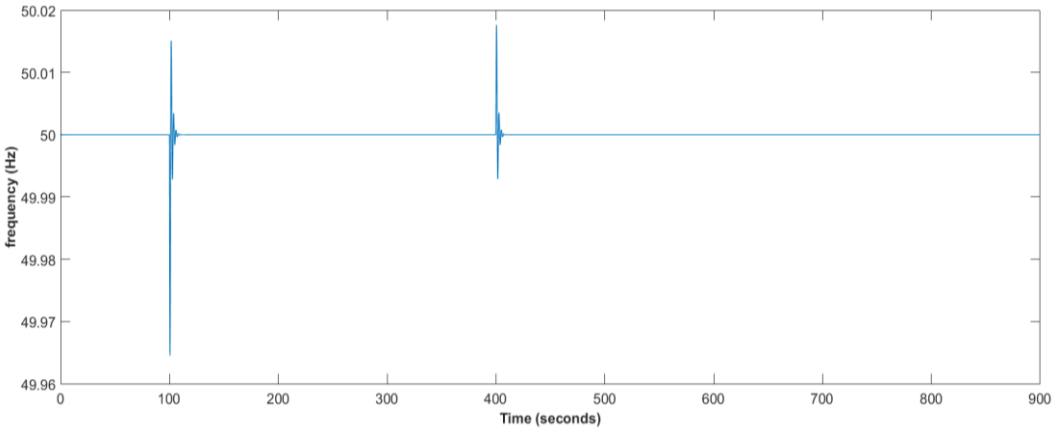

Figure 11: Frequency response for scenario 3

3.4 Scenario 4: Tie-line capacity violation

This scenario is used in order to assess the controller's performance under violation of the tie-lines' limits. To this end, we assume the same configuration and load disturbances as in scenario 1. The basic difference in this scenario is that the capacity of tie-line 121 is only 250 kW. Moreover, the initial operating schedule remains the same (200 kW) while the CSA is equipped with a limit calculation set to 80% of each line's capacity. This means that the specific tie-line already operates at 80% of its maximum allowable power and it cannot accommodate any further increase of power by the CSA. It is worth noting that the 80% limits were selected so that the line maintains a margin of 20% for changes of power during dynamics. Based on these assumptions the load step change in cell 1 leads to the following correction request:

Power Change (kW)	Tie-line ID
2.10	121
26.79	122
128.70	123
157.60	141

It is obvious that the request from tie-line 121 is nearly zero whereas lines 122 and 123 increase their contribution to the correction compared to Scenario 1. By contrast, tie-line 141 request remains unchanged. The BRC output responses and frequency of the system are shown in figures 12 and 13.

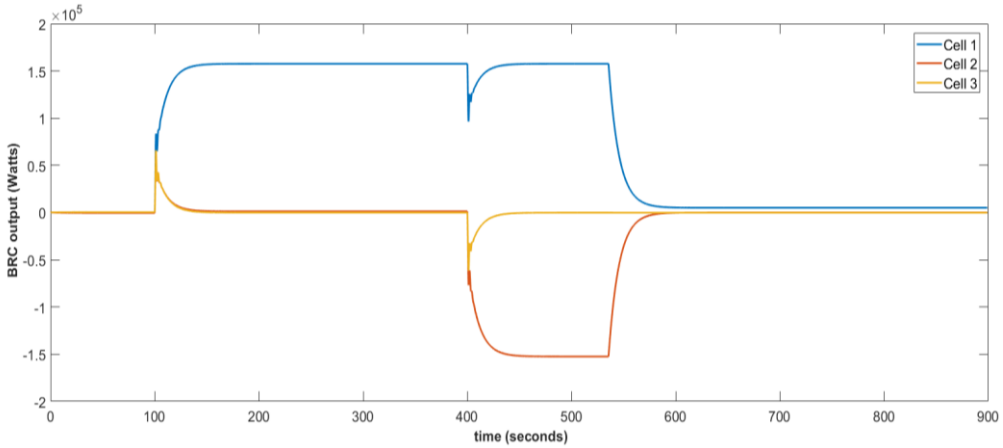

Figure 12: BRC output due to imbalances and deactivation of resources

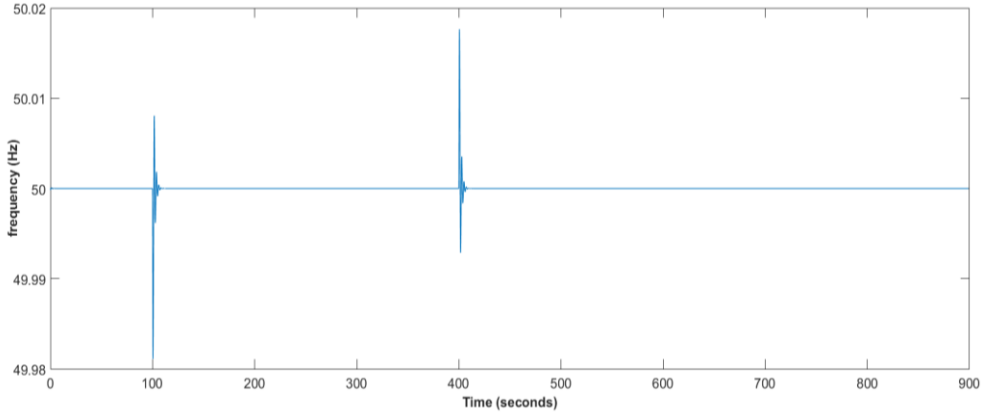

Figure 13: Frequency response

4 Summary and conclusion

In this report the implementation and validation of the stand-alone BSC UC is presented. The validation was based on simulation tests using the modified CIGRE MV reference grid in Matlab/Simulink and in a configuration of four cells. In order to examine the controller behaviour and the system stability, various symmetrical and asymmetrical imbalances were introduced as input disturbances. The results for these scenarios were assessed in terms of negotiation

effectiveness (controller outputs) and system stability (frequency, cell balance). Although the focus was on BSC stand-alone implementation and validation, the tests involved some simplified versions for the FCC and BRC controllers as prerequisites for the use of the BSC functions.

The results for all four implemented scenarios reveal that the proposed control concept is able to effectively negotiate the modification of tie-line set-points between cells, leading to a subsequent deactivation of BRC reserves. In all scenarios the deactivation of reserves was close to the predicted value and, as a result, the cells can effectively benefit from imbalance netting in order to reduce the use of their BRC reserves. The negotiation of the tie-line set-points does not jeopardise the stability of the system even when the set-points are changed with significant time delays or when the capacity of a tie-line is violated. Therefore, it can be safely deduced that the proposed concept and its implementation and testing highlights the benefits of the We-of-Cells concept as these are reflected on the specific control Use Case.

As further steps to the validation analysis, in the frame of ELECTRA lab-scale investigations the specific UC is being validated in conjunction with the selected ELECTRA FCC and BRC controllers in more elaborate simulation tests using the same SRPS as well as experimental validation in laboratory.

ANNEX 5: Primary Voltage Control (PVC)

1 Introduction

The purpose of this annex is to demonstrate by simulations the basic principle of primary voltage control (PVC) and the influence of short circuit impedance characteristics on the performance of this control. Different R/X ratios are tested for the same short circuit power and voltage control capability is verified. An additional, supplementary function estimating grid impedance is also investigated.

2 Methodology

In order to be able to analyze different operating conditions, the simulations have been carried out on a simple network consisting of a flexible energy source, connecting impedance and an infite bus. PVC is a Control Topology Level (CTL) 0 or CTL-1 controller, therefore it is sufficient to limit the grid model to a single component.

The flexibility source used in this example is a generic inverter-coupled energy source with full active and reactive power (PQ) controllability, which can represent a Type4 wind generator, battery storage system, VSC HVDC (voltage-source converters high-voltage direct current) terminal, or etc.

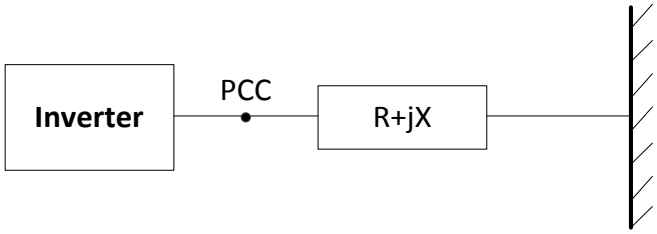

Figure 1: Reference network

The simulations were carried out with the following assumptions:

- Different X/R ratios were tested, namely X/R=5, X/R=1 and X/R=0.2 representing mostly inductive, equal and resistive networks respectively.
- PVC was set to control voltage at point of common coupling (PCC) to 1.0 pu.
- At time t=0.6 s infinite bus voltage was changed to 0.95 for 0.2 s in order to test the response of the resource to grid voltage change.
- The flexibility resource was able to provide both active and reactive power with a negligible time constant $T_s \approx 1$ ms.
- Voltage control utilized PI controller with k_p=0.6 and k_i=4.5 and no droop or line drop compensation was enabled.
- Two cases are compared, i.e. Case A with only reactive power injection and Case B with both active and reactive power injection.

3 Simulation results

3.1 Simulation of the PVC function only

Case A

After the step disturbance in grid voltage is applied the controller reacts by supplying reactive power to the grid. For the cases with X/R=5 and X/R=1 the control process is correct and after a transient the controller restores voltage at 1 pu. The amount of reactive power needed to achieve 1 pu voltage was less for a higher X/R ratio. In other words, the lower the X/R ratio, the more reactive power is necessary to maintain voltage at desired value. For the third case (X/R=0.2) the controller failed to restore voltage even though it used all available reactive power (the converter reached its current limit at 1.3 pu).

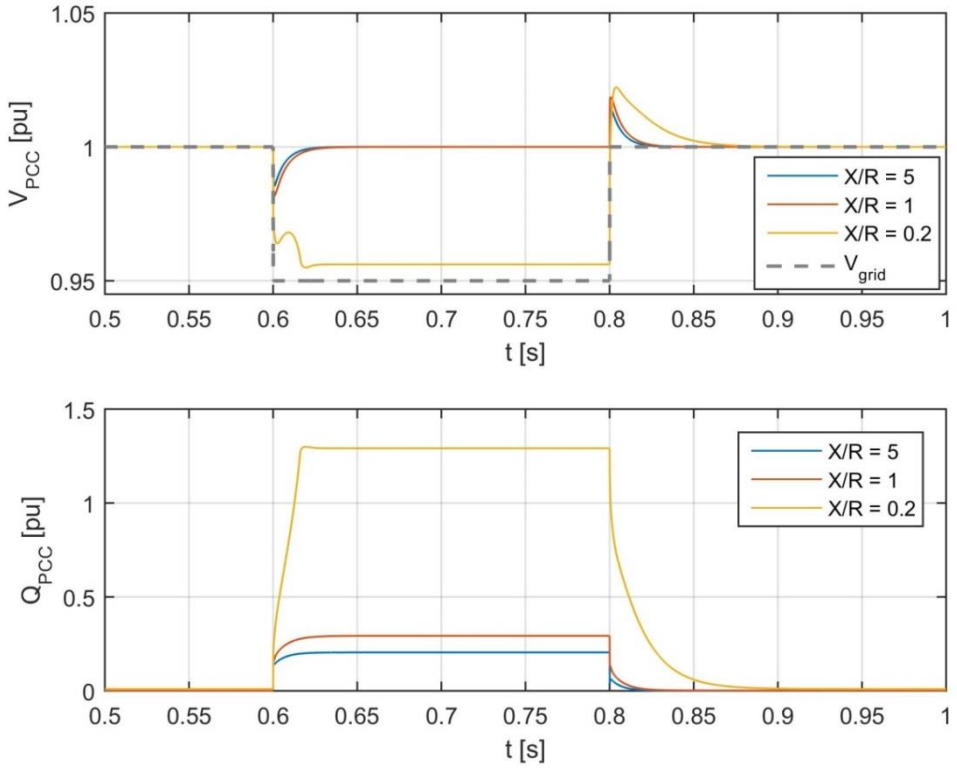

Figure 2: Simulation results for Case A

Case B

The same disturbance is applied, however in this case the controller is actively injecting both active and reactive power in order to control voltage. The amount of injected active power is proportional to the ratio of R and Z, which both are estimated by the Grid Impedance Estimation function. Additional injection of active power, even in small amounts, helps to maintain voltage at reference value, in particular for the resistive network. In order to perform on-line grid impedance estimation (GIE) locally the GIE function is proposed.

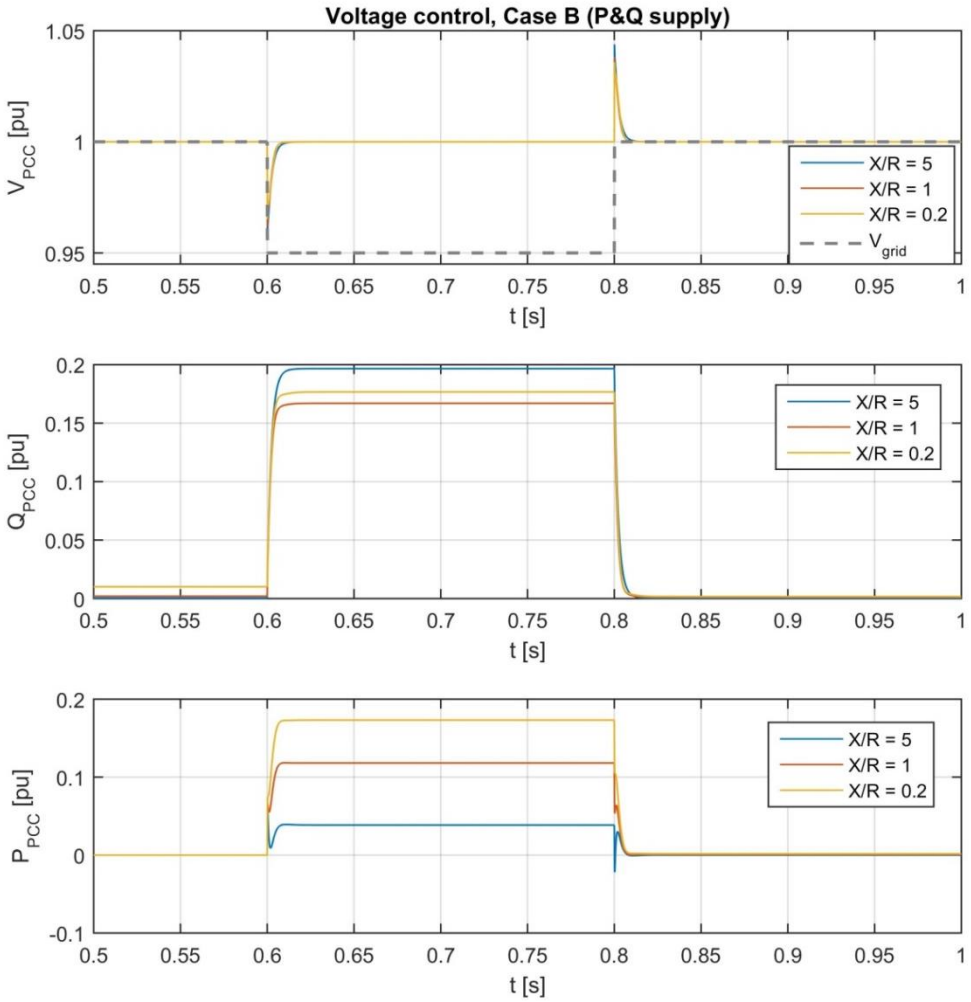

Figure 3: Simulation results for Case B

3.2 Grid Impedance Estimator Function

Grid Impedance Estimator (GIE) is a function estimating current value of complex grid impedance R+jX. GIE consists of two functions working cooperatively depending on system conditions and changes in the estimated values, i.e. grid impedance determination (GID) function and grid impedance following (GIF) function. The performance of these functions is demonstrated by simulations.

Grid impedance determination (GID)

In order to reach a unique solution of GIE estimation equations, samples from two time intervals must be acquired in such a way that during the acquisition period grid impedance and grid voltage should remain constant and the two sets of samples should differ in current generated by the power source at the generator bus. The latter can be achieved either intentionally, e.g. by the tap change action or by the controller of generator or load, or can be a result of a coincidental action such us change of generated power, etc. As a result, measurements of two different operating points are available and used for the estimation of the Thévenin impedance (R_L, X_L) and voltage ($|U_s|$, φ). This effect is presented in Fig. 4. After the initialization of the algorithm the estimates of R and X reach random solution. In order to update them the algorithm increases U_g by 2% for a short period of time at t=1 s and the new operating condition is established. Precise estimates were achieved within 60 ms. Next, at t=2 s the grid voltage U_s is suddenly reduced as an effect of some arbitrary incident in the network. This causes a huge change in the estimates, therefore a new

impulse is ordered and the estimates are corrected again, including new value of system voltage. Same situation is repeated at t=3 s when the external voltage is restored to 1 pu.

Grid impedance following (GIF)

When the algorithm detects no unrealistic change in the estimates of R and X it remains in the grid impedance following mode. In this mode the algorithm does not require any signal injection from the generating source and can detect impedance changes using the same set of equations (7) by assuming that the grid voltage is relatively constant. GIE follows changes of the equivalent grid impedance with a lag depending on the number of samples k and forgetting factor λ. The overall performance of GIE algorithm in following mode is shown in Figure 4 from t=5 s when the grid resistance changed, through t=6 s when grid reactance changed until t=7 s when both resistance and reactance altered. The estimates follow the changes accurately. The dynamics of this process is depicted in Figure 4.

As can be seen from Figure 4, GID mode has been triggered three times, otherwise the algorithm operates in GIF mode. Operating principle and interdependence on the two modes in the whole GIE algorithm is schematically presented in Figure 5. Determination of transition conditions (DTC) is out of the scope of this report. The preliminary approach used here is a set of deterministic conditions, however for more complex applications fuzzy logic can be used.

Performance indicators

The dynamic performance of estimation is investigated for several variants of the number of samples in averaging (k=1..200), which is typical solution in such applications. To reduce GIE response time forgetting factor was introduced into GIE algorithm, three values were tested, $\lambda \in \{1, 0.9, 0.75\}$. Figure 6 presents GIE R_L estimation step response in following mode. Optimal results are achieved for parameters k=25 and λ=0.75 with response time less than 10 ms and maximum obtainable accuracy.

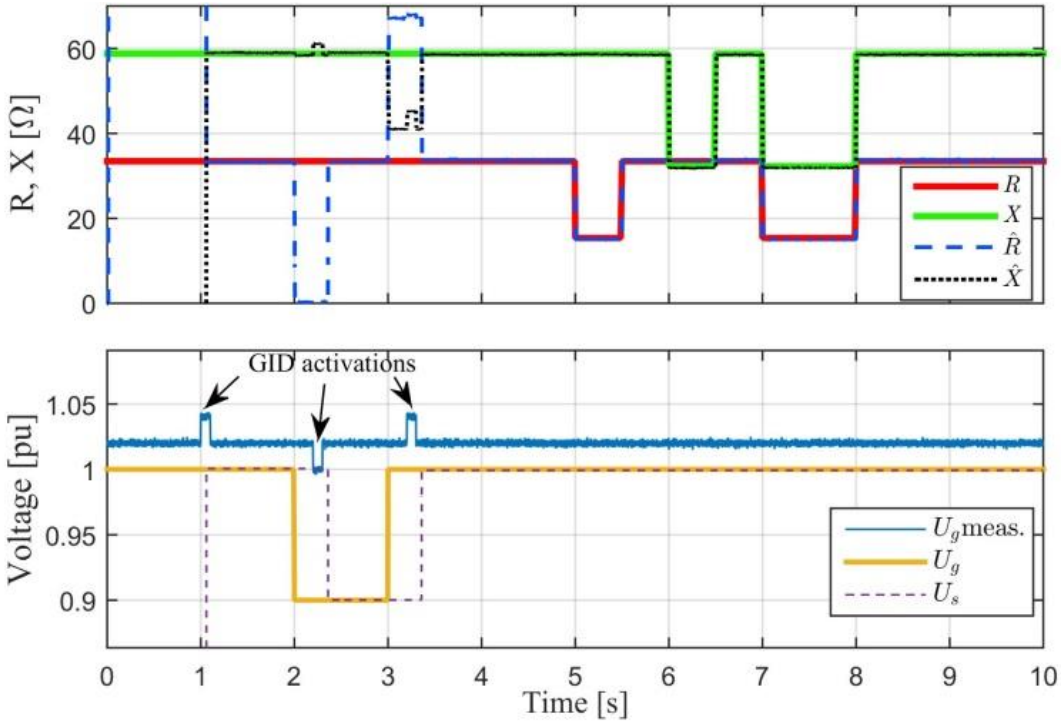

Figure 4: Determination and following-up ability of GIE. Upper window: resistance R_L and X_L of grid impedance and their estimates. Lower window: voltage modulus: U_g and U_s and grid Thévenin-equivalent estimate $\hat{U}_s$. T_p=0.5ms, λ=0.75, k=25

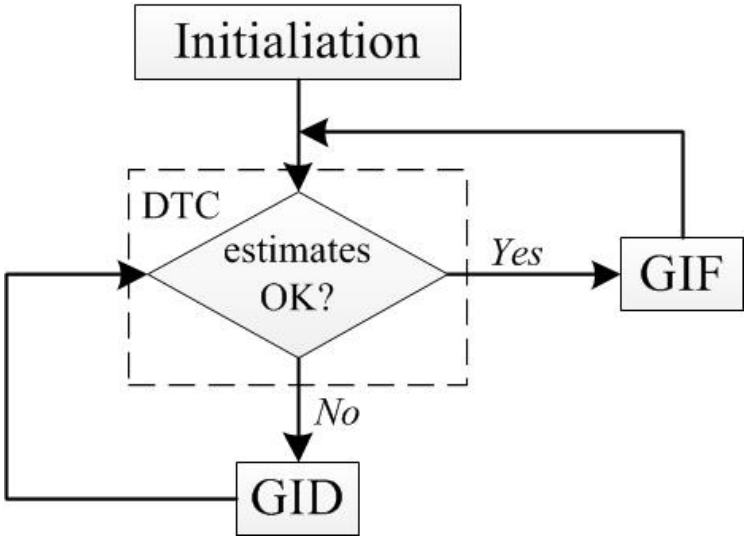

Figure 5: Operation principle of the grid impedance estimation algorithm

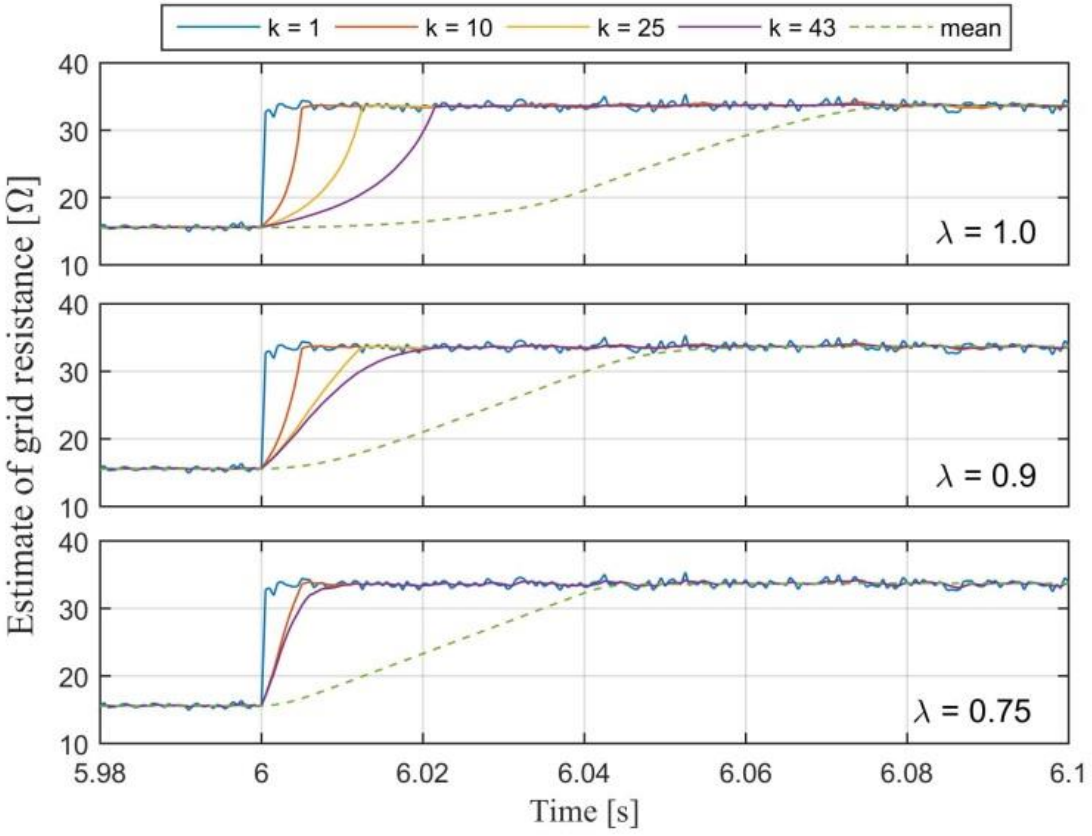

Figure 6. Operation in GIF mode; R_L estimation step response for different values of λ and k and mean value of estimate of R_L(k=25) for moving average n=200 ($\Rightarrow \Delta t$=0.1s, for T_p=0.5ms). T_p=0.5ms

The quality of the estimator is determined not only by the time response but also by estimation precision. Figure 5 presents moving average of least square estimation error (LSE) for n=200 in steady state. The LSE value comes from the measurement error. R_L and X_L estimation with use of only the last samples of U_g and I (k=1) is accompanied by LSE fluctuating around 0.0095 pu. For $k \geq 10$ the mean value of LSE fluctuates around 0.0055 pu which is satisfying. For sample time T_p=1 ms, LSE is on the same level. All simulations were performed on the assumption that noisy signals are supplied to the algorithm. Measurements of voltage (U_g) and current (I) are disturbed by normally distributed random signals (μ=0, σ^2=0.0013, $|\delta| \leq 0.005$).

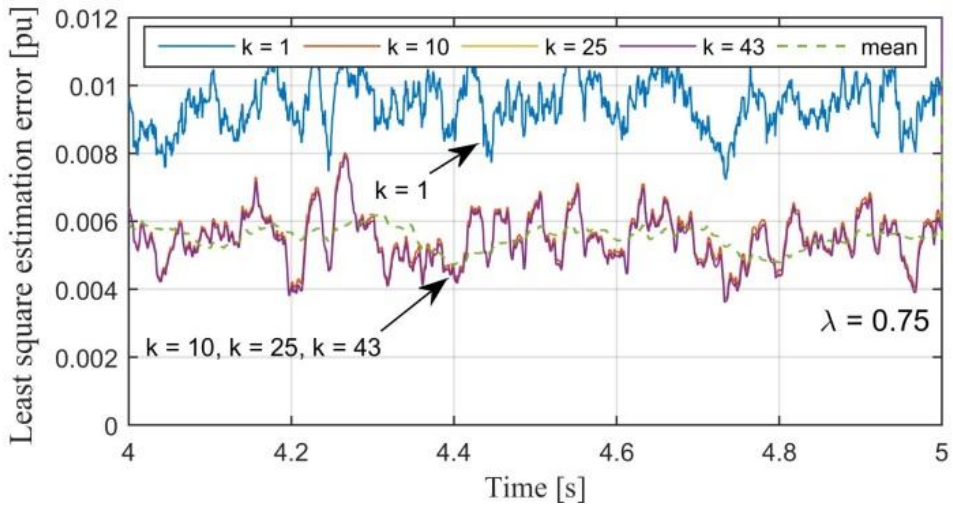

Figure 7. Least square estimation error for different *k*, and moving average of LSE(*k*=25) for *n*=200 (⇒ Δt=0.1s, for T_p=0.5ms). T_p=0.5ms, λ=0.75

4 Summary and conclusion

Numerous solutions exist for local voltage control and in principle the results presented in section 3 bring virtually nothing new. However, the results pinpoint that for specific operating conditions standard voltage control algorithm can be ineffective. These conditions can occur for example due to islanding or due to separation of a cell. Therefore it was proven that by incorporating also the active power into the primary voltage control algorithm effective voltage control can be achieved. In order to be able to do it, on-line grid impedance estimation function is necessary.

The presented grid impedance estimation method operates satisfactorily based on the local measurements only. It is a hybrid of a passive and active method as it switches from one mode to another depending on the situation. It has the capability of estimating parameters of both the Thévenin-equivalent impedance and voltage source.

ANNEX 6: Post Primary Voltage Control (PPVC)

1 Introduction

Post Primary Voltage Control (PPVC) developed in the scope of ELECTRA project aims to provide optimal voltage control for the future electrical grids considering the Web-of-Cells (WoC) concept [1-2]. The process (defined as a Use Case based on IEC 62559 standard) and functions of PPVC defined within the project ELECTRA are required to be validated by stand-alone simulations and laboratory experiments in order to ensure the novelty, accuracy, and benefit of PPVC. In this direction, PPVC Use Case and its functions have to be tested and validated, which will be the main focus of this Annex.

Implementation of PPVC in the ELECTRA project has been carried out with explorative way by different partners testing various paths to achieve the PPVC objectives. Both commercial and open source simulation platforms were utilized. Besides, different test cases were built on CIGRE MV test network in order to create variety for simulation outcomes. The implementation of PPVC functions on simulation platforms and preliminary simulation results of stand-alone PPVC Use Case are explained respectively. After that different test cases that were mainly created based on tap changing and PPVC use case combinations are presented including initial results obtained from simulations and laboratory testing. Finally the preliminary steps are presented for the implementation of the PPVC at a lab scale.

2 Methodology

PPVC has two main functions: PPVC controlling function and PPVC set-point providing function. The PPVC controlling function basically tracks voltage deviations and determines the necessity for the calculation of new voltage set-points, while the PPVC set-point providing function performs Optimal Power Flow (OPF) in order to determine voltage set-points. The implementation of these two function on a simulation platform are described in the following parts, respectively.

2.1 PPVC Controlling

The PPVC controlling function is responsible to check the current voltage measurements in grid nodes and to determine if they are within the safe band defined by regulations. It also acts as an information hub that receives voltage set-point values calculated by the PPVC Set-point Providing function and sends it to the corresponding devices. Additionally, the PPVC Controlling acts as a timer launching the periodic triggering of the PPVC Set-Point Providing function in case there is not out-of-safe band voltage events during the proactive PPVC operation window (15 min). The implementation of the function has been utilized in MathWorks MATLAB-Simulink (see Fig. 1), and it can easily be integrated into any other simulation environment.

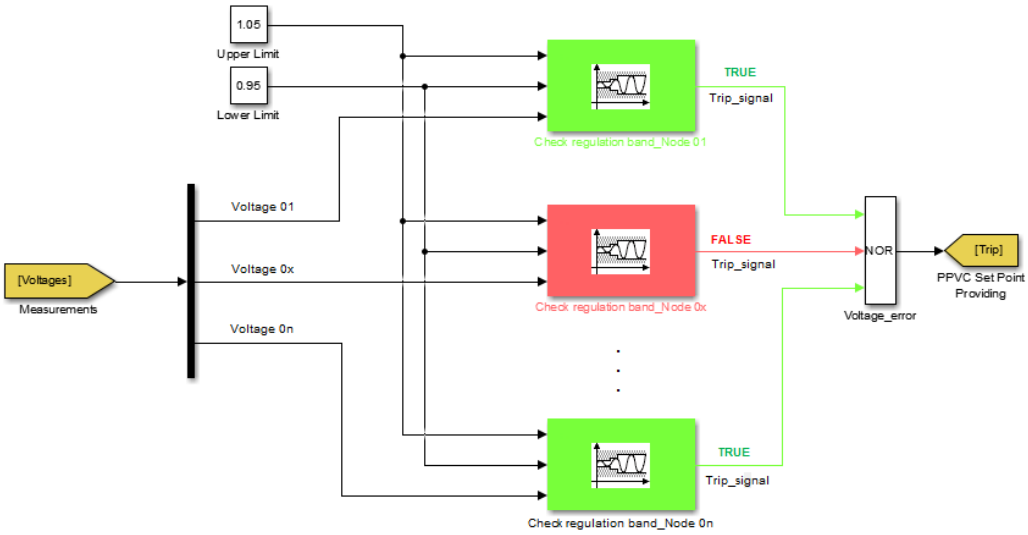

Figure 1: PPVC Controlling function

2.2 PPVC Set-point Providing Function

2.2.1 OPF algorithm in GAMS+MATLAB

There are numerous commercial and freely available simulation tools and solvers to implement OPF algorithm. Nevertheless, some of them are black box tools where the detail process is masked while the others have limited capability on the modification of the OPF. Hence, the project team decided to use the General Algebraic Modeling System (GAMS) to implement OPF in natural mathematical formulation form. GAMS is a high-level modeling system for mathematical programming and optimization. A GAMS implementation of OPF allows a relatively quick adaptation to new situations. For example, an OPF which doesn't take into account the reactive power potential of loads and DGs can easily do so by modifying the formulation in GAMS. This allows a transparent and clear implementation of complex optimization problems such as OPF.

The OPF executed for both routine and emergency processes of PPVC involves objective of loss minimization while respecting the limits of the resources exploitable to voltage control.

The admittance Y can be presented as:

$$Y = G_{ij} + jB_{ij} \tag{1}$$

- Where G_{ij} is conductance of the branch from node *i* to *j* and B_{ij} is succeptance of the branch between node *i* and *j*.
- The algorithm for OPF within PPVC is organized and presented as follows:

Objective:

- The objective of the OPF is the loss minimization and it is formulated as shown in (2).

$$min\left(\frac{1}{2}\sum_{i=1}^{Nb}\sum_{j=1,j\neq i}^{Nb}\left|P_{ij}-P_{ji}\right|\right) \tag{2}$$

Where P_{ij} and P_{ji} are active power flow from node i to j and j to i respectively, Nb is the number of buses in the network. Refer to equations (2) and (3) to see the formulations for P_{ij} and P_{ji}.

Equality constraints:

$$P_{ij} = t^2V_i^2G_{ij} - tV_iV_jG_{ij}\cos(\delta_i-\delta_j) - tV_iV_jB_{ij}\sin(\delta_i-\delta_j) \tag{3}$$

$$P_{ji} = V_j^2 G_{ij} - tV_iV_jG_{ij}\cos(\delta_j - \delta_i) - tV_iV_jB_{ij}\sin(\delta_j - \delta_i) \quad (4)$$

Where V_i and V_j are voltage magnitude at nodes i and j, δ_i and δ_i are voltage angle values for nodes i and j, t is the tap ratio of the transformer without phase shifting.

$$Q_{ij} = t^2V_i^2B_{ij} - tV_iV_jG_{ij}\sin(\delta_i - \delta_j) + tV_iV_jB_{ij}\cos(\delta_i - \delta_j) \quad (5)$$

$$Q_{ji} = V_j^2B_{ij} - tV_iV_jG_{ij}\sin(\delta_j - \delta_i) + tV_iV_jB_{ij}\cos(\delta_j - \delta_i) \quad (6)$$

Where Q_{ij} and Q_{ji} are reactive power flow from node i to j and j to i respectively.

The power flow balance equations at each node are used to define the equality equations for the loss minimization problem. The real and reactive power balance equations at each node i are the following:

$$\sum_{\substack{j=1 \\ i\neq j}}^{N_b} P_{ij} + Pd_i - Pg_i = 0 \quad (7)$$

$$\sum_{\substack{j=1 \\ i\neq j}}^{N_b} Q_{ij} + Qd_i - Qg_i = 0 \quad (8)$$

Where Pd_i and Qd_i are active and reactive power demands (loads) drawn from node i, Pg_i and Qg_i are active and reactive power generation injected at node i.

Inequality constraints:

The thermal limits of the lines were considered:

$$\sqrt{P_{ij}^2 + Q_{ij}^2} < \sqrt{3}|V_N||I_{max}| \quad (9)$$

Where $|V_N|$ is nominal voltage and $|I_{max}|$ is the maximum current for line i to j.

The voltage magnitude at each node in the network is constrained to stay within the allowed voltage range.

$$V_{i,min} \leq V_i \leq V_{i,max} \quad (10)$$

Where $V_{i,min}, V_{i,max}$ are lower and upper voltage limit at bus *i*, respectively.

If active power generation curtailment and reactive power generation control is to be applied on the distributed generators, the inequality constraints in (10) and (11) will hold.

For each generation units connected at each node in the network, the active and reactive power generations are constrained as follows:

$$Pg_{i,min} \leq Pg_i \leq Pg_{i,max} \quad (11)$$

$$Qg_{i,min} \leq Qg_i \leq Qg_{i,max} \quad (12)$$

Where: $Pg_{i,min}, Pg_{i,max}$, $Qg_{i,min}, Qg_{i,max}$ are lower and upper limits at bus i for active and reactive power generation, respectively.

The OPF formulation from (2) to (11) does not include the models for PV and wind turbine inverters reactive power contribution. In addition, the model for battery and CHPs are yet to be included as active and reactive power sources.

Implementation of the OPF

The OPF formulation from (1) to (12) is implemented in GAMS and the required time series data for generation and load are updated by a MATLAB function interfaced with GAMS using GDXMRW. The GDXMRW software gives MATLAB users the ability to use all the optimization capabilities of GAMS. In addition, a MATLAB /Simulink network model is essential for the implementation of real-time simulation using OPAL_RT later on. Hence, the GAMS based OPF linked with MATLAB can be readily used during real-time tests. The MATLAB function not only gives data to the GAMS implemented OPF it also implements the core algorithm for the PPVC controller, which require real-time awareness of the voltage state of all nodes in the network. A simple sketch diagram in Figure 2 illustrates the PPVC implementation using MATLAB and GAMS.

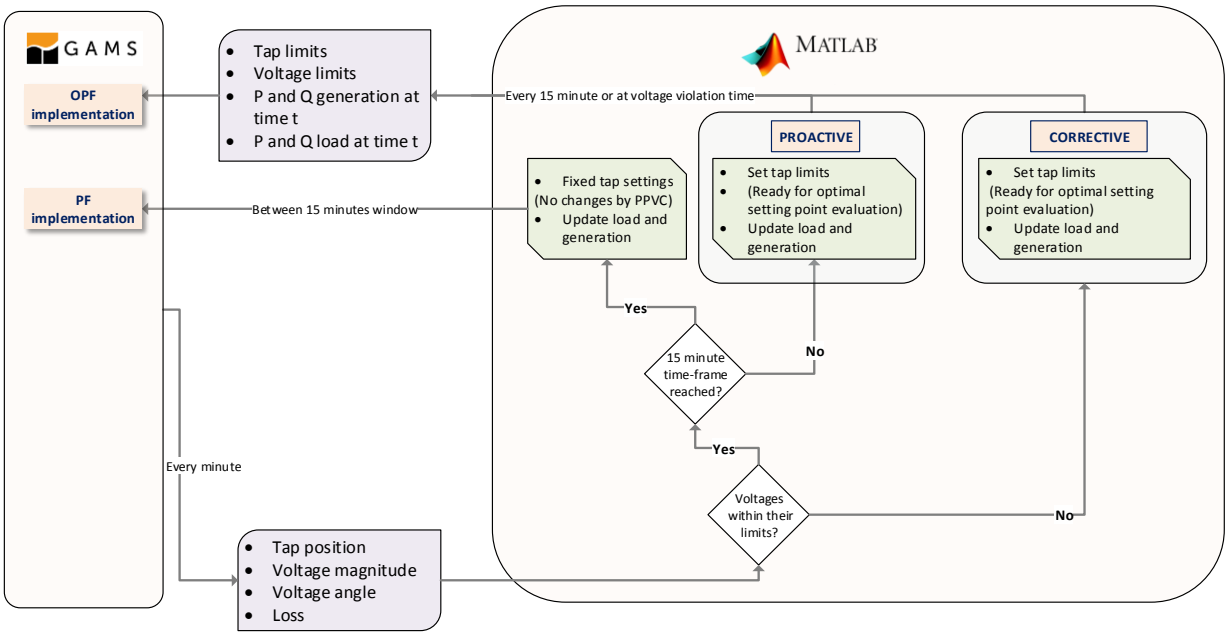

Figure 2: PPVC implementation using MATLAB and GAMS

3 Simulations results

3.1 Simulation results of OPF algorithm in GAMS+ MATLAB

The voltage profiles achieved with the OPF with MATPOWER (MATLAB Power System Simulation Package) and GAMS are compared and shown in Figure 3, for its application to the CIGRE MV benchmark that will be later defined (in section 1.3.1.). In Figure 4, also the computation of the active power losses is compared. These comparisons are needed to validate the GAMS-Matlab OPF implementation to the PPVC problem against the widely-used program, Matpower. As one can see in Figure 3 the differences in the calculated voltage level is in the order of 0.001 pu and that of deference in loss calculation as shown in Figure 4 is negligible. Hence, the GAMS-Matlab OPF implementation can be used for PPVC simulation without losing accuracy. The simulation results of the PPVC implementation using the GAMS-Matlab OPF algorithm is presented in Figure 5.

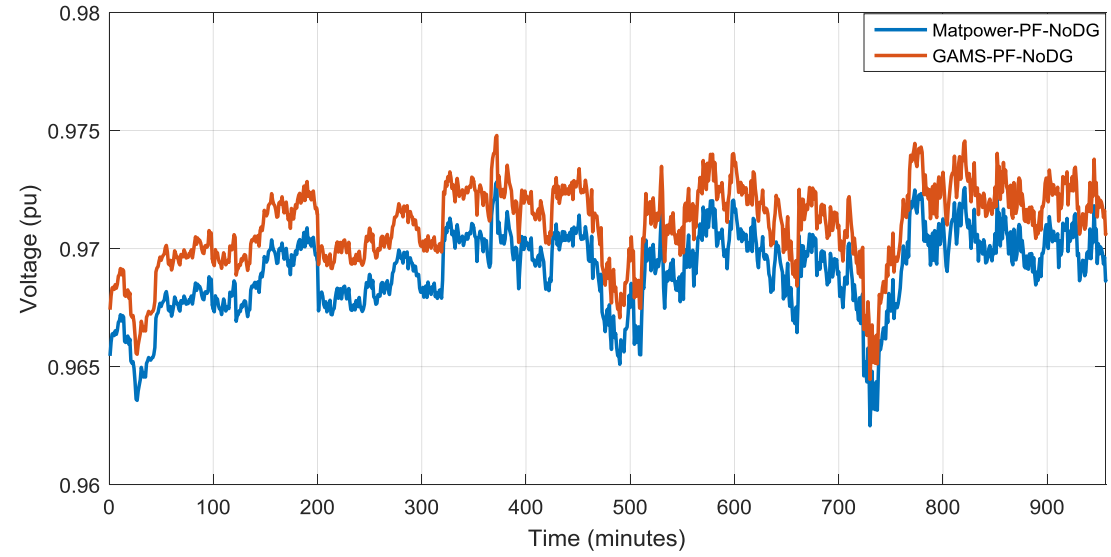

a)

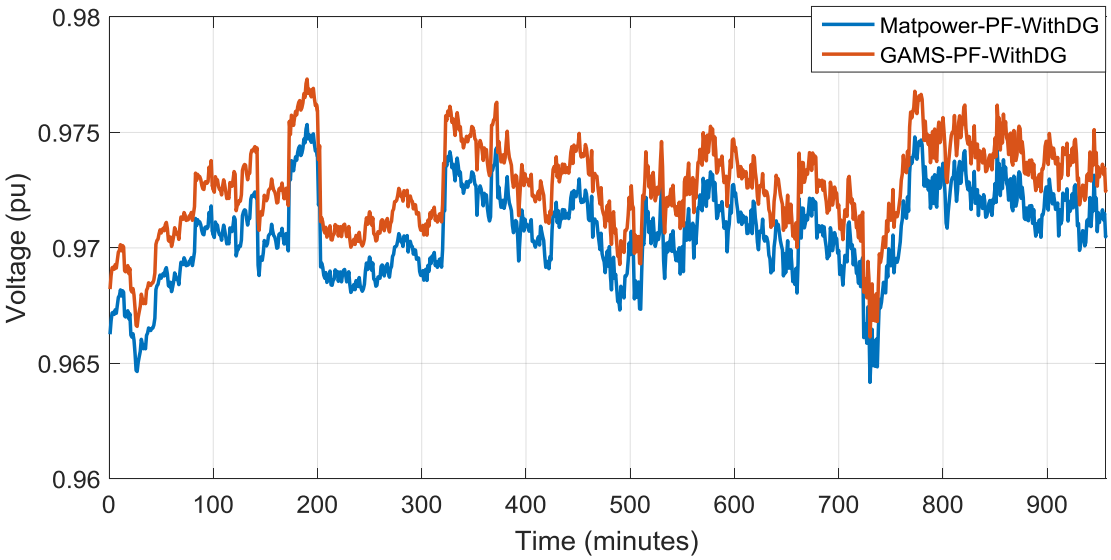

b)

Figure 3: Comparison of voltage profiles between GAMS and MATPOWER for the CIGRE MV network; (a) For a network with no DERs and (b) for a network with PVs and a wind turbine

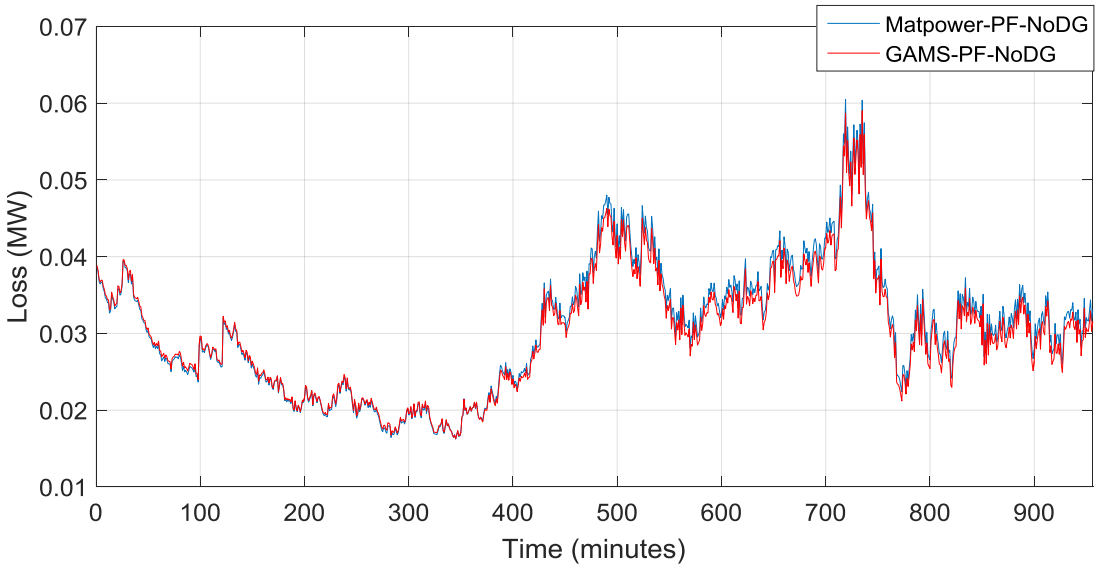

a)

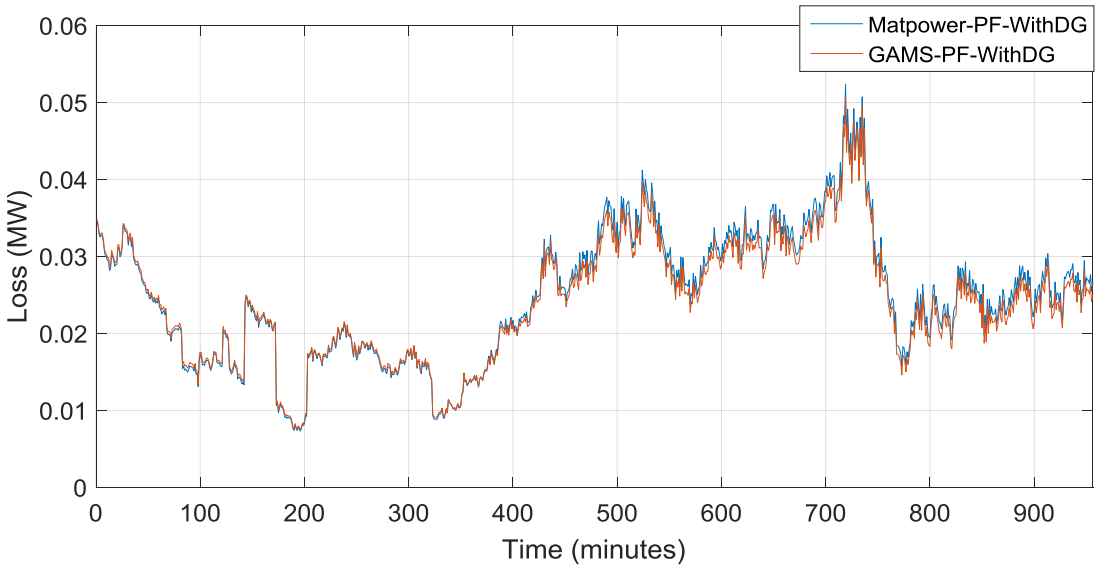

b)

Figure 4: Comparison of power flow results between GAMS and MATPOWER for the CIGRE MV network; (a) For a network with no DERs and (b) for a network with PVs and a wind turbine

The PPVC is implemented as it is described in the Figure 1 and the simulation result is presented in Figure 5. The PPVC controls the On-load Tap Changer (OLTC) in the network optimally by minimizing the loss in the network.

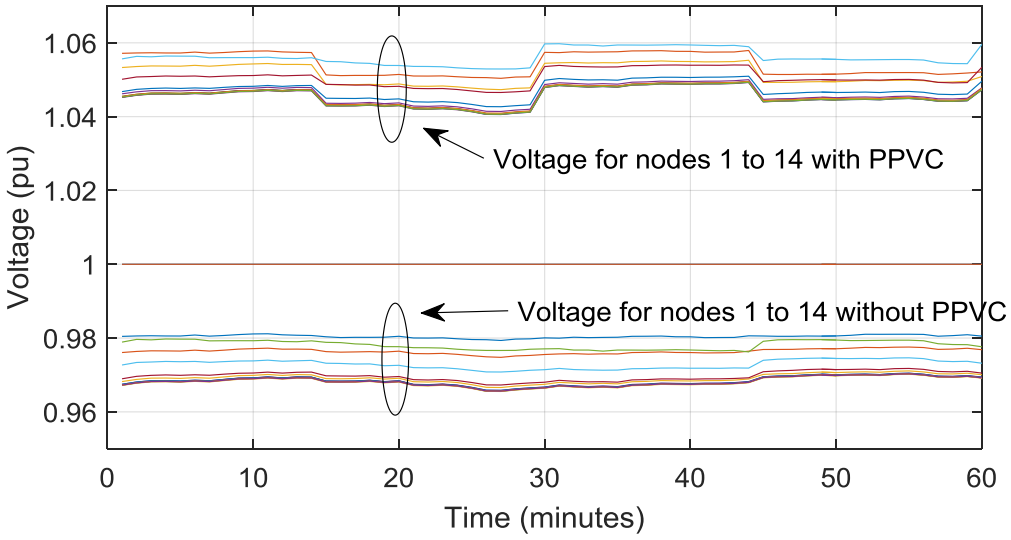

a)

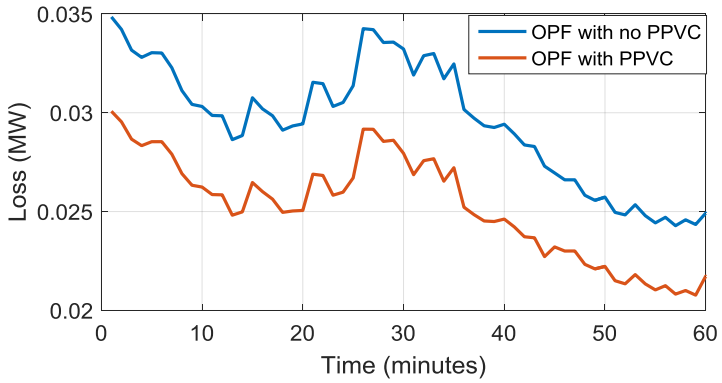

b)

Figure 5: Effects of the implementation of PPVC on the voltage levels (a) and network losses (b)

3.2 OPF algorithm in Python

The Load flow and optimization model was utilized by using pandapower with built of PYPOWER, MATPOWER tool converter to Python.

Pandapower was selected because it is an open source tool external from MATLAB and the tutorials are easily accessible for it. MATLAB/Simulink is emulating the actual grid opposed to pandapower, which represents the grid model. Components and principal data directions are presented in Figure 6.

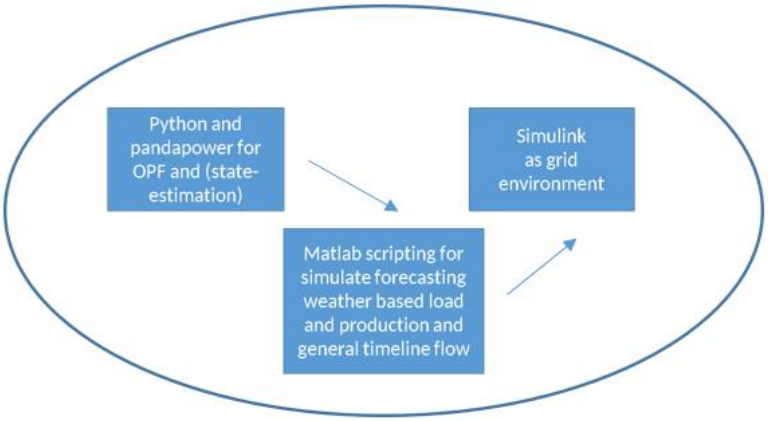

Figure 6: Components in simulation environment

Forecasting is determined based on the weather forecast data used in load and generation forecast as simple functions. Interior point method is applied with PIPES (python package). In addition, since the OPF function is not capable of controlling tap changers, loop of trial error type for the method is built on the top of OPF function. In this way, the OPF is evaluated for all feasible positions of the tap changers, selecting as a final result, the solution with less active power losses in the system.

Pandapower is a joint development of the research group Energy Management and Power System Operation, University of Kassel and the Department for Distribution System Operation at the Fraunhofer Institute for Wind Energy and Energy System Technology (IWES), Kassel. More information about pandapower can be found from official manual [3].

3.3 Stand-alone PPVC UC

3.3.1 Test grid: The CIGRE MV benchmark

For the validation of the stand-alone PPVC Use Case and as a representative WoC, the CIGRE MV European benchmark with DER resources have been selected. In its complex form, the CIGRE MV network contains:

- 8 photovoltic generators
- 1 wind turbine
- 2 batteries
- 2 residential fuel cells
- 1 CHP diesel
- 1 CHP fuel cell
- 2 OLTCs

The grid layout, as it has been implemented in DIgSILENT PowerFactory is displayed in Figure 7. It has four voltage levels: 110kV in the point of common coupling with the grid upstream (yellow), 20kV at the distribution level (dark green) and the DERs connected a 0.4kV (light green). Only the wind turbine is connected at 0.69kV (blue) as it is the usual generation voltage used in Spain (and the data was missing from the original description). The detailed network data used is gathered in Tables 1 and 2 and DER types with their rated powers are shown in Table 3.

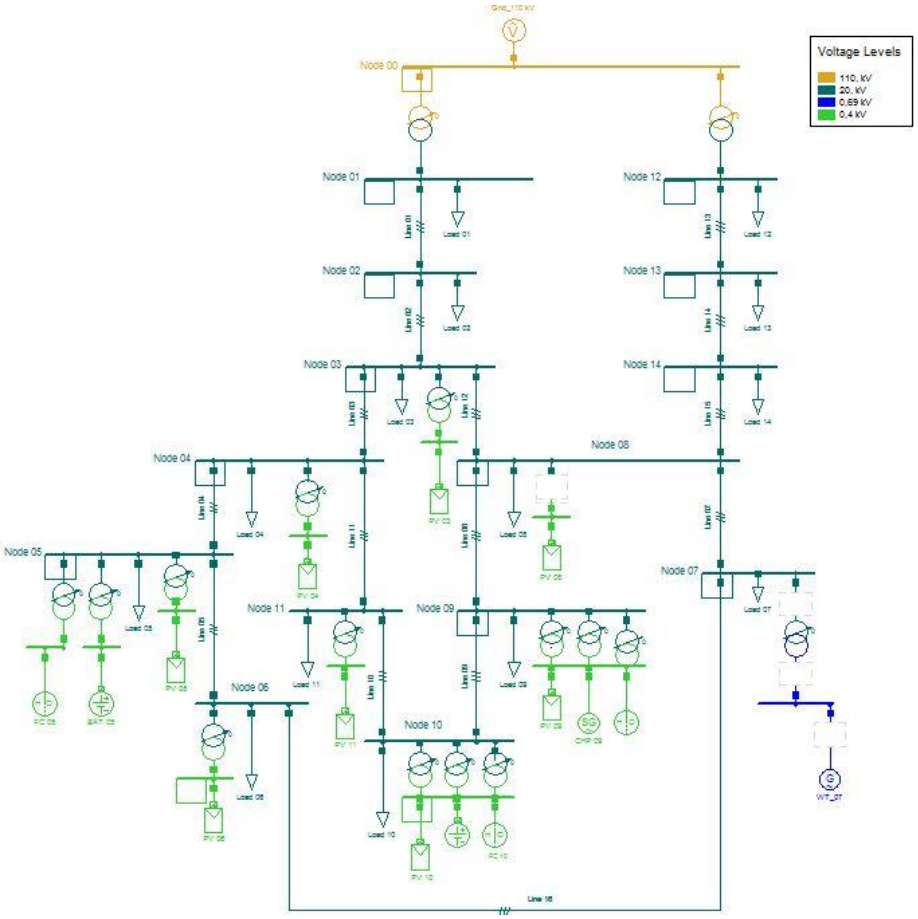

Figure 7: CIGRE MV benchmark with DERs

Table 1: Network data for the CIGRE MV network *1*

	From	To	R_ph (Ω/km)	X_ph (Ω/km)	B_ph (µS/km)	Ro (Ω/km)	Xo (Ω/km)	Bo (µS/km)	l (km)	
1	1	2	0.501	0.716	47.493	0.817	1.598	47.493	2.82	underground
2	2	3	0.501	0.716	47.493	0.817	1.598	47.493	4.42	underground
3	3	4	0.501	0.716	47.493	0.817	1.598	47.493	0.61	underground
4	4	5	0.501	0.716	47.493	0.817	1.598	47.493	0.56	underground
5	5	6	0.501	0.716	47.493	0.817	1.598	47.493	1.54	underground
6	6	7	0.501	0.716	47.493	0.817	1.598	47.493	0.24	underground
7	7	8	0.501	0.716	47.493	0.817	1.598	47.493	1.67	underground
8	8	9	0.501	0.716	47.493	0.817	1.598	47.493	0.32	underground
9	9	10	0.501	0.716	47.493	0.817	1.598	47.493	0.77	underground
10	10	11	0.501	0.716	47.493	0.817	1.598	47.493	0.33	underground
11	11	4	0.501	0.716	47.493	0.817	1.598	47.493	0.49	underground
12	3	8	0.501	0.716	47.493	0.817	1.598	47.493	1.3	underground
13	12	13	0.51	0.366	3.172	0.658	1.611	1.28	4.89	overhead
14	13	14	0.51	0.366	3.172	0.658	1.611	1.28	2.99	overhead
15	14	8	0.51	0.366	3.172	0.658	1.611	1.28	2	overhead

[1] Conseil international des grands réseaux électriques. Comité d'études C6. Benchmark systems for network integration of renewable and distributed energy resources. CIGRÉ, 2014.

Table 2. Network data for the CIGRE MV network *2*

Node	Node	Connection	V1	V2	Ztr	Srated
			[kV]	[kV]	[Ω]	*[MVA]*
0	**1**	3-ph Dyn1	110	20	0.016+j1.92	25
0	**12**	3-ph Dyn1	110	20	0.016+j1.92	25

Table 3. DER types connected in the CIGRE MV network

Node	DER Type	Pmax [kW]
3	Photovoltaic	20
4	Photovoltaic	20
5	Photovoltaic	30
5	Battery	600
5	Residential fuel cell	33
6	Photovoltaic	30
7	Wind turbine	1500
8	Photovoltaic	30
9	Photovoltaic	30
9	CHP diesel	310
9	CHP fuel cell	212
10	Photovoltaic	40
10	Battery	200
10	Residential fuel cell	14
11	Photovoltaic	10

3.3.2 Planning phase: proactive scenario

According to the static data presenting the CIGRE MV grid, dedicated PQ load profiles and generation forecasts have been created based on real measurements, which will be used in the simulation of both the proactive and the corrective scenario. By way of example, the active power profiles of aggregated PV panels are shown in Figure 8.

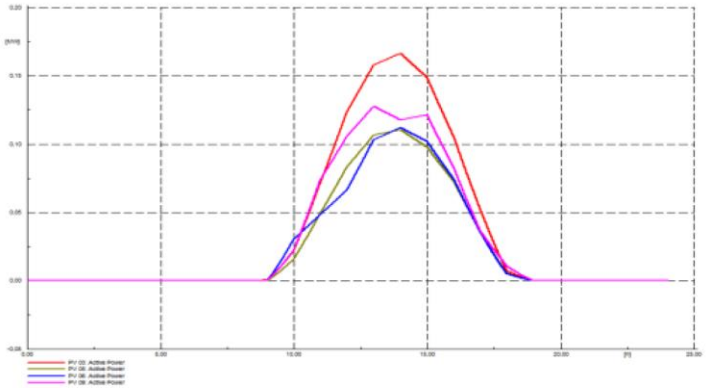

Figure 8: PV voltage profiles

The OPF is responsible to optimize the objective function in order to minimize the active power losses in the grid while respecting the inequality constraints: voltage limits in the nodes, tap

[2] Conseil international des grands réseaux électriques. Comité d'études C6. Benchmark systems for network integration of renewable and distributed energy resources. CIGRÉ, 2014.

transformers and active and reactive power limits in the generators. Every 15 min, the cell operator receive the forecast of the PQ loads and the power generation profiles for the next 15 min for some representative loads, as shown in Figure 9.

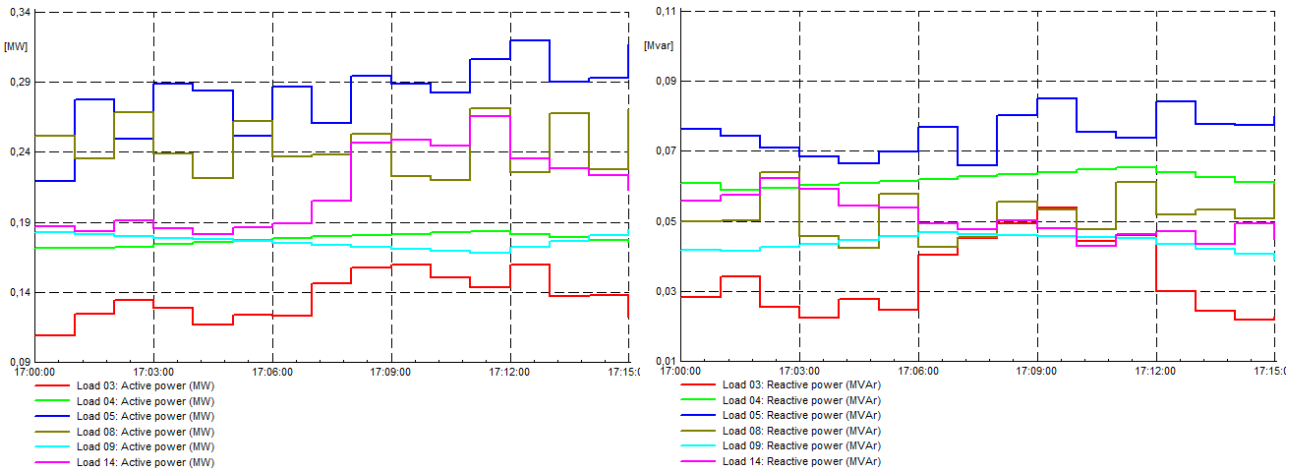

Figure 9: Load profiles

Every 15-min, the OPF process is launched with a resolution ratio of 1 min (according to the sampling ratio of the generation and load forecasts) and thus, the optimized profile set-points are sent to the different PVC/PPVC controllers for the next period. In this preliminary implementation, the lower and upper allowable voltage values are 0.95 p.u. and 1.05 p.u. These limits are indicative temptative because they rely on the grid codes currently in force in every power system and thus, they should be selected according to the regulation applicable, depending on the location of the cell. The cell operator can also consider the droops (Q/U) associated to the DERs in the planning phase as well as the addition of new resources if there is a lack of reactive power reserve (see Figure 10) in order to reduce the response timing by anticipating the activation of resources prior to the voltage event occurrence.

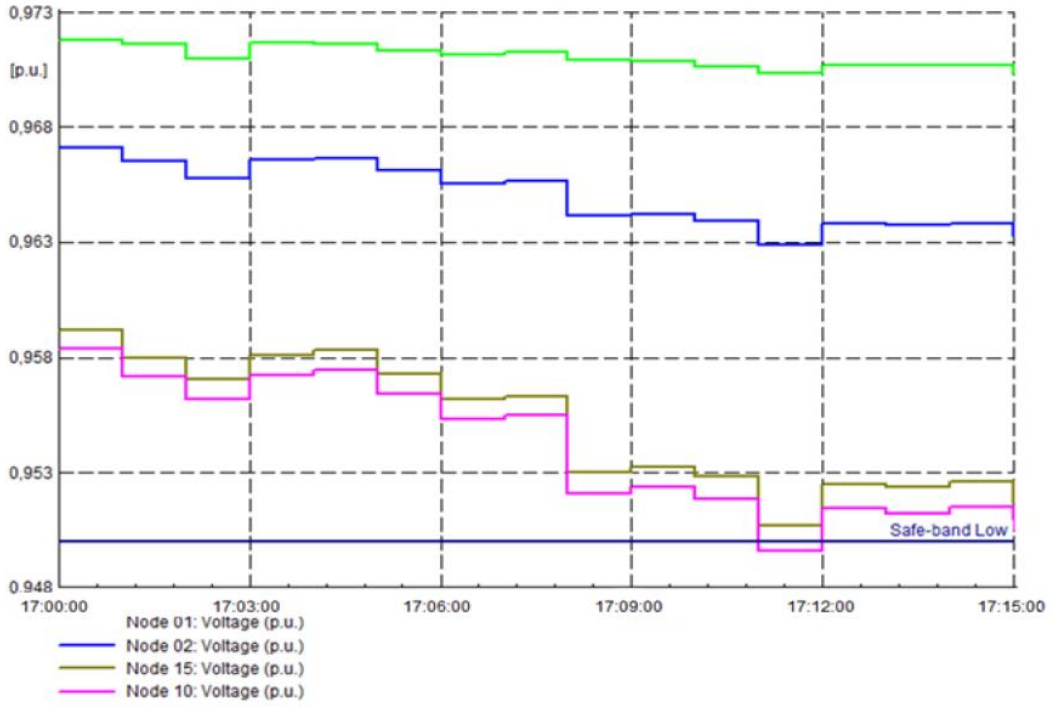

Figure 10: The addition of new resources if there is a lack of reactive power reserve

3.3.3 Operation phase: corrective scenario

In Figure 11 the corrective scenario operation and the results of optimal voltage profiles in representative nodes are shown. The solid lines represent the optimal voltage profiles resulting from the window-ahead planning phase. These profiles already sent to the PPVC devices would remain for the full window if no disturbance happens. In case of an unscheduled event in $t=t_{A'}$ a new OPF process is launched and the optimal voltage set-points are updated (dashed lines)* and, as a consequence, the PPVC resources will react in order to make the voltages in the nodes to reach that optimal.

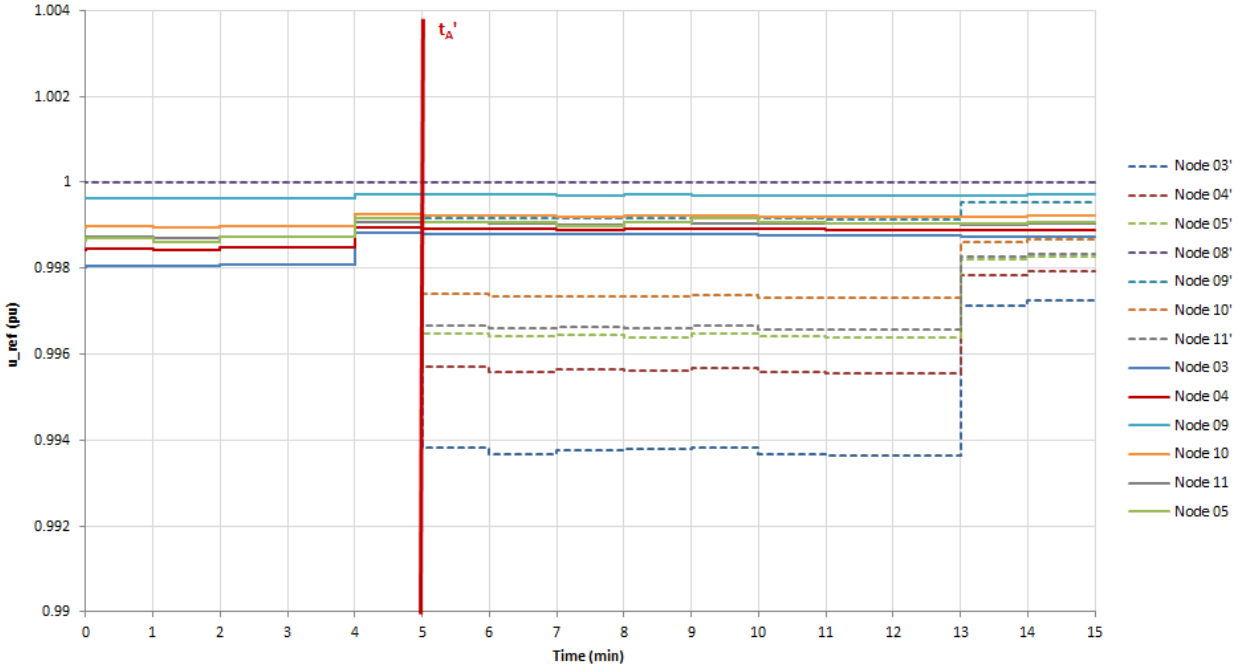

Figure 11: Comparative between optimal profiles with/without unscheduled events

* Notice that the Node 08 is considered in this calculation as the swing bus, so the optimal profile does not change regardless the existence of an unscheduled event

3.3.4 Example cases

Simulation period in each case is set to 15 minutes, which is the proposed length of proactive correction period in post-primary voltage control concept.

Cases under study are:

- Reference case
- PPVC proactive case
- PPVC proactive with fixed tap positions case
- PPVC corrective case

In the reference case, the loading profile in the CIGRE MV network was selected in a way that causes voltage quality issues to the grid. Time window for the simulation was 15 minutes and the time step was one minute. Loading profile for each load node are shown in Figure 12 and Figure 13.

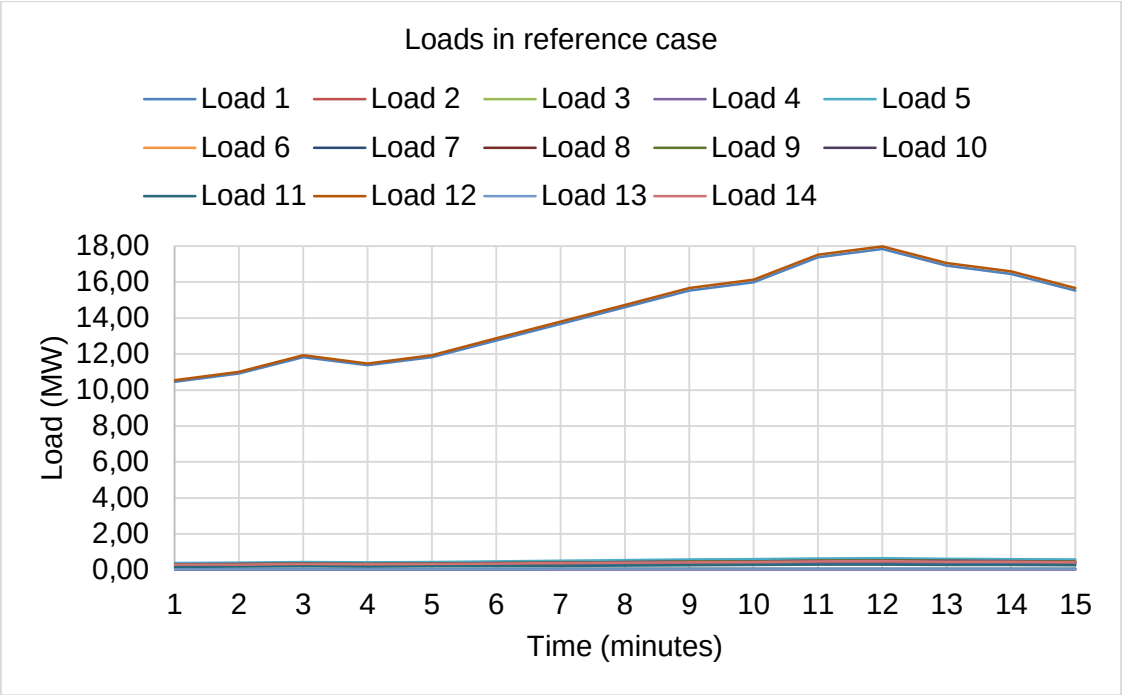

Figure 12: Loads in reference case

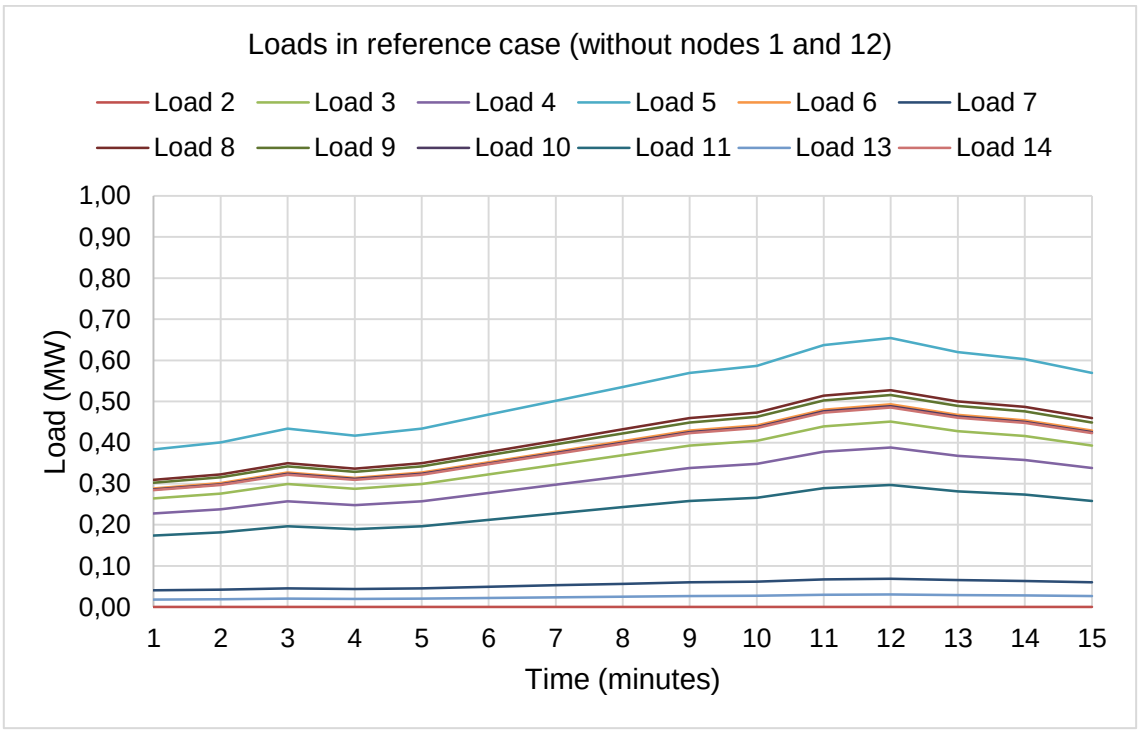

Figure 13: Loads in reference case without nodes 1 and 12

Voltage limits according to European Standard EN 50160 "*Voltage characteristics of electricity supplied by public electricity networks*" for power quality are +/-10 percentage of the nominal voltage [4]. Voltages in reference case simulation for each node are shown in Figure 14.

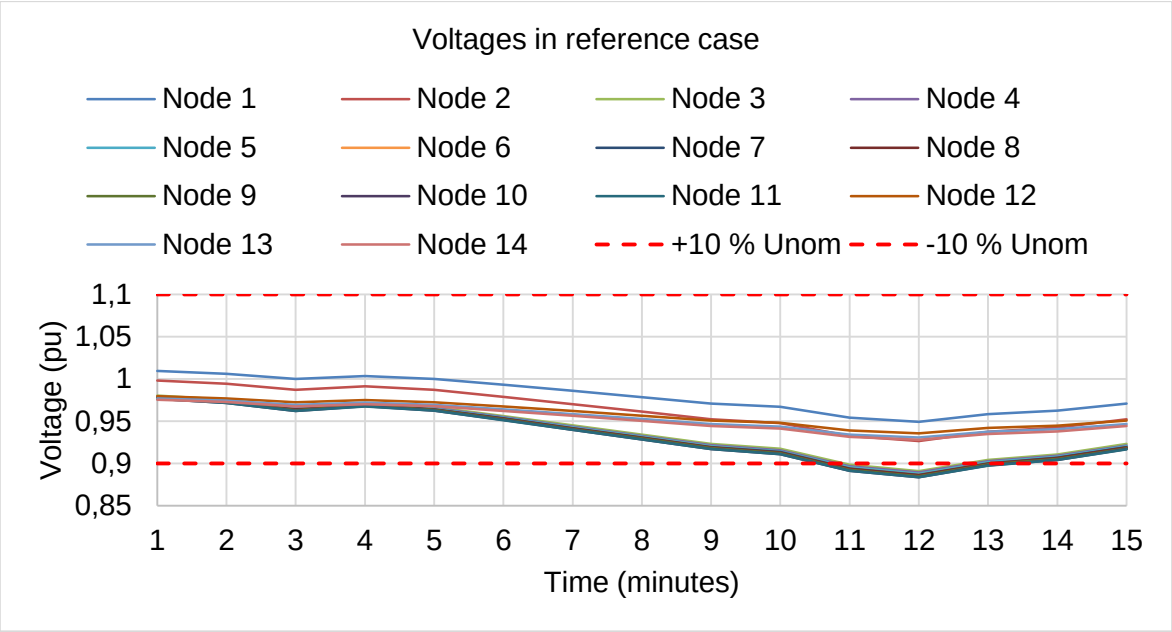

Figure 14: Voltage in reference case

In the reference case, the load is too high and the voltage level drops under the -10 % limit at the end of the simulation period. Therefore, voltage control is needed to avoid the voltage quality issues in the grid.

3.3.5 PPVC proactive case

In the second case, PPVC proactive method was utilized to control the voltage levels in the CIGRE MV network. PPVC proactive function includes transformer tap changers control and PV inverters reactive power control. Voltage limits for the PPVC optimization function was set to 1.05 p.u. and 0.95 p.u. Loading profile was the same one that was used in the reference case simulation. Voltages for each node are shown in Figure 16.

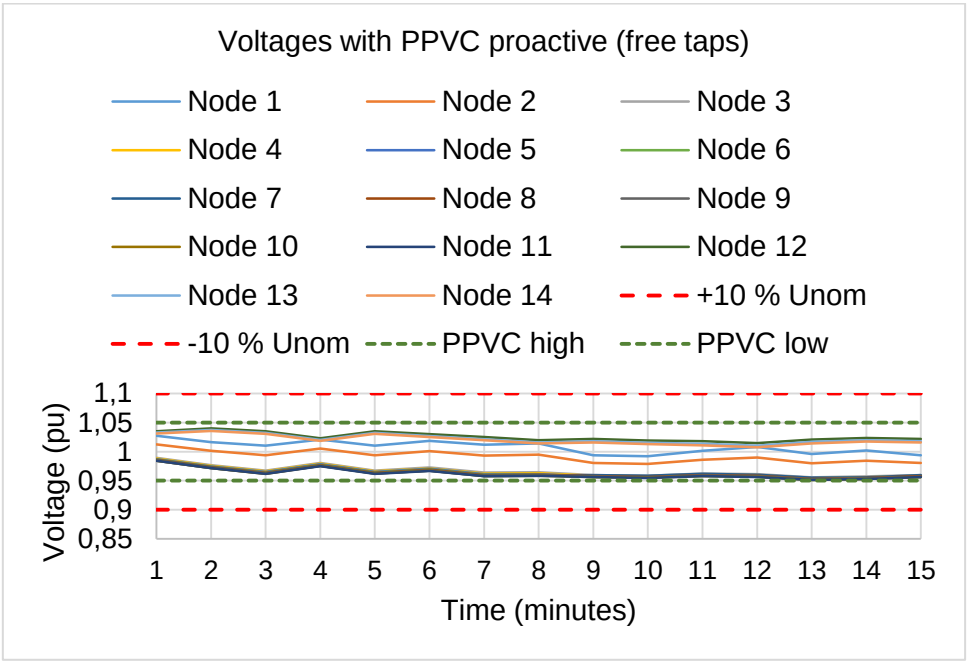

Figure 16: Voltages in PPVC proactive case where tap changer is not limited

As seen from the results, it is possible to keep the voltage level in the grid between the threshold levels with the PPVC proactive function. Although, during the 15 minute period both tap changers changes position quite a lot which might not be realistic. Tap changers positions during the simulation are shown in Figure 17.

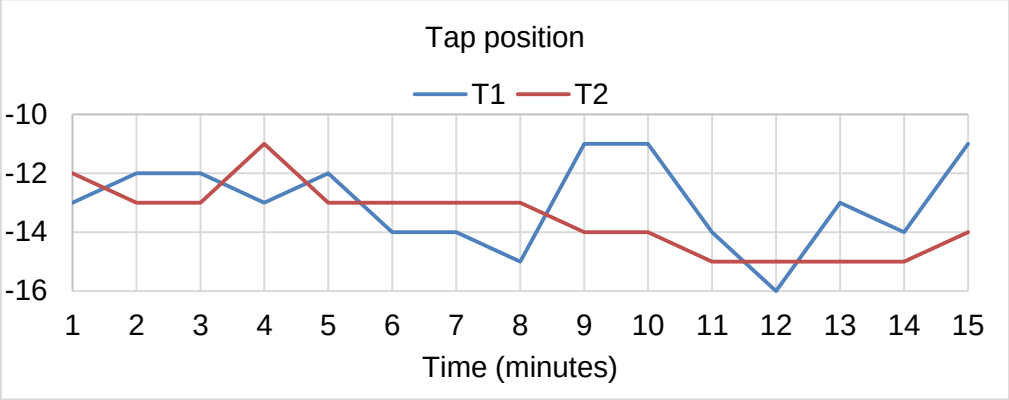

Figure 17: Voltages in PPVC proactive case where tap changer is not limited

As seen from the results, tap changers positions are changed almost every minute, which is not typical. Therefore, also simulation with limited tap changer positions was done. Although load changes almost 100% in the case, which is also not typical for 15 minute period. Fixed tap changer positions in next chapter only refer to fixed value within the 15 min period and position optimized so that it matches the forecast.

3.3.6 PPVC proactive with fixed tap positions

Because changing tap changer position multiple times in 15 minute period might not be realistic, simul ation with fixed tap changer values was also done. Optimal tap positions were calculated for both transformers based on the 15 minute load forecast. This also differentiates the benefit of tap changer and benefit of local reactive power control. Selected tap position for transformer T1 was -15 and -14 for T2 for the whole 15 minute simulation period. Voltage results with fixed tap changer position are shown in Figure 18.

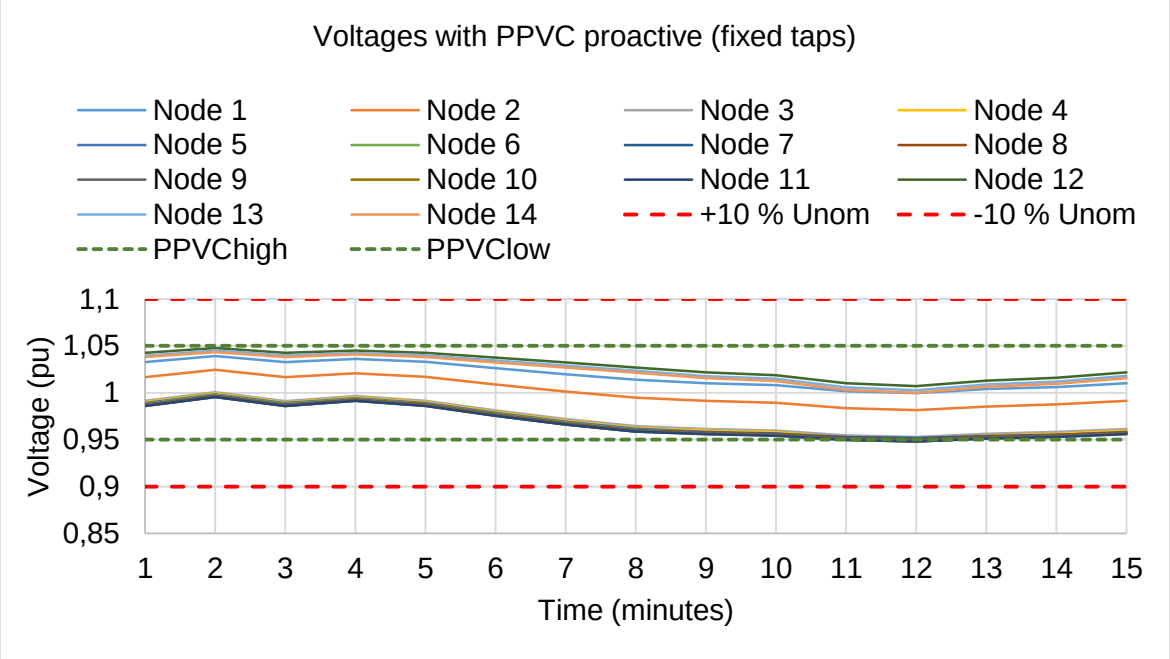

Figure 18: Voltages in PPVC proactive case where tap changer is limited

With limited tap changer positions it is also possible to avoid the voltage quality issue in the grid. In addition to voltage control, PPVC function minimizes the active power losses in the grid and results from different simulation cases are shown in Figure 19.

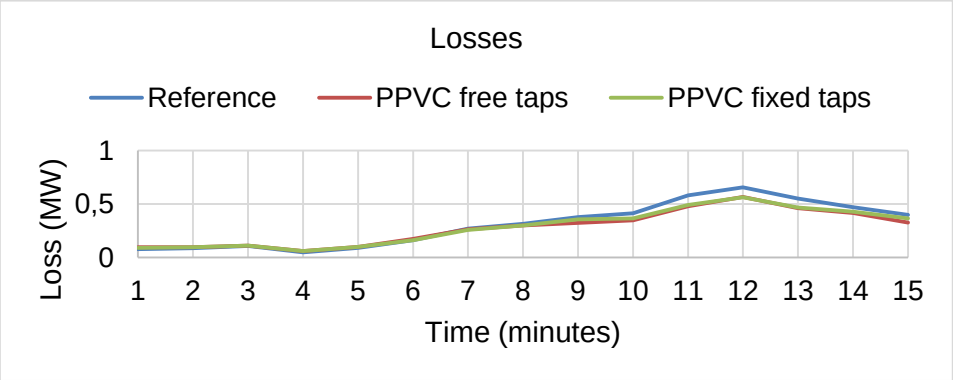

Figure 19: Active power losses in the grid

Results show that active power losses could be reduced with proactive post primary voltage control. During the highest loading situation active power losses are reduced around 100 kW but during the lowest loading situation losses are almost the same. It can also be seen from the results that with fixed tap positions it is possible to reduce active power losses almost as much as in the case where tap changer positions are changing during the 15 minute period.

3.3.7 Corrective method results

PPVC corrective function is utilized for cases where there is sudden voltage deviation. Primary voltage control is the leading control mode in quick voltage deviations and idea is that post primary voltage control joins in and helps in the task of restoring voltage to normal level. In reference case, load is increase step by step so that voltage violation would occur without control like presented in Figure 20.

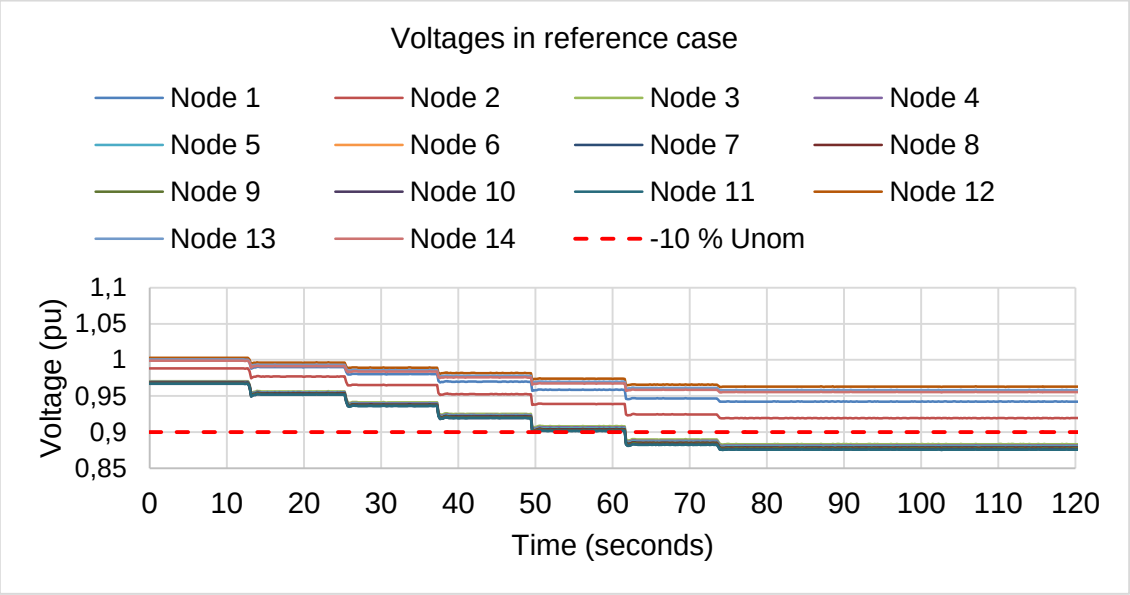

Figure 20: Reference case in PPVC corrective method where load is increasing rapidly

First test is to use just transformer tap changers to control the voltage in the grid. Results are shown in Figure 21.

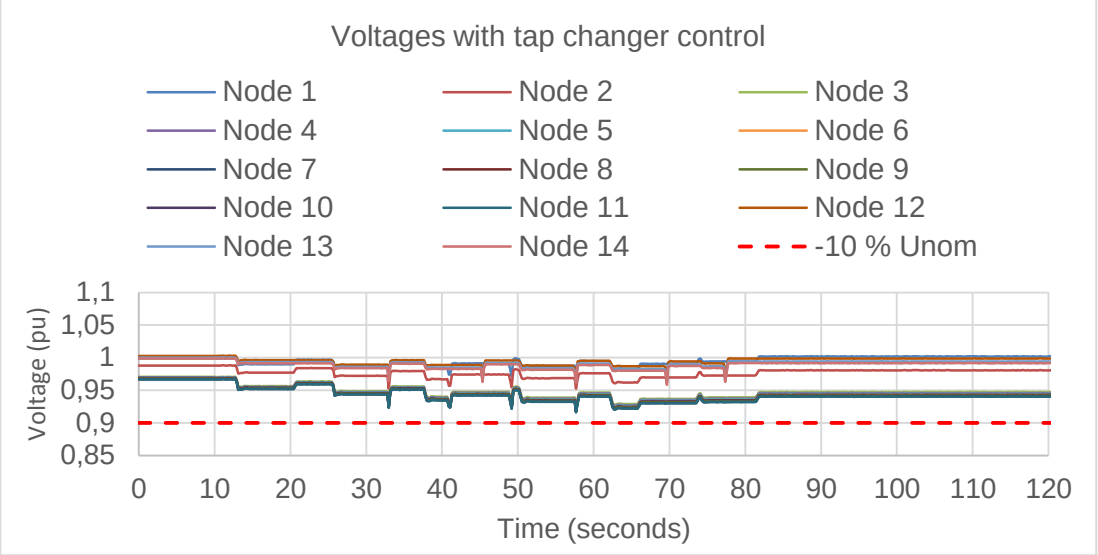

Figure 21: Tap changers recovering voltage

Tap changer manages to recover the voltage level by reacting to each load step. Improvements are achieved when PPVC corrective method is utilized in the simulation. Threshold for PPVC corrective is set to 0.94 pu and when voltage drops under that then the PPVC will start to control the voltage with tap changers and DER unit reactive power control. Results for corrective case are shown in Figure 22.

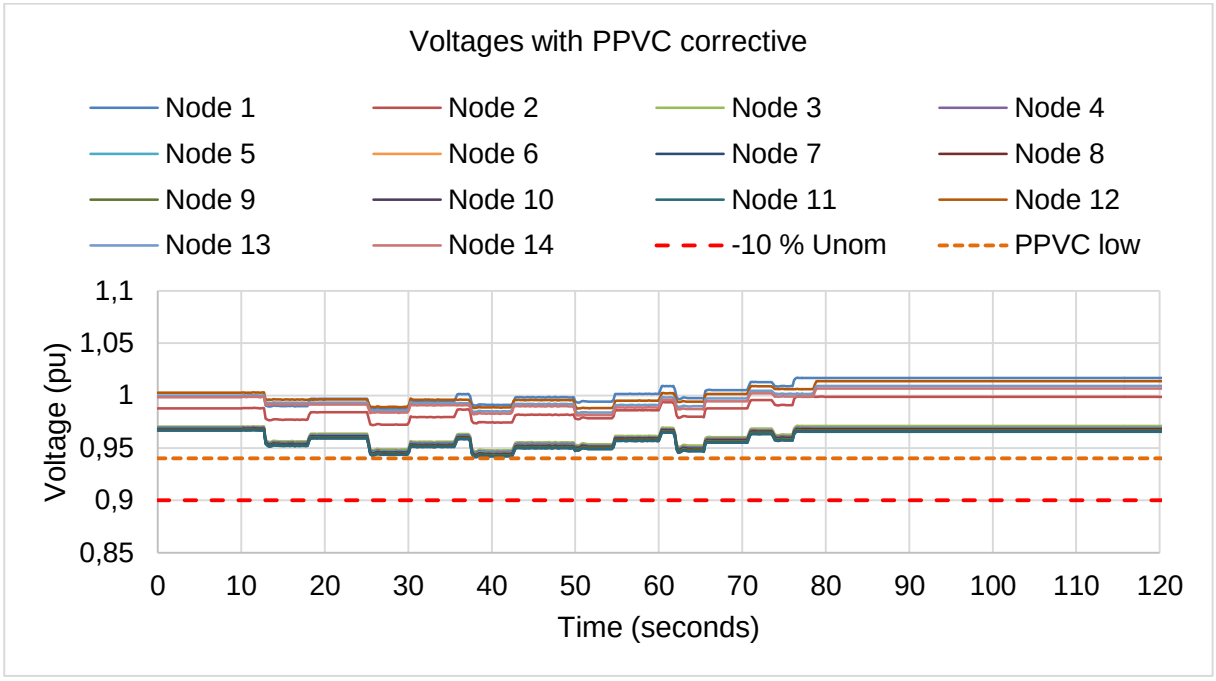

Figure 22: PPVC corrective simulation results

Results with PPVC corrective help to limit the voltage sag compared to transformer tap changers acting alone. This can be better seen in Figure 23 where Node 11 of the CIGRE grid is inspected more closely.

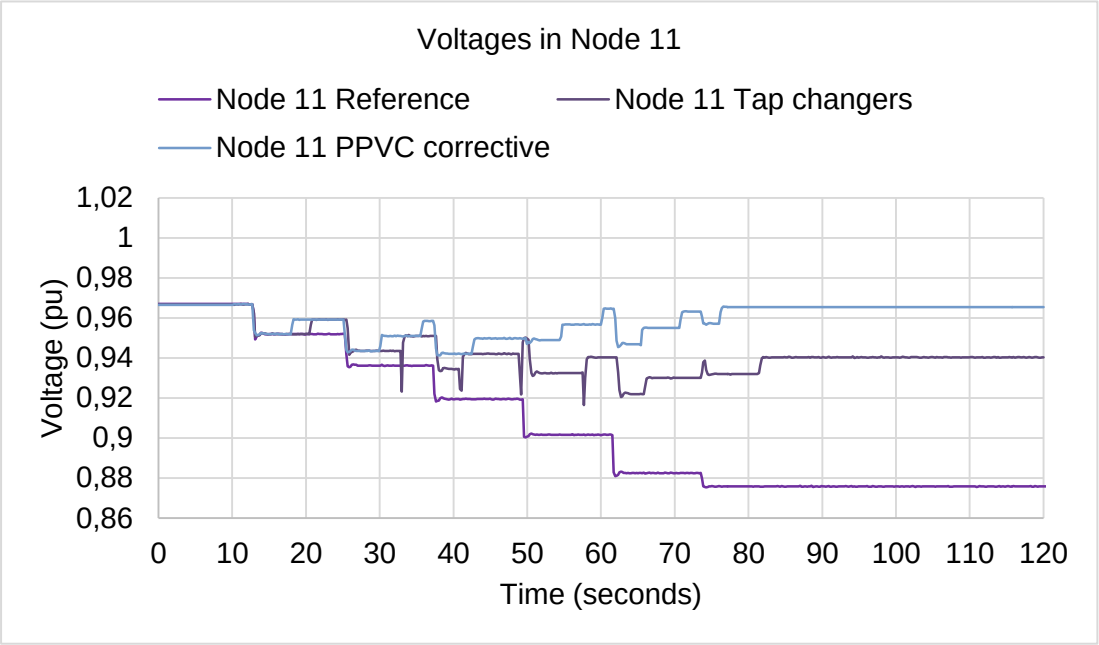

Figure 23: Node 11 voltages compared between three simulations

3.3.8 Analysis of the results from the example cases' simulation

Active power losses were reduced in the study using proactive post primary voltage control in simulations. Although simulations are promising, some critiques can be given to the validity to the method to work in real grid. High activation of tap changer could risk the lifetime of the tap changer. This certainly depends on type of tap changer in question. The major limitation of the study is assumption of non-dynamic load. The load was defined by minute-to-minute basis as fixed value. In real distribution system, however grid load changes with voltage. For example in low voltage measurement in [5], 5 % increase in voltage would increase the load a 3%. This means that benefit would be lost in grid where load follows grid voltage. Simulations would need to be done with dynamic load in optimization model to prevent this from happening. If load is static, optimization wants to increase the voltage to reduce current and therefore losses. Current optimization model used here does not allow dynamic load model and better model would be needed for this.

Corrective simulations were also ran in case where voltage control with only tap changers was compared to corrective post primary voltage control helping in voltage sag recovery. PPVC had significant impact on level of voltage sag and helped in reducing recovery time. Renewable penetration in the grid was not very high, only 2 % of the total load, but reactive power control had still good results. This hints that benefit of PPVC could be larger in system operation perspective than value achieved in loss minimization during normal operationPPVC has significant impact of lowering voltage sag and also voltage recovery is faster. PPVC therefore gives meaningful effect in helping in the corrective case.

3.3.9 Next steps: from simulations to lab experiments

Within the proof-of-concept of the Web-of-cells efforts, the aim is to study and evaluate the response time of PVC+PPVC controllers in the face of topology changes in the network, thus combining the two voltage control UCs and implementing them in a real PHIL installation (power hardware in the loop). The laboratory test starts by implementing real-time simulation using Opal-RT. However, later on there is a plan to replace some of the components with actual hardware leading to PHIL testing. The implementation of the PPVC in the laboratory is illustrated in Figure 24.

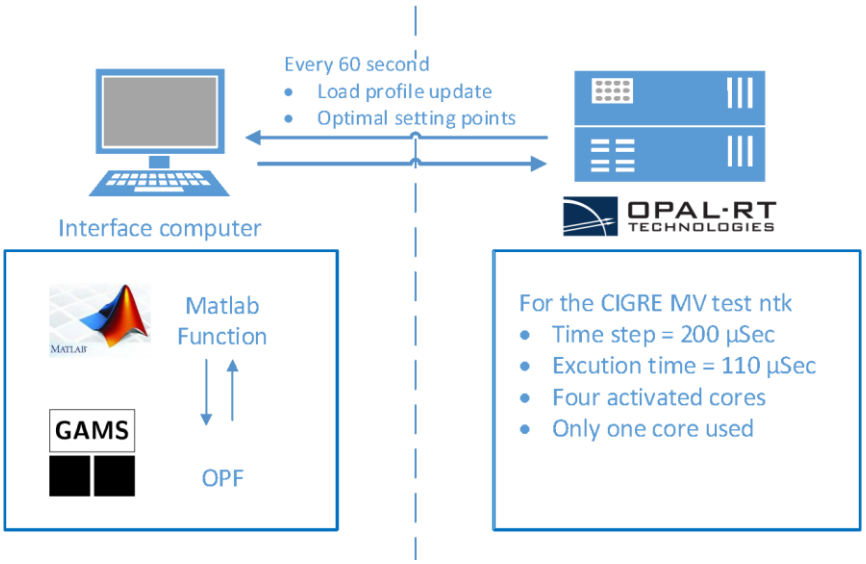

Figure 24: Planned RT-simulation laboratory test

4 Conclusions and further work

In this Annex, the preliminary results for the simulation of the PPVC are shown. It has been clearly demonstrated the benefits of the implementation of the PPVC corrective mode considering the advantages linked to the WoC concept. This improvement is achieved in terms of loss reduction allowing a more efficient operation of the power system, thus enhancing the current voltage control methods used by the grid operators. However, the implementation of the corrective operation mode has demonstrated that the CIGRE MV grid is not the more precise representation of what a cell should be, since the installed DERs compared with the load level are not enough to recover the voltage in case of a severe fault by themselves, lacking enough reactive power reserves coming from DERs. This can only achieved by using the tap changers at the header of the feeders up to very low values of the taps, which is not very realistic. However, this is an issue exclusively depending of the reference grid considered, but not linked to the PPVC voltage control concept itself. Further simulation studies are concentrating on a correct sizing of cells in terms on voltage sensitivity and the improvement of dynamic modelling in order to make the PPVC validation over a full WoC with, as required by the cell concept, self-sufficient cells in terms of voltage control. Also the PPVC testing in the lab with hardware-in-the-loop equipment is foreseen in the framework of WP7.

References

[1] http://www.electrairp.eu (ELECTRA IRP web site)

[2] Brunner, H. “The ELECTRA Web-Of-Cell Architecture in a Nutshell”, ELECTRA project, 2016.

[3] Pandapower manual: http://www.uni-kassel.de/eecs/fileadmin/datas/fb16/Fachgebiete/energiemanagement/Software/pandapower-doc/index.html

[4] Standard, E. N. (2010). 50160. “Voltage characteristics of public distribution systems”, 18.

[5] Bokhari, A., Alkan, A., Dogan, R., Diaz-Aguiló, M., De León, F., Czarkowski, D., Zabar, Z., Birenbaum, L., Noel, A., Uosef, R.E., 2014. “Experimental Determination of the ZIP Coefficients for Modern Residential, Commercial, and Industrial Loads”. IEEE Trans. POWER Deliv. 29. doi:10.1109/TPWRD.2013.2285096